PhD degree in System Medicine (curriculum: Molecular Oncology)

European School of Molecular Medicine (SEMM)

University of Milan

# Dynamic interplay between spectrin, actin and plasma membrane during cell mechanoresponse

Camilla Galli

IFOM, Milan

R11476

Supervisor: Dott. Nils Gauthier

IFOM, Milan

Academic year 2018/2019

*Meglio i nembi sfidare al monte in cima*

*che belar gregge nella valle opima.*

# Table of content

**LIST OF ABBREVIATIONS** **8**

**FIGURE AND TABLE INDEX** **10**

**ABSTRACT** **13**

**INTRODUCTION** **14**

**1. Mechanosensing, mechanotransduction and mechanoresponse** **14**

**2. Spectrin: the phantom of the cell** **17**

2.1. Discovery and description ..... 17

2.2. From electron microscopy to super-resolution: how our knowledge about spectrin has evolved ..... 18

2.3. Spectrin repeats and other important domains ..... 22

2.4. The spectrin family of proteins: different isogens and isoforms ..... 25

2.5. Spectrin mechanical properties in red blood cells ..... 27

2.6. Spectrin in neuronal cells: structure, localization and functions ..... 28

2.7. Erythroid and non-erythroid spectrin involvement in cell signalling ..... 31

**3. Spectrin interaction with plasma membrane and actin** **35**

**4. Plasma membrane organization** **36**

**5. Cytoskeleton organization** **40**

**6. Exo/Endocytosis and intracellular trafficking** **45**

**7. The evolution of the plasma membrane fluid-mosaic model and its interaction with actin cytoskeleton 46**

**AIM OF THE PROJECT 49**

**RESULTS 50**

**1. Spectrin and actin define distinct plasma membrane territories in cells of different origins 50**

**2. Resolving the spectrin ultrastructure with super-resolution microscopy 58**

**3. Spectrin and actin form a complementary and dynamic meshwork at the cell edge level during cell shape remodelling events 63**

**4. Actin nodes as drivers of spectrin organization 69**

**5. Spectrin molecular turnover depend on contractility 73**

**6. The actin-binding ability of spectrin is needed to coordinate spectrin dynamics with changes in cell mechanics 77**

**7. Spectrin and actin respond differently during extrinsic PM challenges 82**

**8. Spectrin concertedly respond with actin during cell compression 84**

**9. Spectrin elastic properties give support to PM during mechanical challenges 88**

**10. Spectrin meshwork is involved in spatio-temporal regulation of clathrin-mediated endocytosis at PM level 90**

**11. CRISPR/Cas9 approach for βII-spectrin knock out MEF cell line generation 95**

12. βII-spectrin depletion leads to αII-spectrin protein degradation 97

13. Spectrin is important for cell shape control in MEF cells 98

MATERIALS AND METHODS 100

1. Cell culture and media 100

2. Plasmids and transient transfections 101

3. CRISPR/Cas9 transfection, plasmid and sgRNA 101

4. Confocal, TIRF and STED Microscopy 102

5. Nearest neighbor distribution (nnd) analysis 103

6. Micropatterning 103

7. Stamping 104

8. Immunofluorescences 104

9. Spreading assay 105

10. Spectrin and actin intensities at the cell edge 106

11. Correlated Spectrin and actin flow velocity analysis (PIV) 107

12. Cytoskeletal Drug Perturbation and osmotic shocks 107

13. Cell stretching 108

14. Cell compression 109

15. Frap experiments 111

**16. Clathrin pits density maps 112**

**17. Statistical analysis 113**

**18. RNA extraction and qPCR analysis 113**

**19. Resource Tables and Schemes 114**

**Schematical representation of the devices used for cell compression/stretching experiments 114**

**DISCUSSION 123**

**1. Spectrin and actin define a universal and 123**

**complementary pattern, suggesting an interchangeable role in PM sustainment 123**

**3. Spectrin is an elastic and continuous meshwork 127**

**4. Spectrin fencing mechanism depends on cycles of condensation/decondensation upon different mechanical stimuli 128**

**5. Spectrin skeleton dynamics is a crucial element for the control of the cell shape and various PM-linked processes 129**

**6. α/β-spectrin heterotetramer stability is necessary for its correct functioning and for cell shape maintentenance 131**

**7. Author contributions 133**

**REFERENCES 134**

**ACKNOWLEDGMENTS 155**

# List of abbreviations

| | |
|---|---|
| **ABD** | Actin binding domain |
| **AFM** | Atomic force microscpe |
| **CAM** | Cell adhesion molecule |
| **CCP** | Clathrin-coated pit |
| **CH** | Calponin homology |
| **CME** | Clathri-mediated endocytosis |
| **CRISPR** | Clustered regularly interspaced short palindromic repeats |
| **EM** | Electron microscopy |
| **ER** | Endoplasmic reticulum |
| **FRAP** | Fluorescence recovery after photobleaching |
| **GFP** | Green fluorescent protein |
| **GPCR** | G protein-coupled receptor |
| **GPI** | Glycosylphosphatidylinosito |
| **HCC** | Hepatocellular cancer |
| **HE** | Hereditary elliptocytosis |
| **HS** | Hereditary spherocytosis |
| **IF** | Intermediate filament |
| **KO** | Knock out |
| **MEF** | Mpuse embryonic fibroblast |
| **MPS** | Membrane-associated Periodic Skeleton |
| **MT** | Microtubule |
| **NCE** | non-clathrin endcytosis |
| **NND** | Nearest neighbour distribution |

| | |
|---|---|
| **PC** | Phosphatidylcholine |
| **PDMS** | Polydimethylsiloxane |
| **PE** | Phosphatidylethanolamine |
| **PH** | Pleckstrin homology |
| **Pi** | Phosphatidyilnositide |
| **PIP2** | Phosphatidylinositol 4,5-biphosphate |
| **PIP3** | Phosphatidylinositol 3,4,5-triphosphate |
| **PIV** | Particle image velocimetry |
| **PM** | Plasma membrane |
| **PPI** | Phosphoinositides |
| **PS** | Phosphatidylserine |
| **QFDERR** | Quick-freezing, deep etching and rotary replication |
| **RFP** | Red fluorescent protein |
| **RTK** | Receptor tyrosine kinase |
| **sgRNA** | single guide RNA |
| **SR** | Spectrin repeat |
| **STED** | Stimulated emission depletion |
| **STORM** | Stochastic optical reconstruction super resolution |
| **TCR** | T-cell receptor |
| **TGF-β** | Transofrming growth factor-β |
| **TIRFM** | Total internal reflection fluorescence |

# Figure and Table Index

**Figure 1. Schematic representation of some mechanical and physical cues to which the cells are exposed. ..... 15**

**Figure 2. Schematic representation of the spectrin heterotetramer and its different conformations..... 18**

**Figure 3. Spectrin skeleton structure in erythrocytes. ..... 19**

**Figure 4. Spectrin cytoskeleton ultrastructure obtained through 3D-STORM..... 21**

**Figure 5. Ribbon representation of spectrin repeats in chicken brain α-spectrin..... 23**

**Figure 6. Schematic representation of spectrin dimer and its interactions. ..... 25**

**Figure 7. Membrane-associated Periodic Skeleton (MPS) in neurons..... 29**

**Figure 8. Plasma membrane organization. ..... 37**

**Figure 9. The three major components of the cytoskeleton. ..... 41**

**Figure 10. Different structures that can be formed by actin filaments..... 43**

**Figure 11. Schematic representation of the clathrin-mediated endocytosis process. ..... 46**

**Figure 12. lipid rafts domains at the plasma membrane. ..... 47**

**Figure 13. Spectrins isogenes have different expression levels in MEFs. ..... 51**

**Figure 14. βII-spectrin and actin define distinct and complementary plasma membrane territories. ..... 52**

**Figure 15. βII-spectrin and actin complementarity is conserved among different cell lines. ..... 55**

**Figure 16. βII-spectrin and actin complementary pattern is maintained in cells grown under different spatial constrains..... 57**

**Figure 17. Schematic representation of the STED experimental design..... 58**

**Figure 18. Calibration of STED system using multicolour Nanoruler. ..... 59**

**Figure 19. STED super-resolution microscopy revealed the intramolecular distance of βII-spectrin in MEFs. 60**

**Figure 20. Spectrin is a continuous meshwork with a constant intramolecular distance. 62**

**Figure 21. Spreading assay as a tool for the study of fast shape changes in fibroblasts.. 63**

**Figure 22. βII-spectrin and actin fluorescences linearly correlate with the area increase during cell spreading. 64**

**Figure 23. During P1 spectrin localizes at the cell body while actin at the cell edge level. 65**

**Figure 24. Spectrin and actin display opposite behaviours during cell spreading. 66**

**Figure 25. Myosin inhibition upon blebbistatin treatment impairs cell spreading. 68**

**Figure 26. Spectrin meshwork moves towards new synthetized actin nodes during untreated cell spreading. 70**

**Figure 27. Spectrin and actin flows cross correlates in terms of speed and directionality. 71**

**Figure 28. Spectrin meshwork locally decondenses and redistributes upon acto-myosin fibers disruption. 72**

**Figure 29. βII-spectrin reacts differently upon treatments with different drugs. 74**

**Figure 30. βII-spectrin turnover relies on myosin-II-dependent contractility. 75**

**Figure 31. βII-spectrin mutants representation. 77**

**Figure 32. βII-spectrin mutants display different dynamics. 78**

**Figure 33. βII-Spectrin WT, ΔPE and ΔABD show different spreading behaviours but similar accumulation at "cracking" zones formed in a spontaneous way. 79**

**Figure 34. ΔABD cells display a negative Δarea/min while WT and ΔPE cells have a positive area increase during spreading. 81**

**Figure 35. βII-spectrin reacts with actin during cell stretching. 83**

**Figure 36. βII-spectrin and actin show opposite reactions to cell compression. ..... 85**

**Figure 37. Compression-induced blebs formation upon cell compression. ..... 87**

**Figure 38. Global and local βII-spectrin reactions upon cycles of osmotic shocks. ..... 89**

**Figure 39. βII-spectrin, actin and clathrin-heavy-chain never show colocalization. ..... 91**

**Figure 40. AP2 specifically localizes in βII-spectrin-voided regions. ..... 93**

**Figure 41. βII-spectrin act as a fence during clathrin-mediated endocytosis. ..... 94**

**Figure 42. Generation of RPTP MEF cell lines βII-spectrin knock out ..... 96**

**Figure 43. βII-spectrin KO leads to αII-spectrin protein degradation. ..... 97**

**Figure 44. βII-spectrin KO lead to a cell area decrease. ..... 99**

**Figure 45. Model of the mesoscale organization and dynamics of spectrin-actin-plasma membrane territories. ..... 124**

**Table 1: Summary table of all spectrin isogenes and their localization. ..... 27**

**Table 2: Summary table of the different spectrin functions in invertebrates and in mammalian cells. ..... 35**

**Table 3: Summary table of all the cell lines used for βII-spectrin screening. ..... 54**

# Abstract

The spectrin cytoskeleton is a major component of the mammalian cell cortex. While long known and ubiquitously expressed, its dynamic behaviour and cooperation with other major components of the cell cortex is poorly understood. Here we investigated spectrin reactions upon different mechanical cues, such as cell-driven perturbations, like cell adhesion, spreading and contraction, or environmentally driven ones, like compression, stretch and osmotic changes. Upon all of these challenges we observed that spectrin meshwork spatially adapts and reorganizes under the plasma membrane together with the acto-myosin cytoskeleton. Working together to maintain cell integrity, both cytoskeletons define specific membrane territories. Actin-rich regions control protrusions, adhesions and stress fibers, whereas spectrin-rich regions concentrate in retractile zones, covering low actin density territories of the cortex. Given this interplay, we wondered if spectrin could be potentially involved in the spatial and temporal regulation of membrane trafficking. We followed spectrin, actin and clathrin dynamics through live TIRF microscopy and observed an inverted correlation between spectrin and actin densities and endocytic capacities, suggesting a spectrin contribution to clathrin-mediated endocytosis. Our results pinpoint a role for spectrin in the support of the lipid bilayer in regions where actin cytoskeleton is not established, creating a fencing mechanism for actin remodelling and cargoes internalization. All these mechanisms potentially unveil why the spectrin family of protein is evolutionary highly conserved and ubiquitously expressed in eukaryotic cells, and might explain its involvement in a broad range of pathological condition.

# Introduction

## 1. Mechanosensing, mechanotransduction and mechanoresponse

Mechanobiology is an emerging field at the interface between biology, physics and engineering focused on the understanding of how changes in the mechanical properties of cells and tissues can contribute to development, cell proliferation and differentiation, both in physiology and in disease.

During the entire life, all the cells are in constant interaction with the surrounding microenvironment and exposed to mechanical and physical cues that need to be sensed appropriately over time for the correct cellular function. Cells are subject to several different forces, including compressive, tensile, fluid shear stress and hydrostatic pressure, each of which plays an intricate part in the shaping, development and maintenance of the tissue.

As shown in the schematic representation in figure 1, every time that a cell proliferates for example, it undergoes tensile forces which regulate the mitosis success and the balanced division of the genetic material between the two daughter cells; cellular polarity acquisition and the consequent migration is regulated by intrinsic forces which play important roles in cytoskeleton remodelling, thus allowing the correct cell positioning and tissue shaping. When in tissues, cells are under constant compressive forces, due to cell-cell or cell-matrix interaction, which are essential for its maintenance and integrity, in order to avoid cell escape, tissue degeneration and the consequent pathology outgrowth. But cells aren't always stuck together within immobile tissues; sometimes they can move across the body, like erythrocytes do in blood vessels, as well as lymphocytes during an inflammation response, and they are under constant shear stress caused by the blood flow. A balanced osmotic pressure between cells and

the external environment is also important for tissue development and stability; whenever cells undergo hypo- or hyper-osmotic changes, they can swell or shrink, thus involving intrinsic forces and players in order to adapt to those variations.

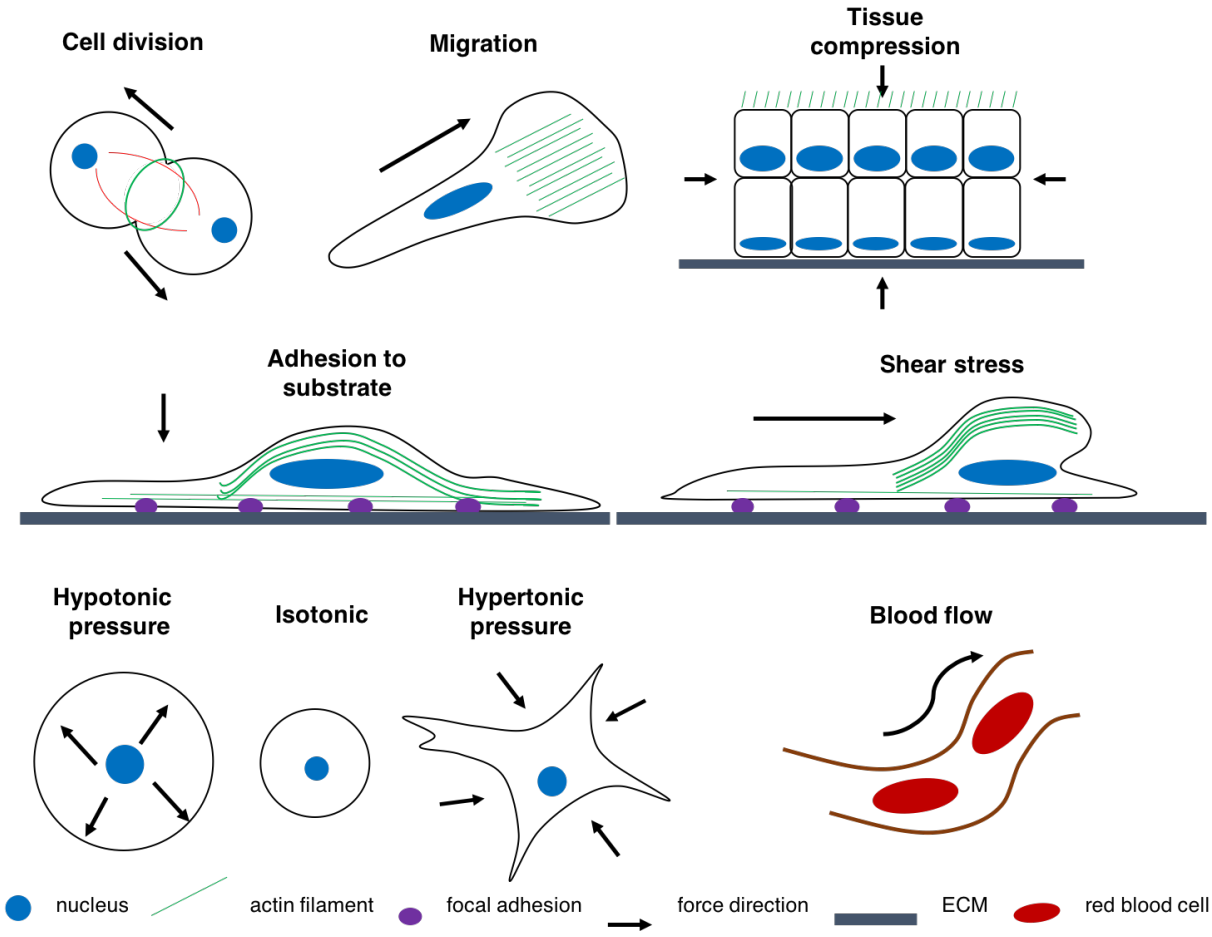


**Figure 1. Schematic representation of some mechanical and physical cues to which the cells are exposed.**

Cells are subjected to several different forces, including compressive, tensile, fluid shear stress and hydrostatic pressure, each of which plays an intricate part in the shaping, development and maintenance of the tissue. During cell division cells undergo tensile forces, while cellular polarity acquisition and the consequent migration is regulated by intrinsic forces which play important roles in cytoskeleton remodelling. Cells in tissues are under constant compressive forces, due to cell-cell or cell-matrix interaction, but when they move in the body, they are under constant shear stress caused by the blood flow. Finally, whenever cells undergo hypo- or hyper-osmotic changes, they can swell or shrink, thus involving intrinsic forces and players in order to adapt to those variations.

Local sensing of the mechanical forces leads to proteins conformational changes that are subsequently transduced into biochemical signals, thus resulting in the activation of downstream signalling pathways, ultimately regulating cell mechanoresponse.

Cell sensing starts in a subsecond to second timescale, while mechanical response takes from second to minutes to occur and involves the rearrangement of the cytoskeleton, myosin recruitment and contraction machinery activation, thus activating a global cellular reaction (Vogel and Sheetz, 2006).

Mechanotransduction is involved in different physiological processes and defects in response to mechanical cues can lead to pathological conditions such as atherosclerosis, arthritis, deafness, osteoporosis, asthma, cancer and a number of developmental disorders, including Kartagener's syndrome and Hutchinson–Gilford progeria syndrome (DuFort et al., 2011).

Cell mechanoresponse to external forces consists on an interplay between different elements such as ion channels, endocytic molecules, focal adhesions, extracellular matrix, acto-myosin cytoskeleton and plasma membrane (PM).

Among them, the acto-myosin cytoskeleton is the most characterized one, and it has been shown that it can interact with other important structures such as the PM and another protein, called spectrin, which has been deeply studied in red blood cells and neurons due to its mechanoprotective role.

In this work, we aimed at a better understanding of spectrin organization, distribution, dynamics and interplay with other molecular players, during cellular mechanoresponses in a different cellular system.

# 2. Spectrin: the phantom of the cell

## 2.1. Discovery and description

Spectrin is a long-known membrane binding protein that has been firstly identified in erythrocytes in 1968 by Marchesi and Steers (Marchesi and Steers, 1968), and its peculiar name is due to the fact that it is the major component of the so called red blood cell "ghost", which is the remaining part of red blood cells after treatment with mild detergents in order to release hemoglobin and other cytoplasmic components (Liem, 2016). Electron microscopy of spreads of erythrocyte ghosts have revealed a polygonal network formed by the association of five to seven extended spectrin molecules at 50-70 degree angles linked together by short F-actin protofilaments (~ 40 nm in length). Spectrin skeleton is coupled with the plasma membrane primarily through its binding to ankyrin protein and several plasma membrane binding domains (Byers and Branton, 1985; Liu et al., 1987; Shen et al., 1986). Spectrins are comprised of α- and β-subunits (280-260 KDa respectively), associated together laterally to form heterodimers, which in turn are associated head-to-head to form heterotetramers with a length that goes from ~ 50 nm (relaxed conformation) (Nans et al., 2011; Ursitti et al., 1991; Ursitti and Wade, 1993) to 200 nm (stretched conformation) (Byers and Branton, 1985; Liu et al., 1987), depending on the different sample processing methods (Pan et al., 2018). In order to form a tetramer, the amino terminus of the α-subunit interact with the carboxyl terminus of the β-subunit (Broderick and Winder, 2005; Liem, 2016). In figure 2 is reported a schematic representation of the α/β-spectrin heterotetramer.

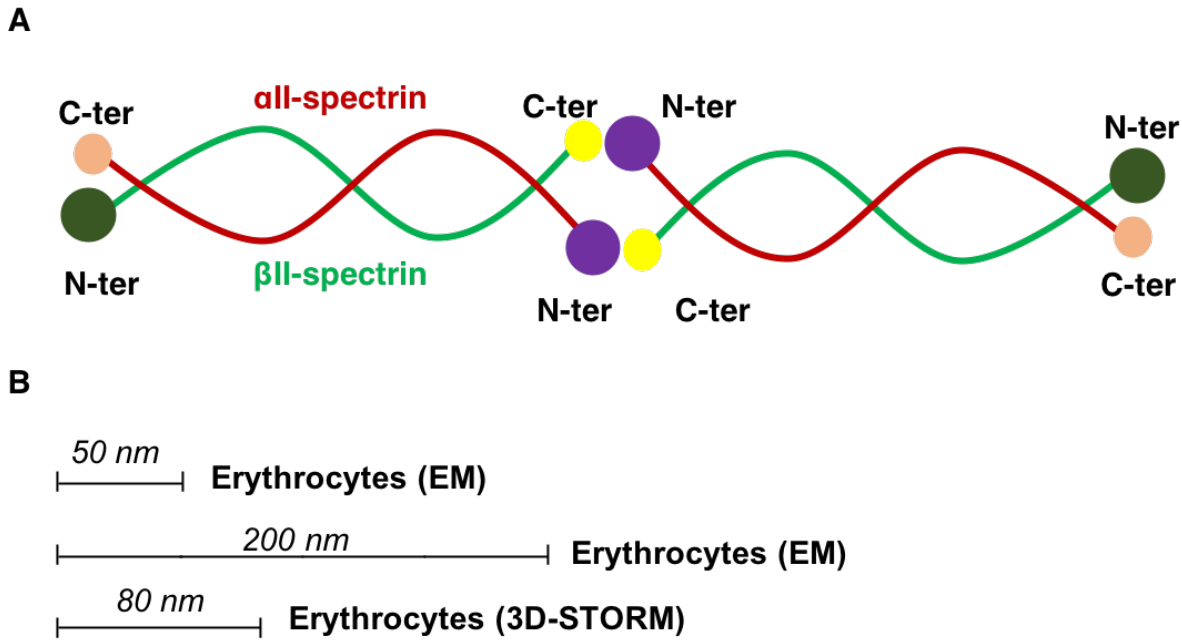


**Figure 2. Schematic representation of the spectrin heterotetramer and its different conformations**

(A) Schematic representation of spectrin molecule. α- and β-subunits associate together to form heterodimers, which in turn can form heterotetramers through the interaction between β-spectrin C-terminus (yellow) and α-spectrin N-terminus (purple). (B) Schematic representation of spectrin conformations described through different microscopy techniques. Electron microscopy studies from different research groups, revealed a molecular length ranging from 50 to 200 nm (Nans et al., 2011; Ursitti et al., 1991; Ursitti and Wade, 1993; Byers and Branton, 1985; Liu et al, 1987). Super-resolution 3D-STORM analysis on fully hydrated erythrocytes revealed 80 nm edge length for the spectrin skeleton (Pan et al., 2018).

## 2.2. From electron microscopy to super-resolution: how our knowledge about spectrin has evolved

Since its discovery in red blood cells, different estimations regarding spectrin's length have been reported. Indeed, an electron microscopy study of artificially spread erythrocytes, revealed for the first time a 200 nm long spectrin tetramer, cross linked by junctional complexes (Byers and Branton, 1985). Few years later, Liu and his group (Liu et al., 1987) found a method to improve spectrin skeleton spreading by using a thin carbon film and then examined it by high

resolution negative staining electron microscopy, thus confirming the 200 nm tetramer length and suggesting that the membrane skeleton exist as an hexagonal lattice, as shown in figure 3. All these observations were in line with the extended full length of spectrin tetramers already proposed by David Shotton years before (Shotton et al., 1979).

On the contrary, results from quick-freezing, deep etching and rotary replication (QFDERR) and atomic force microscopy (AFM) of non-spread spectrin skeleton suggested a denser meshwork, with an average length of 25-60 nm (Swihart et al., 2001; Ursitti et al., 1991; Ursitti and Wade, 1993). More recently, Nans and his group used cryo-electron tomography to evaluate the 3D topology in intact, non-spread membrane skeletons of mouse red blood cells. Their study revealed an average contour length of spectrin filaments of ~46 nm, thus indicating that the native structure of spectrin skeleton is a fraction of its fully extended length (~ 200 nm) (Nans et al., 2011).

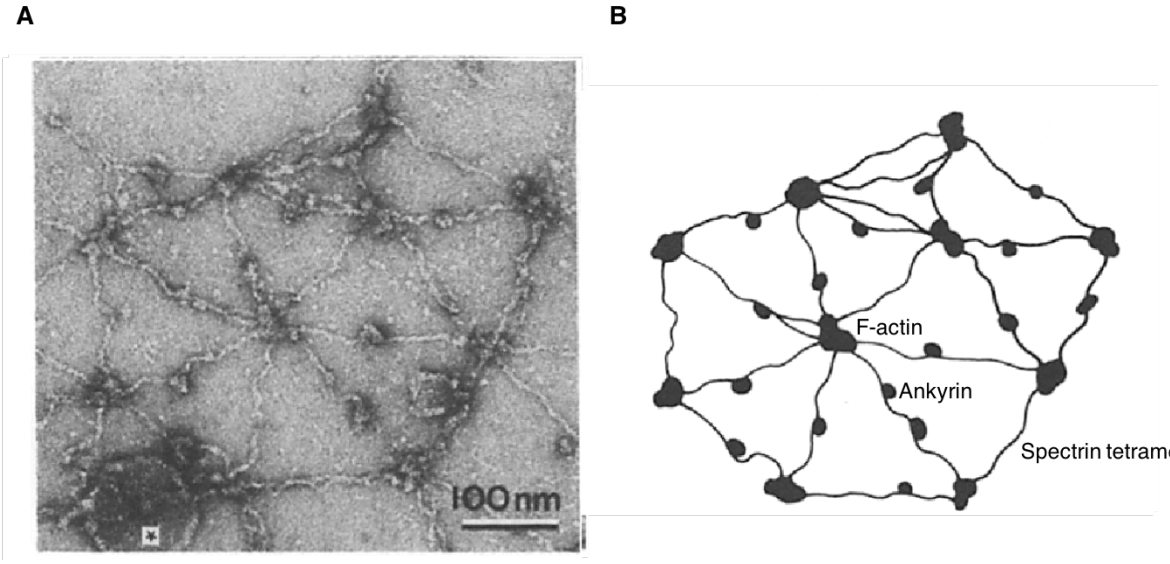


**Figure 3. Spectrin skeleton structure in erythrocytes.**

(A) A high magnification image of the sprectrin meshwork reveals the 200 nm hexagonal lattice of junctional complexes, showing short F-actin filaments cross-linked by spectrin tetramers bound to ankyrin protein. The image was obtained through high resolution negative staining electron microscopy (B) Schematic representation of the the spectrin hexagonal lattice. Adapted from Liu et al., 1987

But all the difficulties in obtaining the native ultrastructure of the cytoskeleton were mainly due to the extensive sample processing necessary for all the previous study, in which samples were dried and often membrane was removed.

Nowadays, thanks to the advent of super-resolution fluorescence microscopy (Huang et al., 2010), it became possible to reach 20 nm optical resolution, and the spectrin cytoskeleton ultrastructure can now be probed in living cells upon minimal sample processing. Indeed, a recent study performed by 3D-stochastic optical reconstruction super resolution microscopy (STORM) on fully hydrated erythrocytes, revealed a ~ 80 nm edge length for the spectrin skeletal meshwork, which is less than half of the above-mentioned results from EM of spread red blood cells cytoskeletons (Pan et al., 2018), as shown in figure 4.

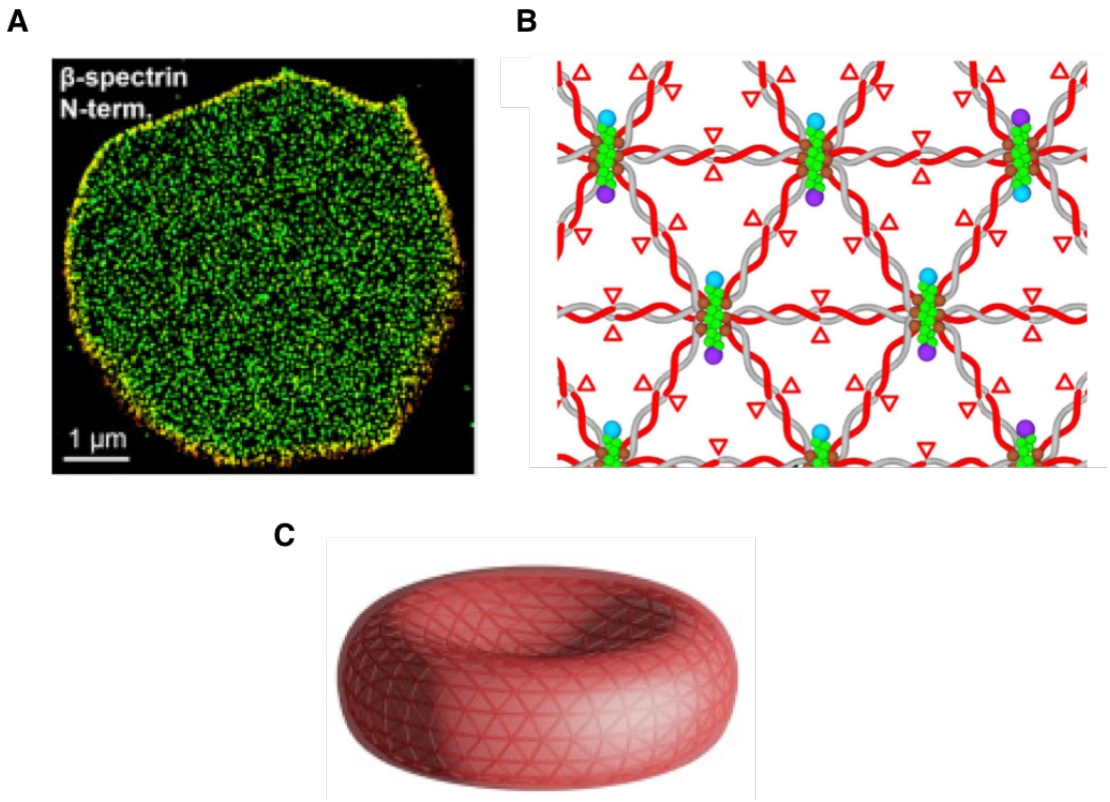


**Figure 4. Spectrin cytoskeleton ultrastructure obtained through 3D-STORM.**

A) 3D-STORM image of the N-terminus of βII- spectrins from fully hydrated erythrocytes. B) Current model of the spectrin-actin cytoskeleton of the erythrocytes. Spectrin tetramers are connected by junctional complexes containing short actin protofilaments (green) and several actin capping proteins (tropomodulin in light blue, adducin in purple and 4.1 in dark red), thus forming a triangle network with the edge lenght of ~ 80 nm. C) Cartoon representing spectrin network at the plasma membrane level of erythrocytes. Adapted from Pan et al., 2018.

These results indicate that the cytoskeleton of resting erythrocytes is in a relaxed state and might be helpful to elastically respond to both stretching or compression, as erythrocytes undergo frequent deformations during circulation toward the blood flow.

Moreover, another recent work made through 3D-STORM, led to the discovery of an actin-spectrin periodic cytoskeleton in neurons with a length of 180-190 nm (Xu et al., 2013).

Even if erythroid spectrin and the non-erythroid one share high structural similarities, there is a substantial difference regarding their length, thus suggesting that spectrin in neuronal

processes is under constant tensile force (Zhang et al., 2017) (see also chapter 2.6. Spectrin in neurons).

All these studies enabled us to understand the spectrin skeleton structure both at macroscopic and nanoscopic level, but still little is known about its mesoscale organization and interaction with other molecules at the level of plasma membrane in systems different from erythrocytes and neurons (Jenkins et al., 2015).

## 2.3. Spectrin repeats and other important domains

Spectrin belongs to the so called "spectrin superfamily" of proteins together with α-actinin, dystrophin, utrophin, plakin, desmoplakin, plectin and nesprins. The common feature among them is the presence of a helical repeating unit, which size can range between 99 and 114 amino acids, referred to as "spectrin repeats" (SRs). Even if the sequence homology between them does not exceed 30% (Leluk et al., 2001), there is a common structural fold shared by all SRs consisting of three helices, two are parallel and one anti-parallel (Djinovic-Carugo et al., 2002), as shown in figure 5.

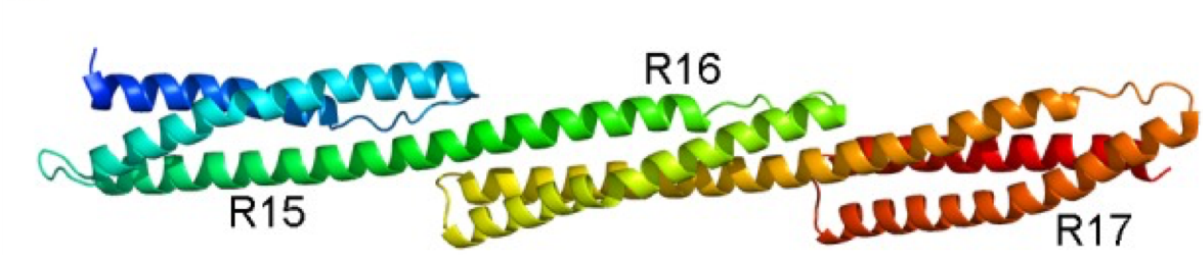


**Figure 5. Ribbon representation of spectrin repeats in chicken brain α-spectrin.**

Representation of three contiguous spectrin repeats (SR15, SR16 and SR17) in chicken brain α-spectrin. Each repeat consists of three heleces, two parallel and one anti-parallel (blue-light blue-green in SR15, green-yellow-orange in SR16, orange-red-dark red in SR17). Consecutive SRs are linked by a helix region (the 'linker') which connects the last helix of one repeat with the first helix of the adjacent one. Adapted from (Autore et al., 2013).

The three helices are mildly curved and wrapped around each other in a left-handed supercoil (Grum et al., 1999). Consecutively arranged repeats are connected through the junction of parallel helices of the following repeats in an uninterrupted helical structure (Kusunoki et al., 2004), and it has been demonstrated that spectrin repeats can reversibly unfold and refold when subjected to forces up to 20 pN, thus propagating the unfolding in a collective way (Discher and Carl, 2001; Law et al., 2003a; Law et al., 2003b). Some repeats appear to be largely unfolded compared to others; this is the case of repeats of different spectrin isoforms, which can be more or less unfolded and, consequently, more or less stable and rigid. Indeed, non-erythroid SRs appeared to be more stable compared to the erythroid one, this could be the reason why brain spectrin is way more rigid compared to other ones (An et al., 2006; Machnicka et al., 2014). It has been shown that typically, 21 complete repeats can be found in α- spectrin, whereas β-spectrin contains just 17 of them (Baines, 2009).

All the above-mentioned characteristics give to spectrin family proteins their elastic properties (Liem, 2016; Zhang et al., 2013) supporting the spectrin flexibility model, according to which spectrin repeats may respond to shearing forces by partially unfolding and acting as a molecular spring (Machnicka et al., 2014).

But spectrin is much more than just an assembly of spectrin repeats (Machnicka et al., 2014); between repeats 9 and 10 of the α-subunit, an SH3 domain, a common structural motif often found in proteins involved in signal transduction, is inserted (Robertsson et al., 2005). Moreover, at the C-terminus of α-spectrin there is an EF- hand domain (which is structurally very similar to caldmodulin-like domain), a $Ca^{+}$ binding domains, which is critical for skeletal integrity by stabilizing CH2-domain-F-actin interactions (Korsgren and Lux, 2010). β- spectrin presents a C-terminal PH (pleckstrin homology) domain, a 100-120 residues of amino acids, able to mediate the binding between the protein and phosphoinositides at the plasma membrane level, that occurs in a wide range of proteins involved in cellular signalling or cytoskeletal organization. Moreover, tandem CH (calponin homology) domains form an actin binding domain (ABD), located at the N-terminus of each of the two β- spectrins (Delalande et al., 2017). Finally, β- spectrin presents an ankyrin binding domain within residues 14-15, responsible for some of the interactions with the plasma membrane. In addition, ankyrin binding domain and PH domain are not the only two ways through which spectrin interacts with the plasma membrane. It has been shown that spectrin can present high-affinity lipid-binding domains, such as phosphatidylserine (PS) -binding domain (present in both α- and β- spectrin isoforms) and phosphatidylethanolamine (PE) -binding domain (present only in the β- one), localized in proximity of the ankyrin-binding site (Wolny et al., 2011). In figure 6 is presented a schematic representation of the α/β-spectrin dimer and all its interactions.

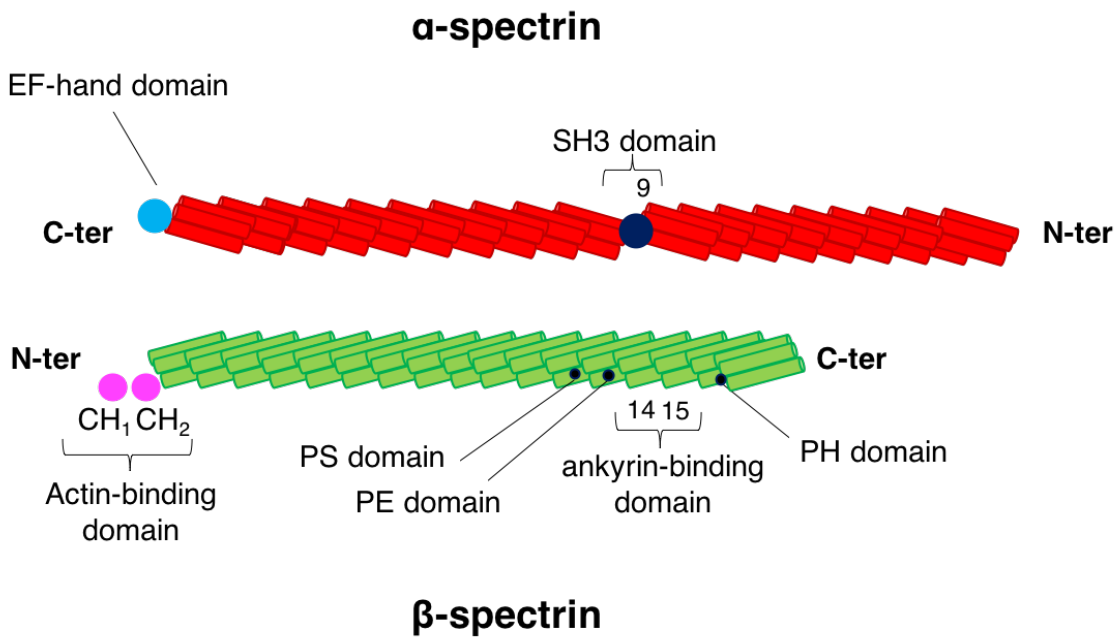


**Figure 6. Schematic representation of spectrin dimer and its interactions.**

In a spectrin dimer, α- and β-subunits lie side-by-side and antiparallel. They are made up of successive triple-helical repeats. Partial repeats at the N-terminus of α-chain and near the C-terminus of β-chain interact either to form the dimer or with another dimer to make a heterotetramer. The β-spectrin N-terminus contains tandem CH domains for actin binding. Triple helical repeats 14–15 bind ankyrin. PH membrane binding domain, is present at C-terminal region of βII-spectrin and PS and PE membrane binding domains are present in proximity of ankyrin binding domain. At the C-terminal region of α-spectrin there is an EF-domain, able to bind $Ca^{+}$, while between repeats number 9 and 10 there is an SH3 domain, involved in signal transduction.

## 2.4. The spectrin family of proteins: different isogens and isoforms

Spectrin proteins are expressed in all metazoan cells, and in mammalians are encoded by seven different genes. Indeed, separate genes encodes for the two major versions of alpha subunits, SPTA1 (the erythroid version) and SPTAN1 (the non-erythroid one), which generate αI- and αII- spectrin respectively. The primary transcript of SPTAN1 can be alternatively spliced, thus resulting in at least 4 (but possibly up to 8) αII- spectrin isoforms (Cianci et al., 1999a).

Four “conventional” β- genes, SPTB, SPTBN1, SPTBN2 and SPTBN4 code for βI-, βII, βIII- and βIV- spectrin, where the first one is expressed in red blood cells only, whereas the other three in all the other nucleated cells (Machnicka et al., 2014).

Finally, another gene, SPTBN5 codes for one giant βV- spectrin (also known as β-heavy); this unusual isoform is unique, since it contains 30 spectrin repeats, may lack the ankyrin-binding capacity and have an SH3 domain.

The expression of the diverse spectrins is tightly regulated in a tissue- and time- specific manner. The αII- spectrin isoforms have a wide tissue expression (Cianci et al., 1999b), while the different β- spectrin variants are distributed to various intracellular locations such as the plasma membrane (βII-spectrin, which is the one most widely distributed among the nucleated cells (Bennett and Baines, 2001; Winkelmann et al., 1990; Winkelmann and Forget, 1993)), the Golgi apparatus and vesicles (βIII-spectrin (Stankewich et al., 1998)), the axon initial segments and node of Ranvier in the central peripheral nervous system (βIV- spectrin (Berghs et al., 2000). βV- spectrin has been shown to be expressed at low levels in many tissues, such as in the outer segments of photoreceptor rods and cones and in the basolateral membrane, in the cytosol of gastric epithelial cells and in the outer hair cells (Legendre et al., 2008; Stabach and Morrow, 2000), see also table 1, where a summary of the different spectrin variants and their respectively localization is reported.

Invertebrates have a smaller repertoire of spectrin genes. *C.Elegans* and *D. Melanogaster* have just one version of α-spectrin, which is very similar to αII-spectrin in mammalians, encoded by spc-1 and I(3)dre3 genes, respectively. β-spectrin is encoded by two different genes: the first one codes for $\beta_G$- spectrin protein, which resembles the βII-spectrin present in mammalian cells (Unc-70/bgs in *C.Elegans* and b-spc in *D.melanogaster*) and the other one (sma 1 in *C.Elegans* and karst in *D.Melanogaster*) encoding for a giant βH- spectrin (which is very similar to the mammalian version of βV- spectrin) (Dubreuil et al., 1989; Dubreuil and Grushko, 1998; Machnicka et al., 2014).

| Subunit | Gene | Localization | Reference |
|---|---|---|---|
| αI | *SPTA1* | • **In RBC**<br>• **A variant also found in brain** | (Winkelmann and Forget., 1993) |
| αII | *SPTAN1* | • **Different isoforms and wide tissue expression** | (Cianci et al.,1999) |
| βI | *SPTB* | • **In RBC**<br>• **A variant also found in brain and muscle** | (Winkelmann and Forget., 1993; Winkelmann et al., 1990; Bennet and Baines., 2001) |
| βII | *SPTBN1* | • **All nucleated cells** | (Winkelmann and Forget., 1993; Winkelmann et al., 1990; Bennet and Baines., 2001) |
| βIII | *SPTBN2* | • **Golgi and vesicular membrane skeletons** | (Stankewich et al., 1998) |
| βIV | *SPTBN4* | • **Neurons (axon, initial segment, nodes of Ranvier)** | (Berghs et al., 2000) |
| βV | *SPTBN5* | • **Low level in many tissues**<br>• **Outer segments of photoreceptor rods and cones**<br>• **Basolateral membrane of gastric epithelial cells**<br>• **Outer hair cell (OHC)** | (Stabach et al., 2000; Legendre et al., 2008) |

**Table 1: Summary table of all spectrin isogenes and their localization.**

Seven different spectrin isogenes can be found in mammalian cells; αI- and βI-spectrins are predominantly expressed in erythrocytes whereas βII, βIII, βIV and βV are expressed at different levels and with different distributions in nucleated cells. Adapted from Machnicka et al., 2012.

## 2.5. Spectrin mechanical properties in red blood cells

Spectrin skeleton provides erythrocytes with two major mechanical properties: resilience and flexibility. These characteristics are necessary to the cells, since they constantly undergo shear stress when circulating in the blood flow, or compression when they pass through thin capillaries.

A first evidence of red blood cells mechanical capacities dates back to the late 60s, when scientists, by using different experimental approaches, such as osmotic swelling (Fung and Tong, 1968), fluid shear deformation (Hochmuth and Mohandas, 1972) and micropipette aspiration (Rand and Burton, 1964), demonstrated the erythrocytes ability to deform and come back to a normal shape, thus being able to sustain external mechanical challenges. Subsequent studies, revealing the peculiar structure of the spectrin molecule and its mechanical properties, finally linked the protein to the elastic characteristics of circulating red blood cells (Elgsaeter et al., 1986).

Given its crucial role in maintaining the stability and the structure of the membrane and, consequently, the shape of a cell, it emerged that spectrin can contribute to several human diseases such as different types of hereditary haemolytic anemia, like hereditary spherocytosis (HS) or hereditary elliptocytosis (HE). Indeed, molecular defects in erythroid spectrin are associated with abnormal shape, increased membrane fragility and decreased cell deformability (Machnicka et al., 2012).

HS for example, is a disease characterized by mechanical abnormalities accompanied with osmotic variations, which can be caused by single base deletion or nonsense mutation in α-spectrin, by the abolition of the β-spectrin initiation codon, or by mutations in ankyrin gene.

Mutations in both α- or β-spectrin, can lead to HE too, a disease mainly characterized by mechanical dysfunction in red blood cells, without changes in osmotic pressure (Delaunay, 2007; Zhang et al., 2013).

## 2.6. Spectrin in neuronal cells: structure, localization and functions

The beauty and the simple geometry of erythrocytes have always intrigued numerous scientists, and for this reasons spectrin has been extensively studied within those circulating cells.

But spectrin is present also in nucleated cells and particularly, in the last years, researchers focused their attention on the neuronal isoform, where the ultrastructural organization of spectrin is quite different from the erythroid one. Thanks to the latest advances in super-resolution fluorescent microscopy (Huang et al., 2010), it became possible to determine the quasi-one-dimensional (quasi-1D) structure of the protein, which seems to be enriched at the axonal level. Here, it has been observed the presence of a Membrane-associated Periodic Skeleton (MPS), both in fixed and live cultured neurons and in brain tissue sections. MPS has been shown to be made of actin-spectrin and other associated proteins. Actin is arranged into ring-like structures wrapped around the circumference of neurites, capped by the protein adducin and connected each other by αII- and βII- spectrin heterotetramers, with an average distance of ~ 190 nm (figure 7).

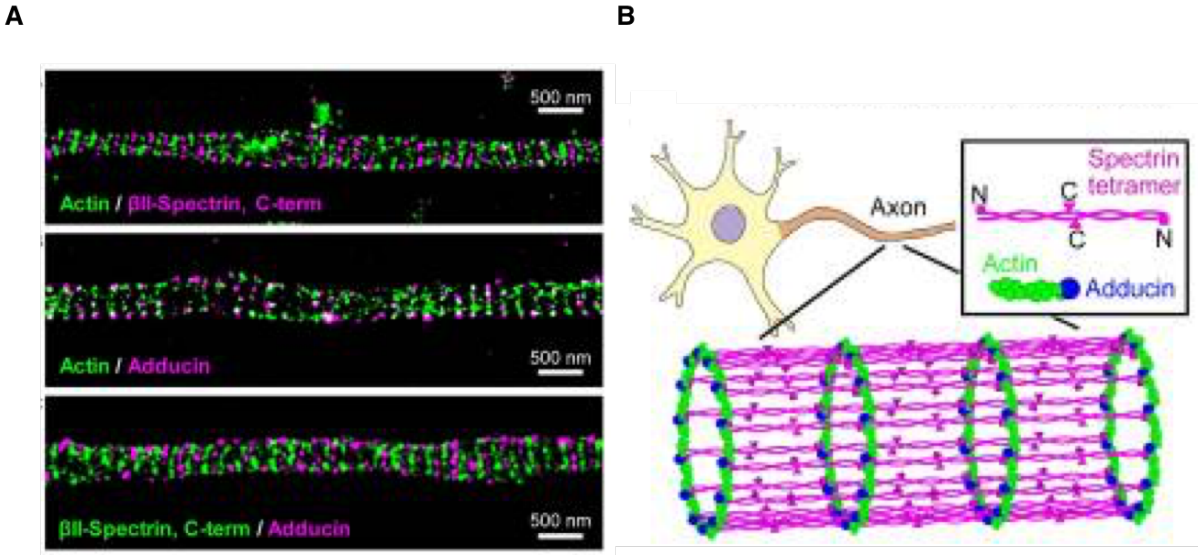


**Figure 7. Membrane-associated Periodic Skeleton (MPS) in neurons.**

A) Two-color, STORM image of (top) actin (green) and C-terminus region of βII-spectrin (magenta), (middle) actin (green) and adducin (magenta), and (bottom) C-terminus region of βII-spectrin (green) and adducin (magenta). B) A model for the membrane-associated periodic skeletn in axons. Short actin filaments (green), capped by adducin (blue), form ring-like structures wrapping around the circumference of the axon. Spectrin tetramers (magenta) connect the adjacent actin/adducin rings along the axon with a periodicity of ~190 nm. The letters "C" and "N" in the legend mark the C-terminus and N-terminus of β-spectrin, respectively. Adapted from Xu et al., 2013.

The MPS is assembled early during axon development, forming initially in the region proximal to soma of the cell and then propagating towards the entire axonal shaft (Wang et al., 2019; Xu et al., 2013; Zhong et al., 2014).

This peculiar MPS is present also, even if with lower propensity in dendrites of neurons, and, in addition, it has been observed that spectrin and actin can form a 2D polygonal lattice structure, resembling the erythroid one, also in the somatic compartment of those cells (Han et al., 2017).

This kind of structure has been reported to be highly conserved in a broad range of neuronal cells across different species, both vertebrates like *Homo sapiens, Mus musculus, Gallus gallus,* and invertebrates such as *Caenorabditis elegans* and *Drosophila Melanogaster,* which, on the contrary, displays an erythrocyte-like polygonal membrane skeleton (He et al., 2016; Pielage et al., 2006).

Given its ubiquitous expression, scientists found out that spectrin can be implicated in various neuronal biological functions. Indeed, it has been shown that spectrin is important for the maintenance of the neuronal polarization, the development and stabilization of axons, as well as for providing them the mechanical stability and for protecting them from mechanical stress (Galiano et al., 2012; Hammarlund et al., 2007; Krieg et al., 2014).

In *Drosophila,* it has been reported spectrin role in axon path finding (Hulsmeier et al., 2007) and in the stabilization of pre-synaptic terminals (Pielage et al., 2005). Moreover, spectrin has been shown to play an important role in human neurological disease, such as spinocerebellar ataxia type 5 or West syndrome (Ikeda et al., 2006; Writzl et al., 2012).

## 2.7. Erythroid and non-erythroid spectrin involvement in cell signalling.

Several decades of studies have implicated all the spectrin proteins in a big array of biological processes, from the maintenance of cell shape and membrane integrity to the control of endocytosis and intracellular trafficking or the regulation of several signalling pathways.

Indeed, given the occurrence of a great variety of isoforms in different cells, spectrin function can vary among different cells as a result of their specialization (Machnicka et al., 2012).

As in red blood cells, where spectrin support their shape and membrane integrity (Salomao et al., 2006), in epithelial cells, knock down of either βII- spectrin or ankyrin G, results in loss of the lateral membrane, expansion of the apical and basal membrane area and conversion of cells from a columnar epithelium to a squamous one (Kizhatil et al., 2007a; Kizhatil et al., 2007b).

Interestingly, it has been shown that βII-spectrin can participate to the maintenance of the lateral order in lipid bilayers through phosphatidylserine interactions (Thompson et al., 2008).

Moreover, both α- and β- spectrins are involved in the nervous system development, by mechanical stability to neuronal contacts (Leshchyns'ka et al., 2003).

But supporting cell architecture and cell morphology is not the only function attributed to spectrin, which indeed, can control the disposition of membrane channels, receptors, transporters and adhesion molecules. Spectrin defects can lead to membrane structure destabilization, neurodegenerative disorders and other pathological processes (Djinovic-Carugo et al., 2002; Komada and Soriano, 2002; Tang et al., 2003).

Interestingly, it has been shown that depletion of αII-spectrin in *D. melanogaster* and *C. Elegans* leads to late embryonic-early larval stage lethality (Dubreuil, 2006; Hammarlund et al., 2007; Moorthy et al., 2000).

For these reasons, it became worthwhile to understand all the consequences of mutations or even depletion of both spectrin proteins in mammalian cells. It has been shown that mice lacking αII-spectrin dye at embryonic level (from day 12.5 to 16.5) because of malformations

of the neural tube and cardiac system. In addition, embryonic fibroblasts derived from E 14.5 knock out mice for αII-spectrin exhibit impaired growth and spreading with a spiky shape, sparse lamellipodia and absence of cortical actin (Stankewich et al., 2011). On the other hand, it has been shown that homozygous SPTBN1 null mice are embryonic lethal due to a loss of TGF-β signalling (Tang et al., 2003), whereas heterozygous βII-spectrin deficient mice developed hepatocellular cancer (HCC) (Kitisin et al., 2007). Furthermore, it has been demonstrated that βII-spectrin knock out MEF cells display defects in DNA damage repair by the homologous recombination pathway (Horikoshi et al., 2016), given its presence in nuclei of human cells (Sridharan et al., 2003; Sridharan et al., 2006). Moreover, spectrin has been associated with the maintenance of chromosomal stability (McMahon et al., 2009).

More recently, a new, unexpected role for α-spectrin in participation in cell adhesion and spreading via its SH3 domain, and its ability to reorganize actin cytoskeleton, have been also proposed (Bialkowska et al., 2005; Metral et al., 2009).

Spectrins has been shown to be involved in other signalling pathways like TCR (T-cell receptor) formation, activation and apoptosis in lymphocytes through its binding to CD45 (Iida et al., 1994). In addition, through its interaction with various proteins that participate in intracellular trafficking, spectrin has been shown to be involved in internalization and transport of different proteins (Devarajan et al., 1997).

Recently, a work performed on *D. Melanogaster* described spectrin ($\alpha/\beta_H$) as a mechanoresponsive protein, involved in the shaping of fusogenic synapses upon shear deformations during muscle cells fusion (Duan et al., 2018). Moreover, another interesting and very recent work, propose an interaction between MyosinIIA and actin-spectrin skeleton in the maintenance of erythrocytes shape stability, thus controlling their peculiar biconcave disk shape (Smith et al., 2018).

Interestingly, αII-spectrin has been found to be part of a list of five genes involved in lung cancer metastasis formations (Sun et al., 2019). Indeed, it has been shown that downregulation

in *SPTAN1 gene* is associated with tumor metastatic progression in patient with lung adenocarcinoma or lung squamous cell carcinoma (Sun et al., 2019).

Finally, a very recent work demonstrated that the spectrin skeleton in neurons can function as a structural platform for GPCR- and CAM- mediated RTK activation and signalling, thus providing a mechanism for the regulation of signal transduction in neuronal cells (Zhou et al., 2019). In table 2 is reported a summary of all the spectrin functions in invertebrates and in mammalian cells.

| Subunit | Gene | Function | Reference |
|---|---|---|---|
| αI | *SPTA1* | • **Support RBC shape and maintains membrane stability and its properties** | (Salomao et al., 2006; Delaunay et al., 2007) |
| αII | *SPTAN1* | • **Maintain cell architecture, morphology and PM stability**<br>• **Modifies cell cycle by altering cell adhesion**<br>• **Engaged in the maintenance of chromosomal stability**<br>• **Involved in lung cancer-associated metastasis formation**<br>• **Nervous system development**<br>• **Cardiac system development**<br>• **DDR involvement** | (Bennet et al., 2008; Metral et al., 2009; Bialkowska et al,2005; McMahon et al., 2009 Sun et al.,2019; Leshchyns'ka et al., 2003; Stankewich et al., 2011; Sridharan et al., 2003) |
| βI | *SPTB* | • **Support RBC shape and maintains membrane stability and its properties**<br>• **Formation of TCR in lymphocytes** | (Delaunay et al, 2007; Iida et al., 1994) |
| βII | *SPTBN1* | • **Engaged in cell morphology and mechanical properties, compaction and accumulation of E-cadherin in the epithelial cell-cell contact**<br>• **Maintenance of later order in lipid bilayers**<br>• **Cell cycle regulation through TGFβ signaling**<br>• **RTK transactivation and signaling**<br>• **Nervous system development**<br>• **HCC cancer involvement**<br>• **DDR involvement** | (Kizhatil et al, 2007; Kizhatil et al, 2007; Thompson et al., 2008; Tang et al, 2003) Zhou et al., 2019; Leshchyns'ka et al., 2003; Kitisin et al., 2007; Horikoshi et al., 2016) |
| βIII | *SPTBN2* | • **Facilitates membrane protein transport via the secretory and endocytic pathways** | (Devarajan et al., 1997; Holleran et al., 2001) |
| βIV | *SPTBN4* | • **Regulates localisation of voltage-gated channels at the axon initial segment and node of Ranvier, synchronizes action potentials, provides multifunctional regulatory platform for sodium channels, plays an important role in the structure and stability of excitable membranes in heart and brain** | (Berghs et al., 1990; Komada et al., 2002) |
| βV | *SPTBN5* | • **Engaged in cell flexibility**<br>• **Engaged in OHCs' electromotility** | (Stabach et al, 2000; Legendre et al, 2008) |
| $\alpha/\beta_H$ *(D.Melanogaster)* | *Spc-1/l(3)dre3* | • **Shaping muscle fusogenic synapses**<br>• **Embryonic and larval development** | (Duan et al.,2018; Dubreuil, 2006) |
| B (*C.Elegans*) | *Unc-70/bgs* | • **Provides stability from mechanical stress**<br>• **Embryonic development** | (Krieg et al., 2014; Hammarlund et al., 2007; Moorthy et al., 2000) |

**Table 2: Summary table of the different spectrin functions in invertebrates and in mammalian cells.**

Different spectrin variants can play different functions among different cells. In mammalian cells, erythroid α- and β- spectrins are mainly involved in the RBC shape support and membrane stability maintenance (Salomao et al., 2006; Delaunay et al., 2007). Non-erythroid αII- spectrin is involved in the maintenance of cell morphology and membrane stability, cell cycle regulation and DNA damage repair, nervous and cardiac system development and its downregulation is associated with lung cancer-associated metastasis formation (Bennet et al., 2008; Metral et al., 2009; Bialkowska et al,2005; McMahon et al., 2009 Sun et al.,2019; Leshchyns'ka et al., 2003; Stankewich et al., 2011; Sridharan et al., 2003). βII- spectrin is involved in the maintenance of cell morphology and membrane stability too, cell-cell contacts formation in epithelial cells, maintentance of lateral order of lipid bilayer, TGF-β signaling pathway, RTK activation and signaling, nervous system development. Moreover βII- spectrin has been shown to be involved in HCC growth and DNA damage repair pathway (Kizhatil et al, 2007; Kizhatil et al, 2007; Thompson et al., 2008; Tang et al, 2003Zhou et al., 2019; Leshchyns'ka et al., 2003; Kitisin et al., 2007; Horikoshi et al., 2016). βIII- spectrin is involved in protein transport via endocytic pathway (Devarajan et al., 1997; Holleran et al., 2001), while βIV- spectrin is mainly involved in the regulation of the localization of voltage-gated channels at the axon initial segent and node of Ranvier, synchronization of action potential, sodium channel regulation and in the maintentance of structure and stability of excitable membranes in heart and brain (Berghs et al., 1990; Komada et al., 2002). Finally, βV- spectrin has been found to be involved in cell flexibility and in the OHC's electromotility (Stabach et al, 2000; Legendre et al, 2008). In *D. Melanogaster* spectrin has been shown to be involved in the formation of fusogenic synapses in muscle cells, and in the embryionic and larval development (Duan et al.,2018; Dubreuil, 2006), while in *C. Elegans* it has been associated with stabilizagtion from mechanical stress and embryionic development (Krieg et al., 2014; Hammarlund et al., 2007; Moorthy et al., 2000). Adapted from Machnichka et al., 2012.

# 3. Spectrin interaction with plasma membrane and actin

As already mentioned (see paragraph 2.3. spectrin repeats and other important domains), spectrin can harbour different domains that enable its interaction with both plasma membrane and actin cytoskeleton, thus suggesting the presence of a coordinated network between these

three elements in supporting the cell in both physiological conditions and under mechanical perturbations.

# 4. Plasma membrane organization

The plasma membrane (PM) is the structure that encloses all the cells, defining the boundary between the external environment and the cytosol ((Pontes et al., 2017a; Pontes et al., 2017c; Singer and Nicolson, 1972) and in almost all cells it represents a physical inelastic barrier with a given area that adheres to the underlying cytoskeleton (Gauthier et al., 2012). It is about 5 to 10 nm wide and it is composed by a continuous double layer of amphipathic lipids and proteins held together mainly by non-covalent interactions, as shown in figure 8.

From the physical point of view PM can be represented as a non-stretchable barrier (it can be stretched 2-4 % before rupturing (Morris and Homann, 2001), while mechanically, it is characterized by a low shear modulus (as a result of the fluid nature of lipid barrier s, 4-10 x $10^{-3}$ N/m (Engelhardt and Sackmann, 1988; Evans, 1973; Henon et al., 1999), a high elastic modulus ($10^{3}$ N/m) (Hochmuth and Mohandas, 1972; Hochmuth and Waugh, 1987) with variable viscosity and a bending stiffness strongly influenced by membrane proteins and cytoskeletal elements.

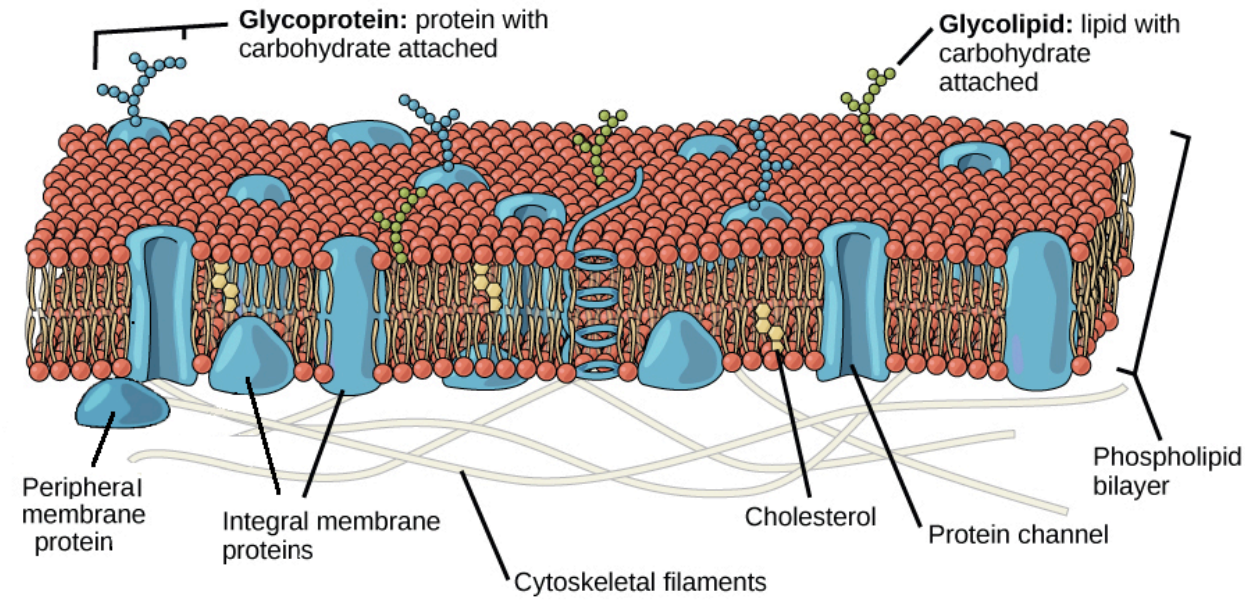


**Figure 8. Plasma membrane organization.**

Image taken from Wikipedia. Schematic representation of the plasma membrane structure, which is composed by a double layer of amphipathic lipids and proteins held together mainly by non-covalent interactions. The lipids found inside the plasma membrane are mainly phospholipids, sterols and glycolipids. proteins are the second main building element and they also can be divided in two different types: peripheral and integral proteins. Moreover, some of these proteins can bear on their surface a complex sugar, this modification gives them the name of glycoproteins.

The lipids found inside the plasma membrane are mainly phospholipids, sterols and glycolipids, and all of them serve as main backbone structure of the plasma membrane.

But lipids are more than just a simple element of the membrane architecture, they also provide a self-assembled barrier to the cells, avoiding random movements of water-soluble elements in and out of the cell. Moreover, lipid composition can also determine the physical state of a membrane and regulate cell functions by providing precursor of chemical messengers. Finally, thanks to the high flexibility of the lipid bilayer, membranes can undergo deformations and shape changes during several processes such as migration, cell division or fusions.

Given spectrin ability to interact with the PM through its lipid-binding domains, and since phospholipids are the major components of the plasma membrane, we will focus on their structure and functions.

Phospholipids have an amphipathic nature due to their peculiar composition, indeed, they possess a hydrophilic head, which spreads over the outer surface and is made by glycerol, phosphate and a small polar compound, and one hydrophobic tail composed of two fatty acid chains facing the interior of the cell.

According to different modifications on their phosphate groups, phospholipids can be divided in several subclasses, such as phosphatidylserine (PS), phosphatidylethanolamine (PE), phosphatidylcholine (PC) and phosphatidylinositides (PI).

In mammalians, PC is the most abundant phospholipid (40-50% of total phospholipids), whereas PE and PS account for approximately 20% and 3-15% respectively of the total phospholipids (Vance and Steenbergen, 2005; Vance and Tasseva, 2013).

It has been shown that PS and PE are not equally distributed in membranes of different mammalian cells and, interestingly, compared to other tissues, brain is the one with the highest density (~ 40-45 % of total phospholipids content). PS concentration can also vary among different organelle membranes within the same cell, and it is generally higher at the plasma membranes and endosomes, while it is very low in mitochondrial inner membranes (which is enriched in PE). Normally asymmetrically distributed across the double leaflet of the plasma membrane (with higher concentration in the inner, compared to the outer one), PS can move in the bilayer and be exposed on the cell surface as a signal for apoptosis cascade start.

Due to its abundance in the brain, PS has been proposed to have a main role in the correct functioning of the nervous system (Mozzi et al., 2003); in addition, it has been recently discovered to have function in targeting proteins to phagosomes (Yeung et al., 2008), in membrane trafficking and recycling endosomes.

On the other hand, there is evidence for supporting a role for PE in membrane fusion regulation of membrane curvature and regulation of contractile ring disassembly during cytokinesis of mammalian cells (Emoto et al., 1996; Pecheur et al., 2002).

Taken together, all these notions reveal an important role for PS and PE to membrane structure maintenance, metabolism and other fundamental biological processes.

Even if present in a very small concentration in the plasma membrane (less than 1%), phosphatidyilnositides (PIs) play important roles in many fundamental biological processes, such as the regulation of cellular signalling, acquisition of cellular polarity, cytoskeletal dynamics, regulation of cellular adhesions, motility or cytokinesis (Shewan et al., 2011). Their characteristic polar head group is composed by cyclic *myo*-inositol $(CHOH)_6$), and can be further phosphorylated, thus giving rise to seven different isoforms of PIs, also known as phosphoinositides (PPIs) (Falkenburger et al., 2010; Shewan et al., 2011). The most abundant PIs at the plasma membrane level are phosphatidylinositol 4,5-biphosphate (also called $PIP_2$) and phosphatidylinositol 3,4,5-triphosphate (also known as $PIP_3$). Particularly, $PIP_2$ has been shown to be involved in the regulation of actin polymerization and in the establishment of membrane-cytoskeleton interactions, thanks to its ability to bind a Pleckstrin Homology (PH) domain, a 120 amino acids sequence that share similarity with two regions in pleckstrin, and it is present in a large number of cytoplasmic proteins (Lemmon, 2007).

But lipids are not the only components of the plasma membrane; proteins are the second main building element and they also can be divided in two different types. The first one, the peripheral proteins, can be loosely attached, through non-covalent interactions, either to the membrane surface or to a second group of proteins called integral proteins which are firmly embedded into the lipid bilayer. Moreover, some of these proteins can bear on their surface a complex sugar, this modification gives them the name of glycoproteins.

These proteins are responsible for several plasma membrane biological functions, such as cell-cell interactions, endo/exocytosis regulation, they can also function as receptor for cargoes

internalization, or they can be carriers or channels, helping the transport of substances and ions across the lipid bilayer.

# 5. Cytoskeleton organization

Plasma membrane is the essential block for the architecture and structure of the cells, but it can't operate alone. Indeed, it is in constant interaction with the cell cytoskeleton, a network of filaments, whose role is to support the plasma membrane, give shape to the cell, position the organelles, provides tracks for the transport of vesicles and allow the cells to move.

In order to fulfil all these functions, the cytoskeleton integrates the activity of a multitude of proteins, and although the name, which contains the word "skeleton", could remind something fix and hard, like our body skeleton, it is not a rigid structure at all.

It is rather a highly dynamic 3D complex composed of three main types of protein filaments: actin microfilaments, microtubules and intermediate filaments. All these three structures are built by a repetitive assembly of small subunits, held together by non-covalent interactions, which allows them to continuously reorganize by fast assembly and disassembly, see also figure 9.

Among them, actin filaments are the one with the most studied interactions with the plasma membrane; indeed, several important cellular functions (i.e. cell migration, endocytosis) depend on this association.

Actin microfilaments are linear polymers of the globular protein G-actin, which polymerizes into filament structures (F-actin), which appears as a two-handed helix wrapped around each other (Holmes et al., 1990).

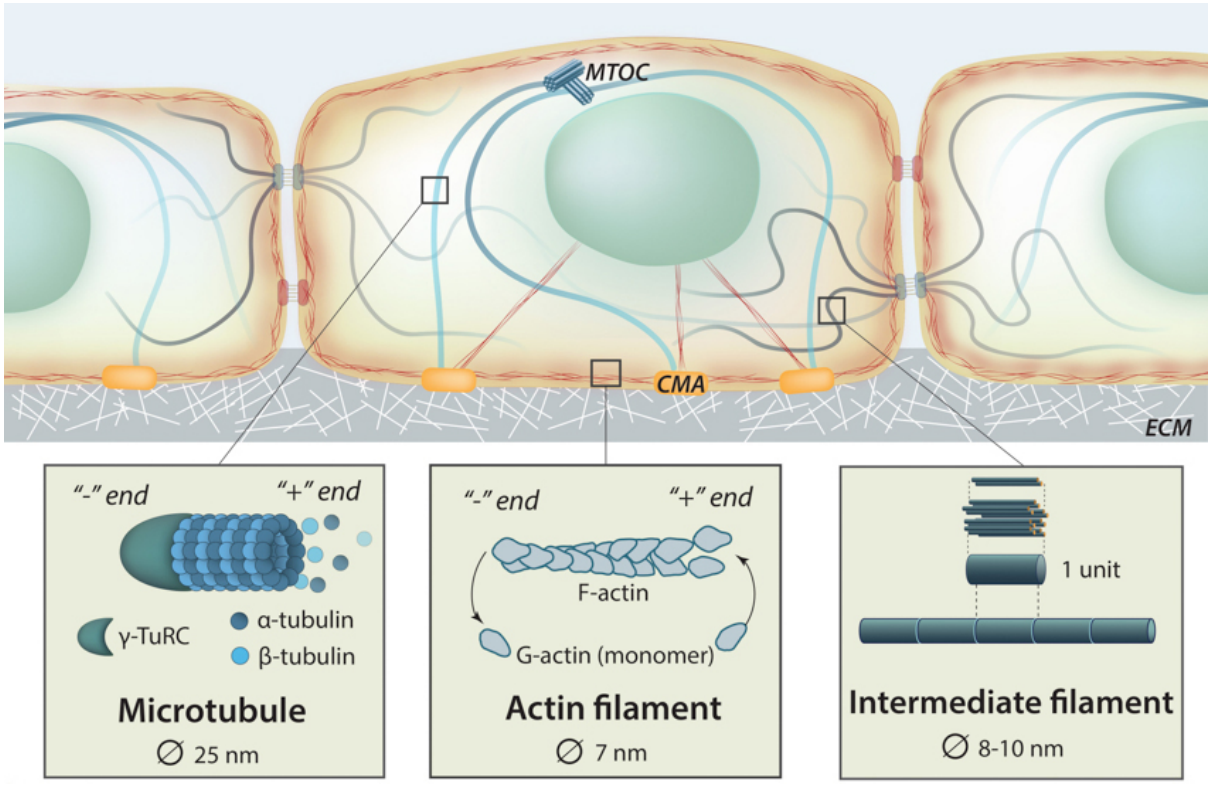


**Figure 9. The three major components of the cytoskeleton.**

Image taken from https://www.mechanobio.info. Schematic representation of the three main component of the cellular cytoskeleton: the microtubules, the actin microfilaments and the intermediate filaments. Microtubules are 25 nm diameter structures formed by lateral association or around 12-17 α and tubulin protofilaments into a regular helical lattice. Actin microfilaments are built up from the globular protein G-actin, which polymerizes into filament structures (F-actin), with a diameter of 7 nm. Intermediate filaments are 10 nm in diameter and many microns long.

The actin filaments are the narrowest one with a diameter of ≈ 7, they can reach a length of around 30-100 nm *in vitro,* and they are very flexible structures, with a viscoelastic modulus of 100-1000 Pa (Burlacu et al., 1992; Helfer et al., 2005).

Actin filaments can form a large variety of structures, such as the actin cortex, stress fibers, lamellipodia or filopodia, which play fundamental roles in generation of physical forces within the cells.

Actin cortex is a thin crosslinked network of actin, myosin and over other hundred actin-binding proteins (ABPs), that lies underneath and is tethered to the plasma membrane, and it is the major determinant of the cell shape and surface stiffness, enabling cells to resist mechanical stresses. Among the several ABPs found to localize at the cortex level, we can find crosslinking proteins such as α-actinin, filamin and fimbrin, or proteins involved in contractility generation like myosins, tropomodulin and tropomyosin. Despite its importance, little is known about how actin cortex is generated, but recent studies revealed a fundamental role for mDia1 and Arp2/3 proteins in cortical actin nucleation (Bovellan et al., 2014; Salbreux et al., 2012).

It has been shown that myosin-II can pull on actin fibers, thus generating contractility in the network, and giving rise to cortical tension, a key driver to changes in cell shape like the ones observed during cell migration, cell division or tissue morphogenesis (Chalut and Paluch, 2016; Chugh and Paluch, 2018).

Another important structure formed by actin are the stress fibers, actomyosin bundles which are the major contractile structures within the cells.

Stress fibers are composed by bundles of 10-20 actin filaments, which are crosslinked together by α-actinin and usually anchored to focal adhesions (Tojkander et al., 2012), and hence they are important for mechanotransduction within the cell. At least four types of stress fibers have been identified in mammalian cells; there are dorsal stress fibers, ventral stress fibers, transverse arcs and the most recently identified perinuclear actin caps, which play an important role in the sensing of forces at the level of the nucleus. At the leading edge of migratory cells, we can find lamellipodia, thin, sheet-like membrane protrusion. These structures are generally devoid of organelles and they are instead composed by a dense and highly dynamic network of actin filaments. The force generated by the polymerization of actin filaments, induce membrane protrusion and, thus, the lamellipodia growth (Giannone et al., 2004; Ponti et al., 2004). Moreover, at the free front of the protruding lamellipodium, we can also find thin membrane protrusions, called filopodia. These structures are 60-200 nm in diameter and contain parallel

bundles or 10-30 actin filaments, they are usually oriented towards the protruding membrane of the cell, and their principal role is to sense the surrounding environment (Korobova and Svitkina, 2008). In figure 10 are reported the different types of structures formed by actin within the cell.

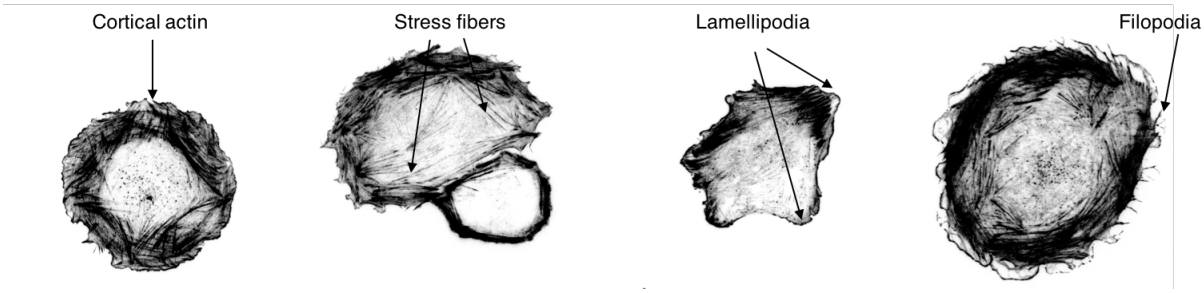


**Figure 10. Different structures that can be formed by actin filaments.**

Representative TIRF images of MEF cells fixed and immunostained for endogenous actin. Different actin structures having different functions are shown. From left to right: cortical actin, stress fibers, lamellipodia and filopodia (Scale bar: 10 μm).

The structure and dynamics of actin cytoskeleton are regulated by a wide number of actin-binding proteins. Among them there are proteins that promote nucleation of new actin filaments (Arp2/3 complex, formins, Cobl, Spire), others involved in its depolymerization (ADF/cofilins, gelsolin). Crucial roles are also played from proteins involved in actin filament elongation like Ena/VASP and Eps8 (Chesarone and Goode, 2009; Ono, 2007).

The second system of cytoskeletal filaments are microtubules: long hollow cylinders that are approximately 25 nm in diameter and vary in length from 200 nm to 25 μm. they are formed by lateral association of around 12-17 protofilaments into a regular helical lattice. Each protofilament consists of repeating units of alpha (α) and beta (β) tubulin heterodimers, all pointed in the same direction. Microtubules are among the stiffest structures founds in animal cells; despite this they are often bent by strong internal cytoskeletal forces and display a resilience to shear and twist. They often serve as tracks for the transport of membrane vesicles

in the cell, carried by the motor proteins kinesin and dynein, but also play an important role in cell shape and polarization (Odde et al., 1999; Pampaloni and Florin, 2008; Sato et al., 1988).

The third and latest cytoskeletal type of filaments are the intermediate filaments (IF), which, as their name suggest, are thicker than actin filaments, but thinner than microtubules. They are 10 nm in diameter and many microns long; they have important role in intracellular organelles positioning and dynamics, and in providing mechanical strength to the cell. IFs lack polarity, they have a high tensile strength and they are resistant to compression, twisting or bending forces. They can interact with plasma membrane especially through desmosomes and hemidesmosomes (Goldman et al., 2012; Kottke et al., 2006).

All of these cytoskeletal elements are structurally distinct and independent, but in order to exert their role properly, they need to interact each other and with the plasma membrane. A typical example of this cooperation is the acto-myosin cortex, which lies directly under the plasma membrane. Changes in cortical tension lead to microtubules and IFs interactions; on the contrary, microtubules polarization allow the loose of the actin polarity and the subsequent formation of focal adhesions and stress fibers (Bershadsky et al., 1996).

The interplay between cytoskeleton and plasma membrane is important for providing adhesion sites to the cell and as a source of signaling molecules that regulate cytoskeleton dynamics and remodeling. In turn, cytoskeleton determine biochemical and biophysical properties of the plasma membrane, such as tension, shape, composition, mobility and recycling of its constituents.

Finally, from the biological point of view, their interplay is a key regulator of several events like cell migration, endo-/exo- cytosis, membrane trafficking, cell-cell or cell-matrix adhesion.

# 6. Exo/Endocytosis and intracellular trafficking

Among the above-mentioned cellular mechanisms, exo- or endocytosis and membrane trafficking are two important examples of membrane-cytoskeleton cross-talk.

Exocytosis is a fusion process, which involves the formation of membrane-bound vesicles containing cellular products, merging with the plasma membrane in order to release the content in the extracellular environment.

The revers process, endocytosis is a well characterized one which involves a wide number of proteins having the role to internalize nutrients and biomolecules and to deliver them to different cellular regions. During this process patches of membrane are invaginated and delivered to specialized organelles, like Golgi or lysosomes, where they are degraded. Several different endocytic pathways have been described in eukaryotic cells: clathrin-independent endocytosis, caveole dependent endocytosis, micropinocytosis, phagocytosis and the clathrin-mediated one (Howes et al., 2010; Mayor and Pagano, 2007).

Clathrin-mediated endocytosis (CME) is a key process in vesicular trafficking that transport a wide range of molecules from the cell surface to the interior of the cell (Kaksonen and Roux, 2018).

Clathrin-mediated internalization is multi-step process which starts with the initiation of the endocytic site, which consists in the formation of a membrane invagination called pit, followed by the cargo recruitment and the subsequent clathrin coat assembly. Clathrin-coated vesicle budding can finally happen in a dynamin-dependent way. Once detached from the parent membrane, the pit is uncoated and recycled back to the plasma membrane for another internalization cycle, while the vesicle content is released for intracellular trafficking events (figure11).

All of these steps, particularly membrane bending and fission, require the participation of both plasma membrane and the actin cytoskeleton, indeed, increase in membrane tension or actin

polymerization impairment lead to inhibition of endocytic uptake and vesicles formation (Kaksonen and Roux, 2018; Kaksonen et al., 2006; McMahon and Boucrot, 2011).

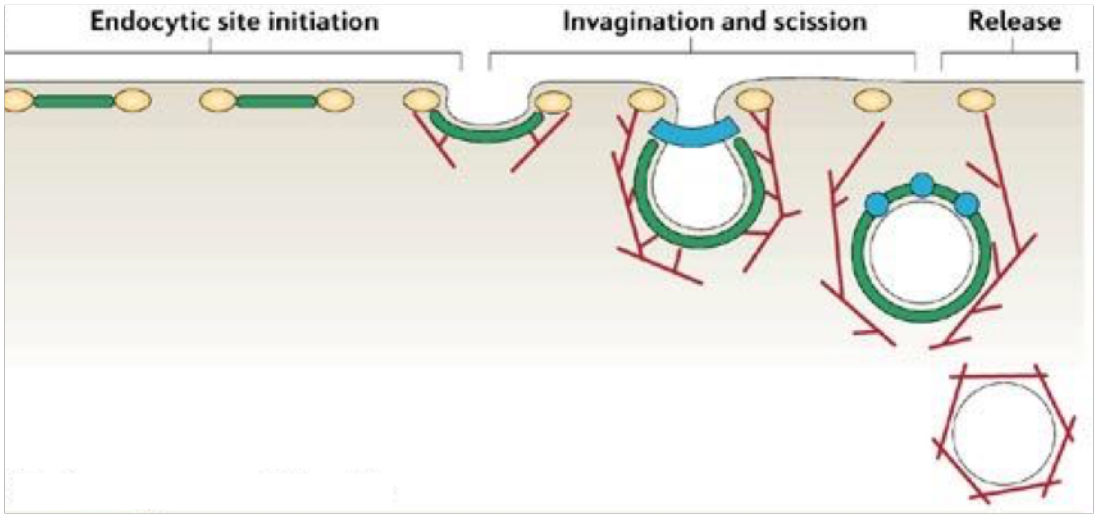


**Figure 11. Schematic representation of the clathrin-mediated endocytosis process.**

Clathrin-mediated internalization is multi-step process which can be divided in: 1) initiation of the endocytic site, consisting in the formation of membrane invaginations called pits, 2) cargo recruitment at the PM level, 3) clathrin coat assembly, consisting in the rectruitment of clathrin from cytosol to PM, 4) clathrin-coated vesicle scission, mediated by dynamin protein and 5) pits uncoating, after which, clathrin machinery its recycled back for another round of vesicle formation. Adapted from Kaksonen et al., 2006.

# 7. The evolution of the plasma membrane fluid-mosaic model and its interaction with actin cytoskeleton

Since 1972 the PM has been described as two-dimensional continuous fluid bilayer of lipids with freely embedded proteins (the fluid-mosaic model) able to move within one plane (Singer and Nicolson, 1972).

Then, it became obvious that the fluid-mosaic model needed to be implemented by including the interaction of extracellular matrix and membrane-associated cytoskeletal proteins, able to influence the distribution and mobility of integral proteins (Andrade et al., 2015; Jacobson et

al., 1995). Recent studies proposed the existence in the plasma membrane of particular microdomains enriched in glycosylphosphatidylinositol (GPI)-anchored proteins, sphingolipids and cholesterol usually called “lipid rafts” (figure 12) (Sezgin et al., 2017).

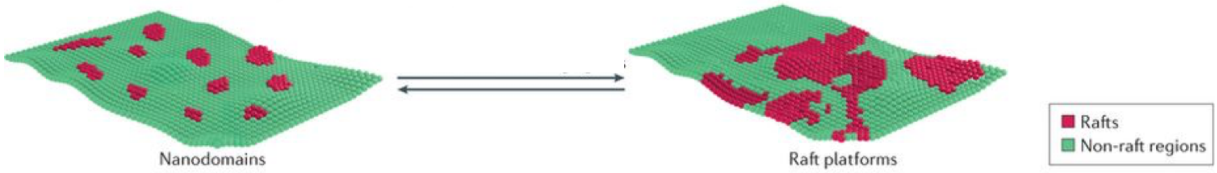


**Figure 12. lipid rafts domains at the plasma membrane.**

Schematic representation of the lipid rafts domain at the plasma membrane levels. Adapted from (Sezgin et al., 2017).

It has been suggested that these domains have important role in a wide range of biological processes, including several signalling transduction pathways, cell adhesion and migration, exo/endocytosis or apoptosis (Munro, 2003; Nicolson, 2014). Not only lipids, but also proteins can laterally segregate along the PM into microdomains that can be stabilized by cholesterol and, to a lesser extent, by actin. Recently, it has been shown that many of these membrane domains components can form nanoclusters at the PM level. These clusters can be driven by remodelling contractile platforms in the inner leaflet that are called “asters”, which are composed by actin filaments and myosin motors (Gowrishankar et al., 2012), able to immobilize PS-containing chains in the inner leaflet, which in turn can interact with elements in the outer leaflet, thus facilitating the formation of such nanoclusters (Raghupathy et al., 2015).

While researchers made a lot of advances in the knowledge of how these nanoclusters are formed, it is still unclear how asters are formed, what triggers myosin activity and how actin binds to PS at the membrane level. A recent study from Satyajit Mayor group, shows how a mechano-chemical cascade regulated by the integrin receptor family, can direct the nanocluster

formation, by RhoA signalling cascade activation, which in turn triggers actin-nucelation (Kalappurakkal et al., 2019).

Overall it has been proposed a cooperative action of a hierarchical three-tiered mesoscale domains organization composed by membrane compartments with a diameter of 40-300 nm, rafts domains on the scale of 2-20 nm of diameter and dynamic protein complex domains which size goes generally from 3 to 10 nm in diameter, which are fundamental for membrane functioning (Kusumi et al., 2012).

# Aim of the project

During last decades, research on cellular membranes and actin skeleton has mainly focused on their composition and organization at nanoscale level, but there is still a gap of knowledge that need to be filled in order to understand the mesoscale organization, dynamics and regulation of this complex network made by PM, acto-myosin cortex and several other elements which role still need to be characterized.

In this context, we focused our attention on spectrin, a protein that, as already described before (see chapter 2. Spectrin: the phantom of the cell), is able to interact both with plasma membrane and actin cytoskeleton and which is known for its mechanoprotective properties in erythrocytes and other kind of cells.

We specifically focused on βII-spectrin, the most abundantly expressed among the β subunits in mammalian nucleated cells (Derbala et al., 2018), which harbours an N-terminal actin binding domain (ABD), that is not present in the α- counterpart.

In order to answer our questions, we applied to the cells different types of mechanical perturbation and followed them through live imaging fluorescence microscopy, providing a comprehensive analysis of spectrin behaviour during cell mechanoresponse. We showed that spectrin is a major dynamic component for shaping the mesoscale-topological organization of the cell cortex during cell- or environmentally-driven mechanical stimuli. Spectrin does so by complementing actin distribution and dynamics over the PM and by cooperating with the actin cytoskeleton in ensuring membrane stability during mechanical challenges, preserving cell integrity. Given this interplay between spectrin, actin and PM, we also proposed spectrin as putative regulator of (CME) and intracellular trafficking, by complementing actin-driven picket-and-fencing mechanism

# Results

## 1. Spectrin and actin define distinct plasma membrane territories in cells of different origins

Spectrin has been largely studied in erythrocytes and in neuronal axons, where it has been shown to adopt different configurations (see chapter 2. Spectrin: the phantom of the cell), while its organization in other cell types is far less accurately depicted.

Here we aimed at describing in detail the spectrin-actin macromolecular organization in mammalian cells by different genetic backgrounds of physiological and pathological relevance. We used mouse embryonic fibroblasts (MEFs) as cellular model, which have been already characterized in the lab for their spreading behaviours, plasma membrane and actin cortex dynamics (Gauthier et al., 2009; Giannone et al., 2004). Moreover, these cells express higher levels of αII- and βII-spectrin, compared to βIII, βIV and βV isoforms, as reported in the qPCR analysis reported in figure 13.

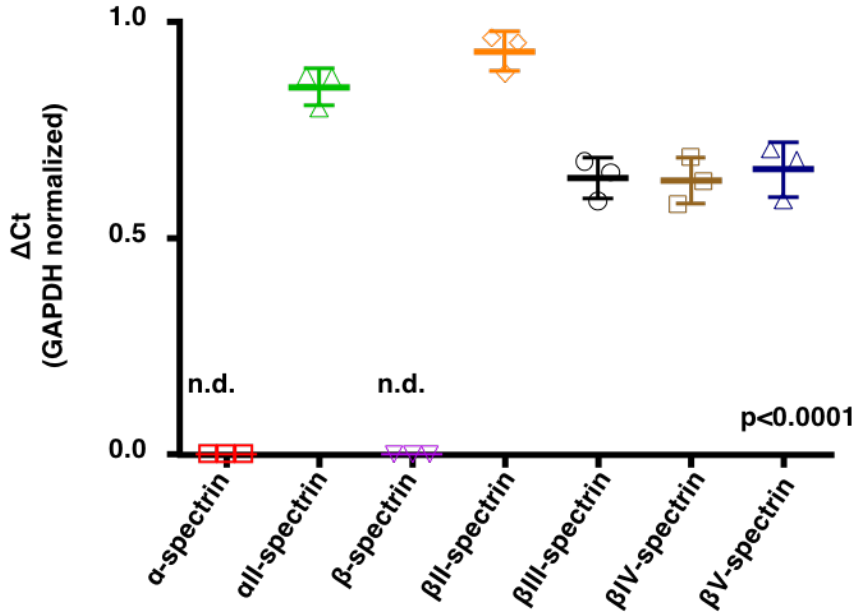


**Figure 13. Spectrins isogenes have different expression levels in MEFs.**

Gene expression analysis of different spectrin isoforms in MEFs used for this study, measured by qPCR (n=3, n.d.=not detected, Statistical analysis: one-way ANOVA with multiple comparison, $p < 0.0001$). The genes sptan1 and sptbn1 encodes for αII and βII spectrin respectively.

We used TIRF (Total Internal Reflection Fluorescence) microscopy for the majority of our experiments since the evanescent wave produced enabled us to observe only a thin region (~ 200 nm) of the specimen, such as structures strictly related to the cellular basal membrane. Indeed, the difference between images acquired with TIRF or EPI fluorescence is evident, since it is possibile to discriminate structures typical of the basal level, such as stress fibers or focal adhesions (TIRF), or of the cell body, like the nucleus (EPI), as shown in figure 14A (left).

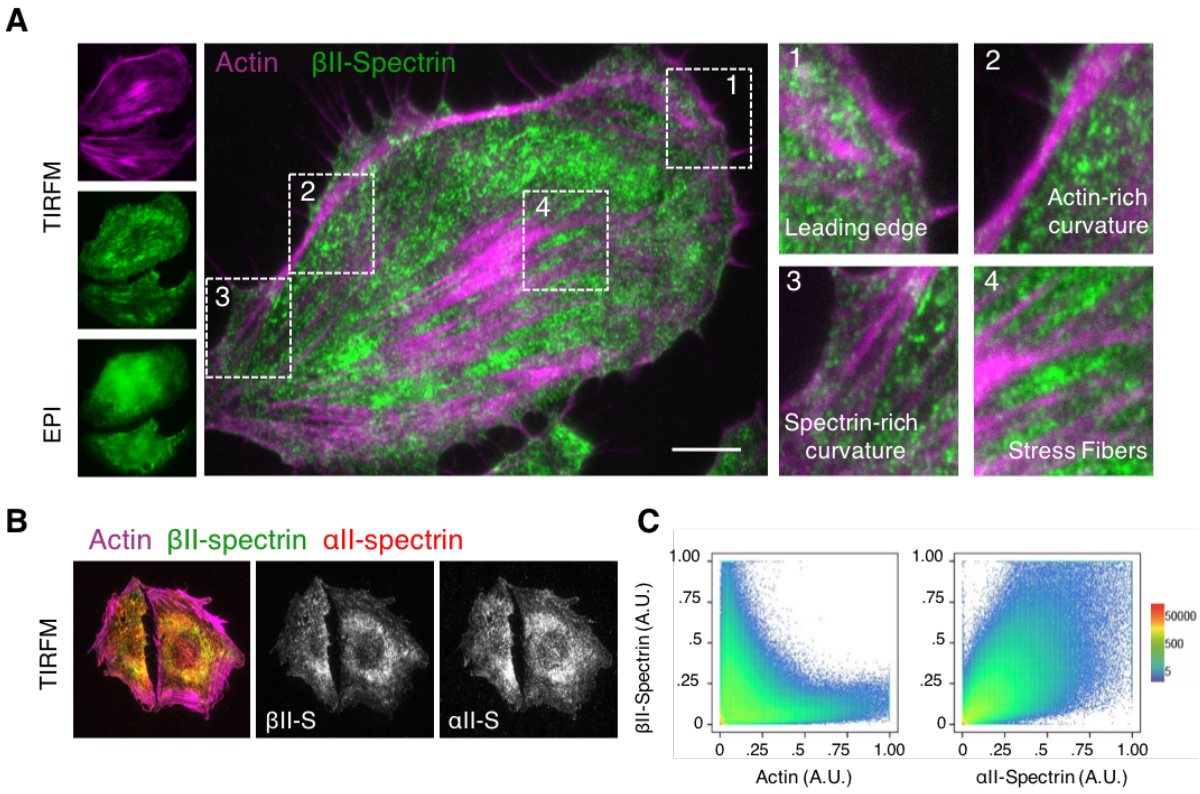


**Figure 14. βII-spectrin and actin define distinct and complementary plasma membrane territories.**

A) MEFs immunostained for endogenous βII-spectrin (green) and F-actin (magenta), observed by simultaneous TIRFM and EPI-fluorescence microscopy (scale bar: 10 μm). Four different cell zones are highlighted (dashed boxes, 1-4), displaying regions by distinct morphological features. B) Representative images of MEFs immunostained for βII-spectrin (green), αII-spectrin (red) and F-actin (magenta), visualized by TIRFM. Correlation analysis of pixel intensities between the different channels are reported in the two scatter plots on the right (C).

Immunolabelling of endogenous βII-spectrin and actin, revealed a peculiar complementary pattern at the cell cortex level between the two proteins; particularly, we observed a βII-spectrin grainy pattern filling the empty spaces left between actin filaments and that was completely excluded from actin-rich leading-edge zones, such as lamellipodia and filopodia, as shown in figure 14 A (middle).

Overall, we identified four different subcellular regions in which this well-defined pattern was conserved and which well represented the complementarity between actin and βII-spectrin: 1) leading edge, 2) actin-rich zones 3) spectrin-rich zones and 4) stress fibers (Figure 14A, right). Interestingly, actin-depleted membrane curvatures, were highly enriched in spectrin and *vice versa,* thus highlighting the interchangeability of the two proteins in supporting the PM regions of otherwise apparent morphological similarity.

Since βII-spectrin is known to form dimers together with its counterpart αII-spectrin, we co-immunostained MEFs for the two endogenous isoforms and actin, thus revealing a perfect colocalization between the two spectrins, whereas they were both completely excluded from the actin enriched zones, as shown in figure 14 B.

Using R studio software, we were able to perform correlation analysis of the pixel intensities within different channels (actin/βII-spectrin and αII-spectrin/βII-spectrin), we then realized two different scatter plots that clearly show the inverted correlation between actin and βII-spectrin, as reported in figure 14 C (left), and a direct correlation between the two spectrin isoforms, as rapresented in figure 14 C (right).

This well-defined arrangement was conserved in many other cell types of both human and murine backgrounds, primary and immortalized, derived from normal or pathological tissues (in table 3 is reported a summary of all the cell lines used for the screening and their characteristics).

| *Tissue* | *Name* | *Type* | *Species* |
|---|---|---|---|
| **Connective** | MEF RPTP | Mouse embryionic fibroblasts | Mouse |
| | MEF-3T3 | Mouse embryionic fibroblasts | Mouse |
| | HS27 | Human foreskin fibroblasts | Human |
| **Epithelial** | RPMI | Skin malignant melanoma | Human |
| | A431 | Epidermal carcinoma | Human |
| | MCF-10A | Normal breast cells | Human |
| | MDA-MB 231 | Breast, adenocarcinoma | Human |
| | HeLa | Cervix, adenocarcinoma | Human |
| | HUVEC | Human umbilical vein endothelial cells | Human |

**Table 3: Summary table of all the cell lines used for βII-spectrin screening.**

Spectrin/actin complementary pattern was conserved in many other cell types of both human and murine backgrounds, primary and immortalized, derived from normal or pathological tissues.

Here, the complementarity between the two proteins was evident when cells were imaged both at the whole-cell level (3D laser scanning confocal microscopy), and at the basal level (TIRFM microscopy), as shown in figure 15 A (white arrows indicating the complementary zones) and in the scatter plots (obtained as described above) reported on the right of each immunofluorescence image. Furthermore, for all the different cell lines characterized, we extrapolated the Pearson's correlation coefficient (r), which was always lower than 1, thus confirming a non-linear correlation between the two proteins (Figure 15 A).

Finally, we tested its ubiquitous expression, even if at different level of expression, as shown in western blot image reported in figure 15 B.

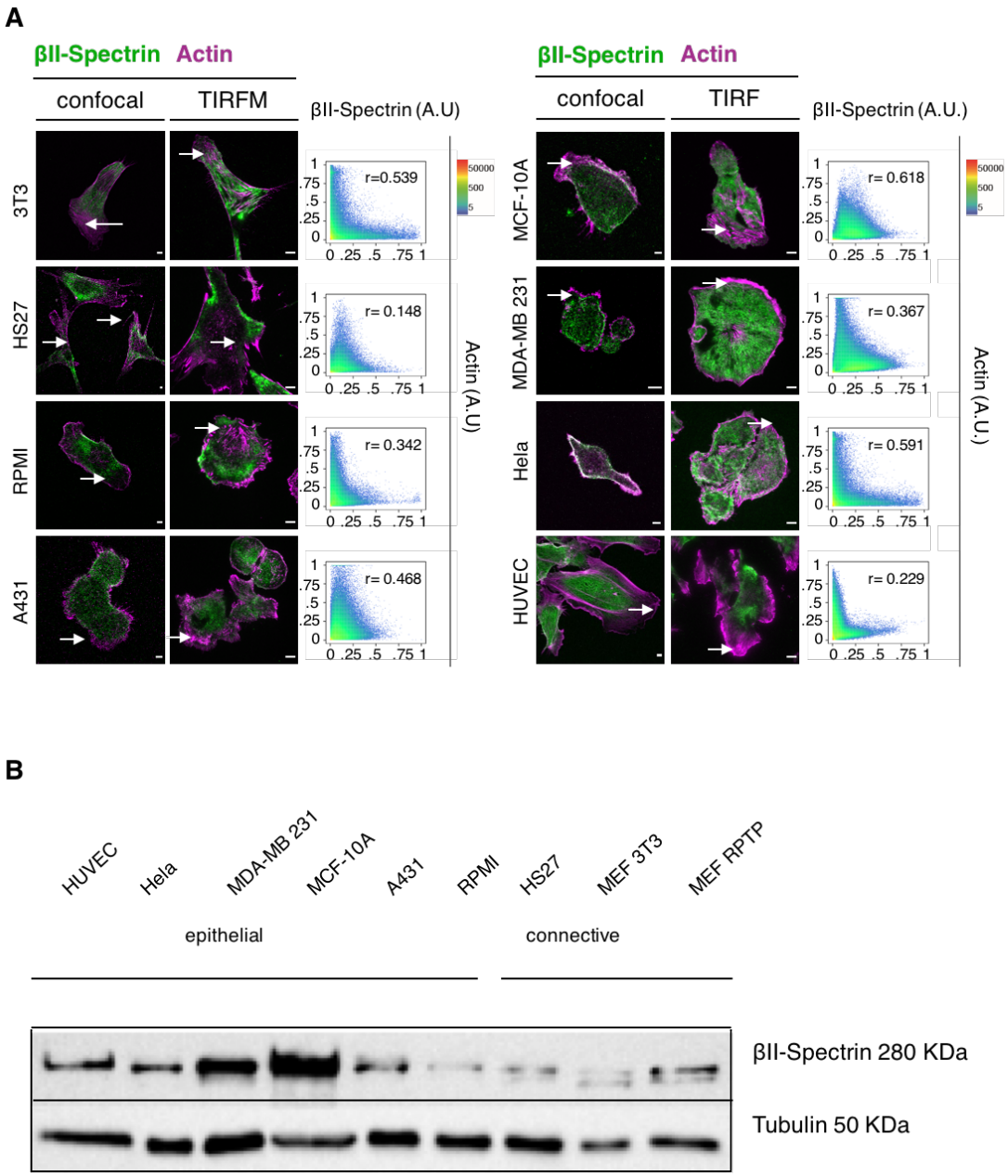


**Figure 15. βII-spectrin and actin complementarity is conserved among different cell lines.**

A) Confocal and TIRFM images of different cell lines immunostained for actin (magenta) and endogenous βII-spectrin (green), arrows indicate peculiar complementary zones (scale bar: 10 µm). Cross-correlation analysis by scatter plot between the two channels and Pearson's correlation coefficients are reported for TIRFM images. B) βII-spectrin protein expression in different cell lines analyzed by western blot in total cell lysates.

However, since the complementary pattern between spectrin and actin that we observed reflected the behaviour of cells seeded on adhesive substrate only, we wondered how was the cortical organization in non-adhesive zones like the apical part of the cell.

In order to answer our question, we applied micro-contact printing techniques to create fibronectin coated lines, on which cells were able to attach, interleaved by non-adhesive substrate, thus mimicking the cell apical cortex and enabling the use of TIRF microscopy resolution over the non-adherent membrane zones.

In those conditions, the exclusion between actin and spectrin was conserved, even in all the four subcellular regions that we identified, particularly at the level of stress fibers and focal adhesions, which were highly enriched in actin, as reported in figure 16 A.

Moreover, by fixing our cells on fibronectin coated micro-patterns, we imposed them different shapes, from non-polarized (circle shape, diameter = 38.4 μm, low number of stress fibers) to an extremely polarized one (crossbow shape, length = 92 μm, high number of stress fibers) and confirmed the absence of spectrin from leading edge zones, as well as the progressive acquisition of complementary pattern at the stress fibers level upon polarization. (Figure 16 B top).

Finally, by transfecting the cells with a GFP tagged βII-spectrin, we were able to observe the same complementary pattern between actin and spectrin, thus, validating the exogenous βII-spectrin construct as a tool for all the investigations that we have performed regarding the dynamic aspects of this exclusion during mechanoresponse (see paragraphs 6 to 10) (figure 16 B, bottom).

Taken together, all these results show the importance of the complementarity between spectrin and actin. Indeed, the enrichment of spectrin in regions where plasma membrane is not covered by actin and vice versa, suggested us distinct but compensatory roles for the two different skeletal meshwork in the mechanical support of the cell membrane.

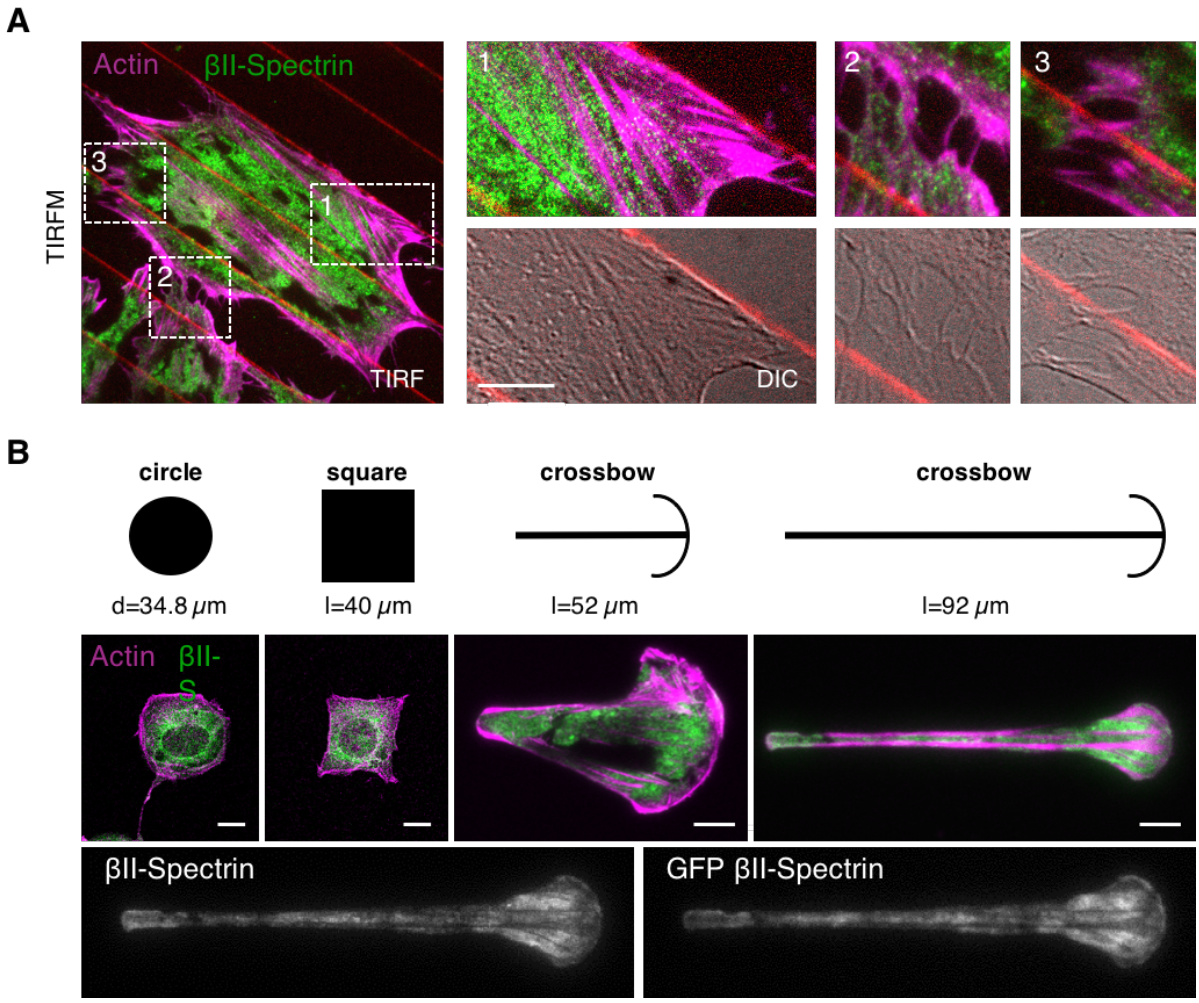


**Figure 16. βII-spectrin and actin complementary pattern is maintained in cells grown under different spatial constrains.**

A) MEFs seeded between adhesive fibronectin lines (red) and non-adhesive substrate (black), are visualized by TIRFM (endogenous βII-spectrin in green and actin in magenta, scale bar: 5 μm). Three different zones are highlighted by the dashed boxes: 1-2) cell adhesions, 3) cell-cell contact. B) Different geometries have been imposed to cells: circle and square (confocal), short and long crossbow (TIRFM). Immunostaining for endogenous βII-spectrin (green) and F-actin (magenta) are shown. Cell on the longer crossbow is transfected for GFP-βII-spectrin, immunostained for both endogenous and GFP-transfected proteins (scale bar: 10 μm).

# 2. Resolving the spectrin ultrastructure with super-resolution microscopy

Once we defined the spectrin meshwork distribution and the formation of territories of complementarity with actin, we wondered if it would have been possible to resolve the ultrastructure of the protein and measure the intramolecular distance in our MEF cells.

In order to do this, we applied stimulated emission depletion (STED) microscopy on our fixed samples.

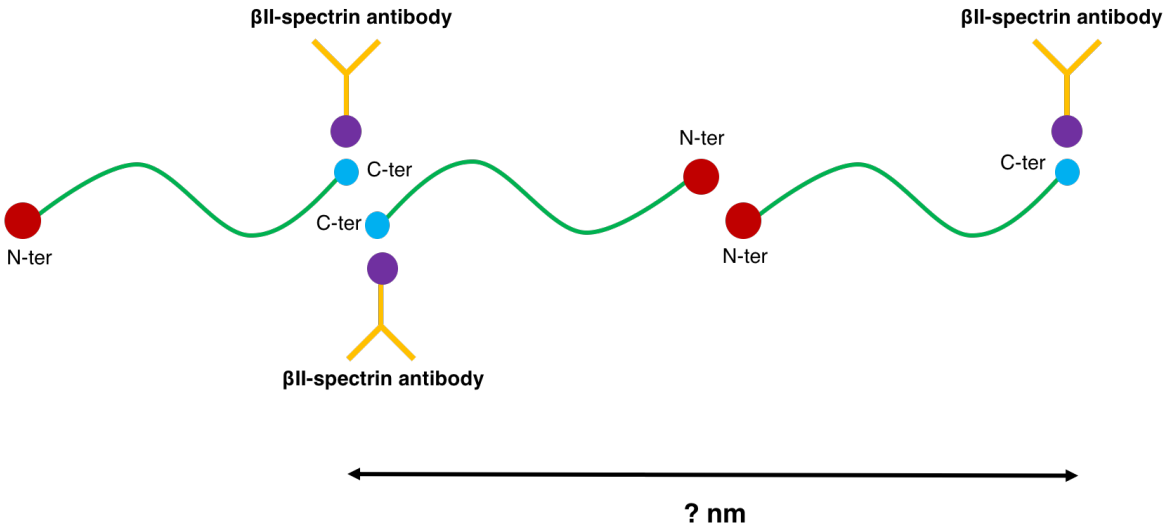


**Figure 17. Schematic representation of the STED experimental design.**

C-terminal regions of βII-spectrin are localized in the inner part of the tetramer while N-terminal regions in the outer one. By using an antibody anti βII-spectrin which was able to recognize the C-terminus of the molecule, we have been able to measure the intramolecular distance of the protein.

STED is a fluorescence microscopy technique that overcomes the diffraction limited resolution of 200 nm of conventional microscopes. The enhanced resolution is essentially based on the switching off the fluorescence of dye molecules by stimulated emission using intense laser light in the outer regions of the diffraction limited excitation focus. This intense radiation causes almost all of the excited molecules to return to the ground state. Fluorescence from the

remaining excited dye molecules in the center of the excitation focus is then detected and used to form the high-resolution images (Hell and Wichmann, 1994).

In order to obtain an even higher resolution, we used the so called "gated STED", by applying a time gate to the images that we collected (Castello et al., 2016).

We fixed our cells and immunostained them with an antibody able to recognize the C-terminus of the βII-spectrin protein, which is positioned in the inner part of the tetramer; in this way, we aimed at measuring the distance between the C-termini of two different spectrins, thus resolving the length of the spectrin molecule, as depicted in the scheme in figure 17.

Before starting with our analysis, we verified the reliability of the microscope, by using a STED multicolour Nanoruler (GATTA quant) containing three emitting points with two fluorophores: ATTO 647-ATTO 594-ATTO 647 and fixed distances between them (140 nm between the two 647 fluorophores and 70 nm between the 594 and the 647 one) as shown in figure 18 A.

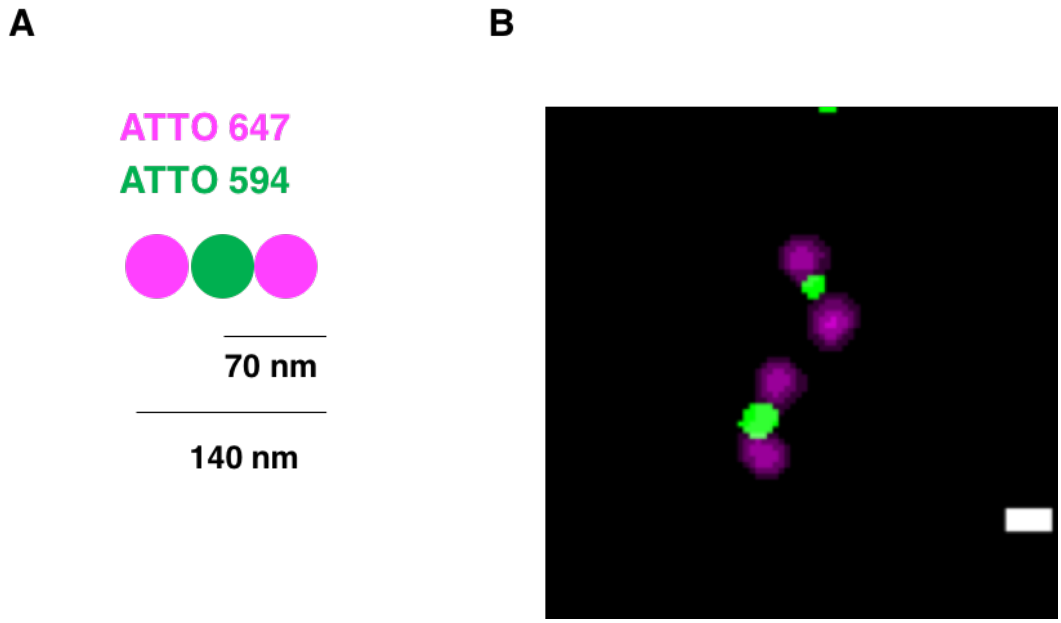


**Figure 18. Calibration of STED system using multicolour Nanoruler.**

A) Schematic representation of the STED Nanoruler used for microscope calibration. Distance between ATTO 647 (magenta) and ATTO 594 (green) fluorophores is 70 nm, while distance between the two ATTO 647 fluorophores is 140 nm. B) Image of STED Nanoruler obtained with our microscope. Scale bar: 50 nm

This enabled us to calibrate our system and to start with our acquisitions and measurements (Figure 18 B).

We firstly acquired images of the entire cell, then chose a restricted area and zoomed in it, and finally, we acquired both confocal and STED images of the selected zone of the cell (figure 19 A).

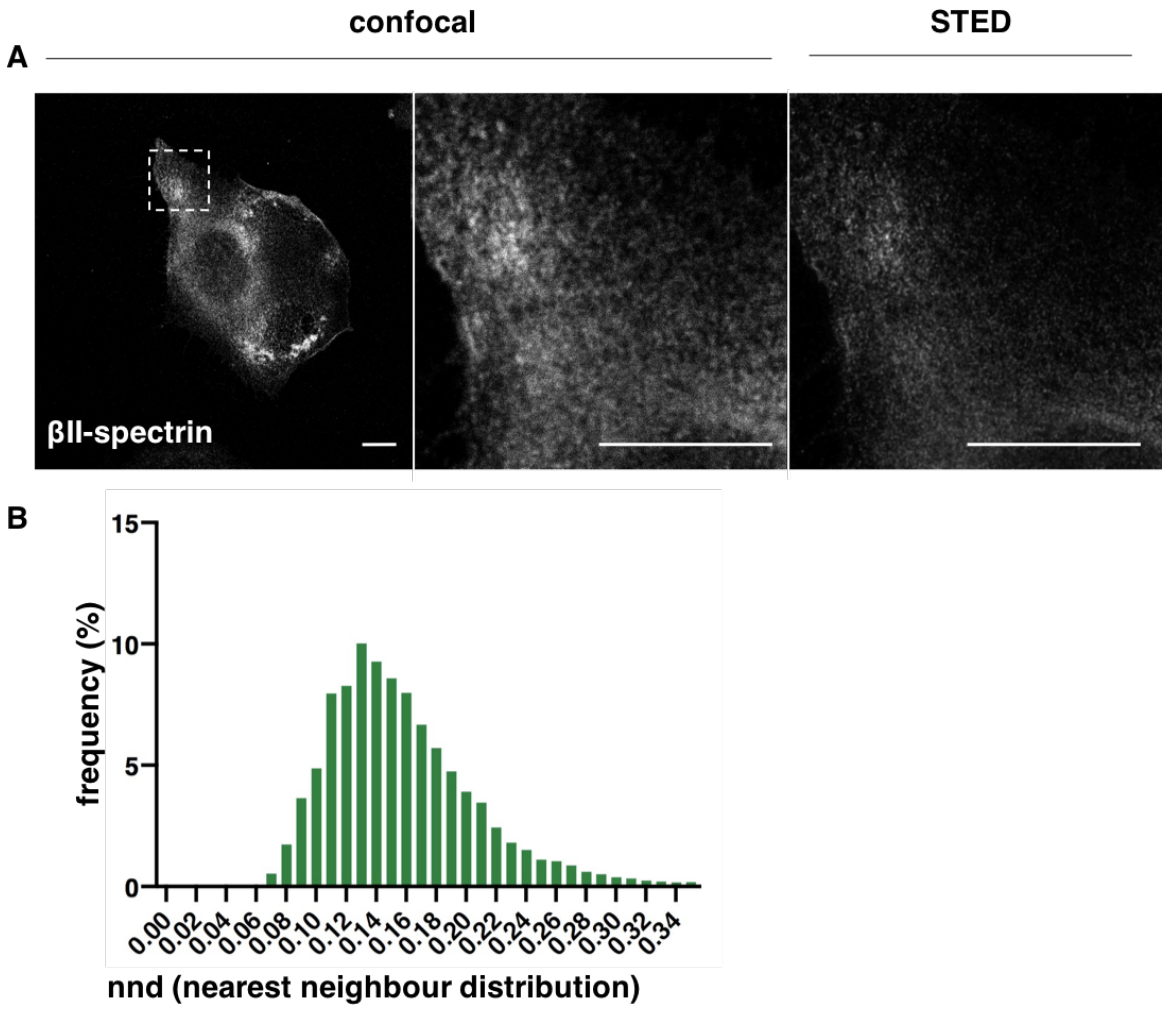


**Figure 19. STED super-resolution microscopy revealed the intramolecular distance of βII-spectrin in MEFs.**

A) MEFs fixed, immunolabelled for endogenous βII-spectrin and analyzed by 3D confocal microscopy (zoom 1X, left, zoom 5X middle), and STED microscopy (same region of confocal image at zoom 5X, right). Scale bar: 10 μm. B) Cumulative frequency distribution plot of the nearest neighbor distribution of βII-spectrin molecules measured from STED images (n= 10 cells, Mean: 0.160 ± 0.065; Median: 0.149).

We performed our analysis by measuring the nearest neighbor distribution (nnd) within each cell, which is defined as the probability distribution of the distance from one point to the nearest or closest neighboring point.

Interestingly, from our analysis, which were performed on 10 different cells, we obtained a cumulative frequency distribution, revealing a peak at 150 nm, as shown in figure 19 B, consistent with the distances described before in literature (see also Introduction section, paragraph 2.2 From electron microscopy to super-resolution: how our knowledge about spectrin has evolved).

By deeply focusing on the images that we obtained, we were able to discriminate different spectrin distributions within the same cell; indeed, some zones seemed to be more enriched in spectrin while others way more less.

We wondered if we could have been able to quantitatively measure such differences, by calculating the nearest neighbor distribution among all the different regions and by comparing them.

We subdivided our images into 2 $\mu m^2$ grids (figure 20 A) and measured the nnd within each of them. We thus obtained multiple distributions, from which we extrapolated the means that were subsequently plotted together as represented in the graph in figure 20 B.

Surprisingly, we didn't observe any significant fluctuation among the different zones, despite the evident differences in spectrin density, as reported in figure 20 A-B. Indeed, we found that apart from those regions where the number of values was too low, the majority of the distributions revealed a nearest neighbor distribution around 150 nm, thus suggesting that spectrin is a continuous meshwork lying underneath the plasma membrane, with a constant intramolecular length. The presence of regions with different spectrin densities, suggested that spectrin in MEF cells is less homogeneous compared to other cellular systems such as erythrocytes or neurons where the structure appear more regular.

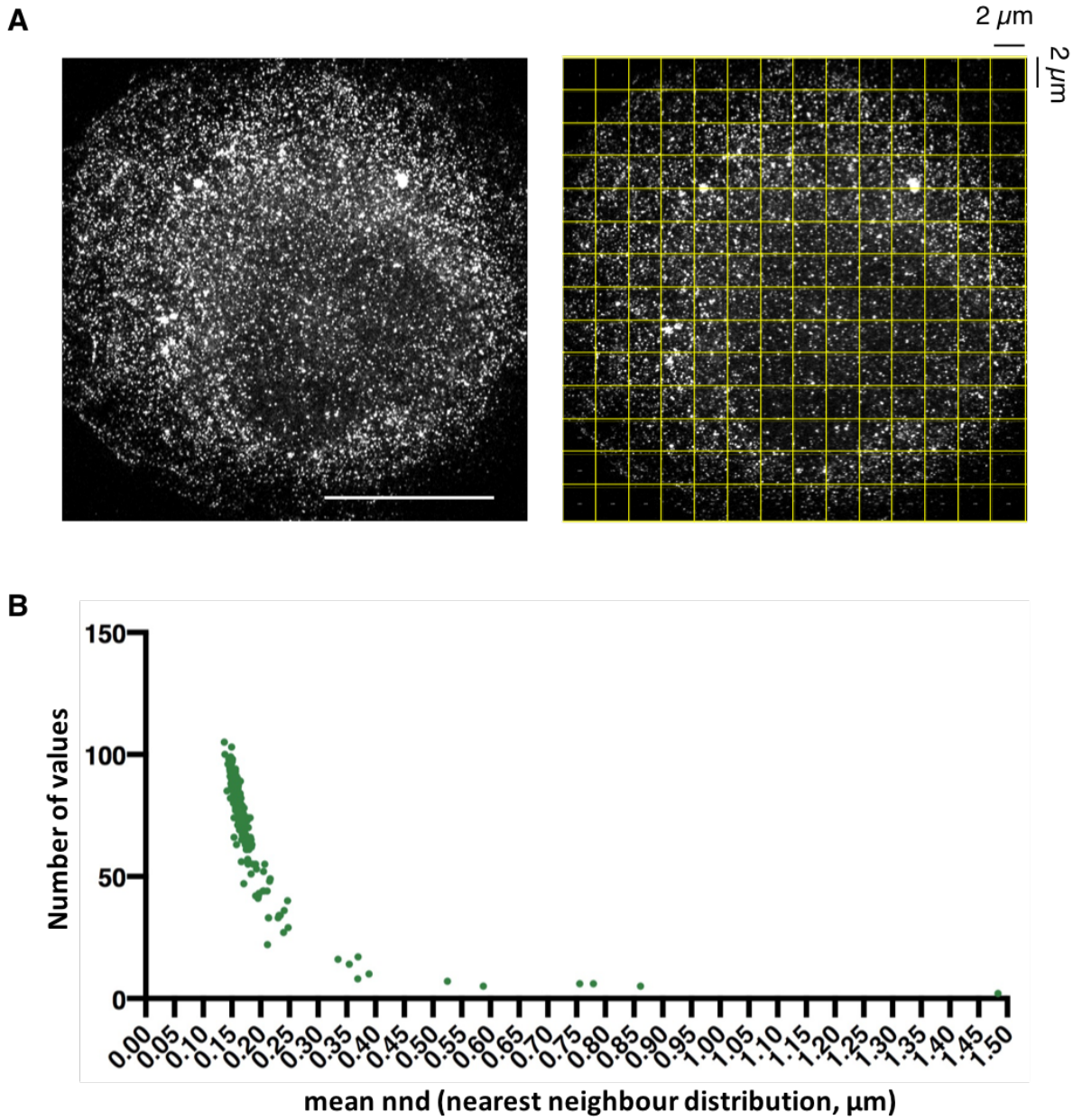


**Figure 20. Spectrin is a continuous meshwork with a constant intramolecular distance.**

A) MEFs fixed, immunolabelled for endogenous βII-spectrin and analyzed by STED microscopy (left), were subdivided into 2 $\mu m^2$ grids (n of grids= 196) (right), scale bar: 10 μm. B) Nearest neighbor distributions were measured for each grid, and the mean of every distribution was plotted in the graph.

We next asked how the two proteins behave during cytoskeleton maturation and cell shape remodelling in living specimens.

# 3. Spectrin and actin form a complementary and dynamic meshwork at the cell edge level during cell shape remodelling events

In order to understand how spectrin skeleton is de-novo assembled and remodelled during cell dynamics, we performed cell spreading assay onto adherent substrate using live-TIRF microscopy. This assay has been widely used in the past to study fast cells shape changes and to monitor cytoskeleton maturation from naïve suspended cells to fully attached and polarized ones.

Cell spreading is a multi-phases process characterized by an initial engagement with the substrate (P0), followed by an isotropic growth of the cell area.

During this phase, known as P1, which lasts few seconds, cells use membrane reservoirs in order to flatten and spread, and an Arp2/3 actin polymerization machinery is activated.

As soon as they have no more reservoirs to use, in order to increase their area, cells undergo a temporary increase of the membrane tension leading to a transition (T) to a contractile phase of spreading, called P2, characterized by local activation of exocytosis, cycles of acto-myosin driven cycles of protrusion-contraction and a final acquisition of focal adhesions and migration polarity, as depicted in the scheme reported in figure 21.

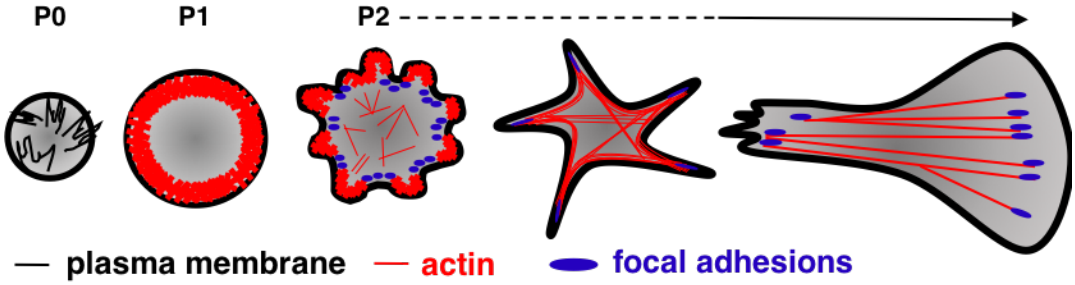


**Figure 21. Spreading assay as a tool for the study of fast shape changes in fibroblasts.**

Schematic representation of the different phases occurring during fibroblasts spreading on fibronectin-coated surfaces. The morphological changes in terms of cell shape, actin cytoskeleton (red), focal adhesions formation (blue) and PM organization (black) are drawn.

Fibroblasts have been already characterized for their spreading characteristics and dynamic behaviours, (Gauthier et al., 2009), and they can be considered now as a model of cell-driven mechanoresponse.

We first fixed our cells at different time points after seeding (5' and 20', in order to increase the chances to find cells in P1 and P2 phases) and immunostained them for endogenous βII-spectrin and actin.

Interestingly, we identified a linear correlation between the amount of endogenous spectrin and the projected cell area in the TIRF plane (p=0.729, n=376 cells), reflecting the ability of spectrin to constantly associates with the PM facing the coverslip (figure 22). Actin instead deviate more significantly from linearity as a result of multi-modal behavior during different spreading phases (p=0.538, n=376 cells), like transition from lamellipodia-driven behavior in P1 to stress fiber during polarization (Iskratsch et al., 2014).

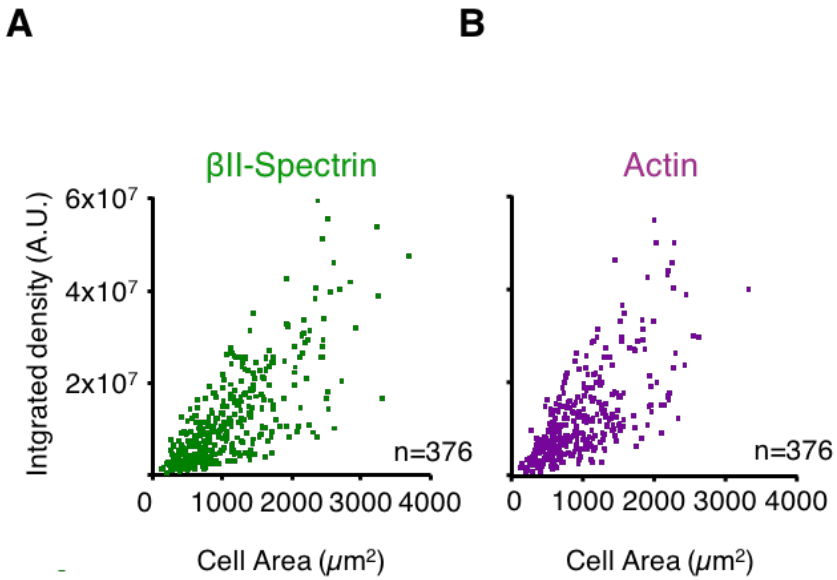


**Figure 22. βII-spectrin and actin fluorescences linearly correlate with the area increase during cell spreading.**

A-B) Cells fixed at different time points after seeding (between 5-20 minutes) and immunolabelled for endogenous βII-spectrin and F-actin. Projected cell area and fluorescence integrated intensities in TIRFM for the two proteins are reported, displaying linear correlation (n=376 cells).

Moreover, we acquired images of cells, both stained for endogenous βII-spectrin and actin or transfected with GFP- βII-spectrin, during P1 phase by 3D scanning confocal microscope, and observed spectrin being organized as a punctate cage-like meshwork around the entire cell body while it was completely excluded from the actin-enriched edge of the cells, in all the two conditions, accordingly with our previous results (figure 23 A-B).

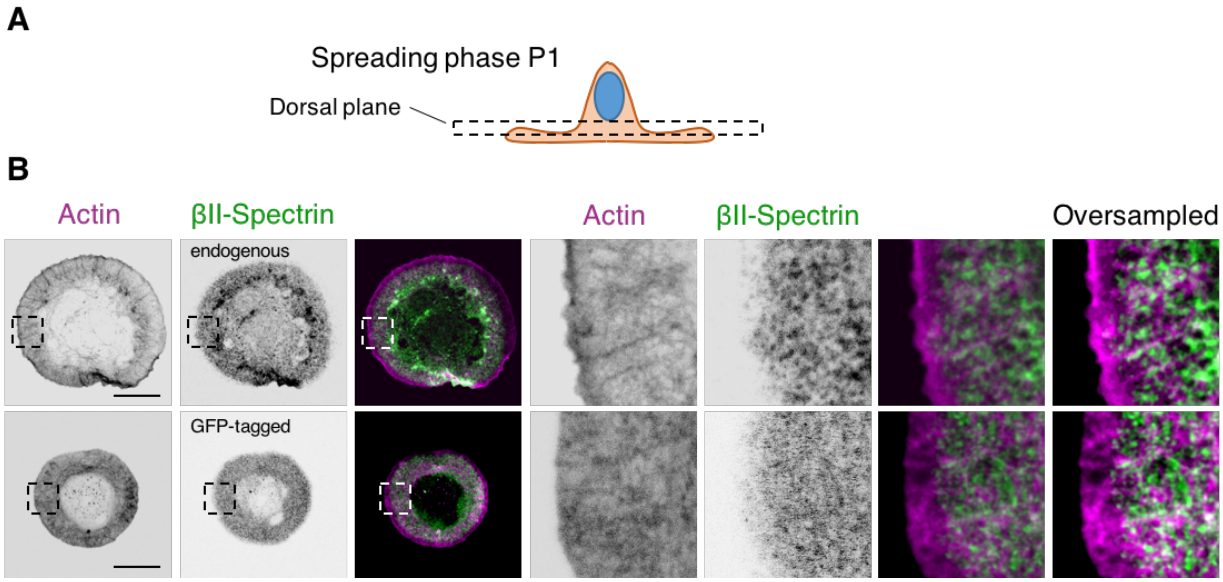


**Figure 23. During P1 spectrin localizes at the cell body while actin at the cell edge level.**

A-B) MEFs fixed during P1, immunolabelled for endogenous F-actin (magenta) and βII-spectrin (green, endogenous and GFP-tagged), and analyzed by 3D confocal microscopy. Optical sectioning is optimized to resolve the cortex on the cell dorsal plane during P1, as shown in the cartoon (scale bar: 20 μm).

We then performed spreading assays on living cells expressing GFP- βII-spectrin and RFP-actin, after seeding them directly at TIRF microscope.

During all spreading phases, we could observe an interplay between the two cytoskeletal structures, since actin engaged into protrusive lamellipodia that promoted cell area growth, and spectrin was enriched, again, at the cell body level and in retracting plasma membrane patches, showing a passive-like behaviour, thus suggesting opposite but compensatory roles in supporting PM during continuous shape remodelling (Figure 24 A).

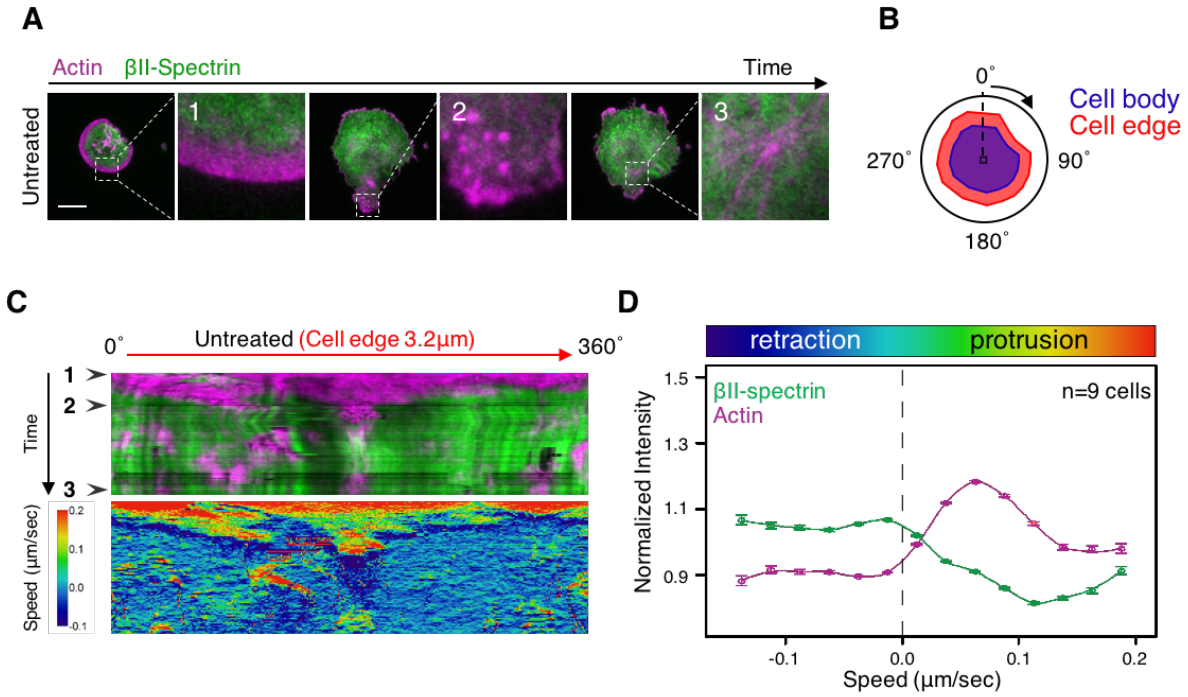


**Figure 24. Spectrin and actin display opposite behaviours during cell spreading.**

A) Cells are visualized by live TIRFM and representative images at relevant time points are shown (green: GFP-βII-spectrin, magenta: RFP-actin, scale bar: 20 µm). Peculiar mechanisms are highlighted by white dashed boxes and zoomed in panels 1-3. In 1 is shown a typical non-contractile phase (P1), while the contractile phase (P2) is shown in 2. In 3, coalescent actin nodes contribute to the maturation of the actin cytoskeleton. B) Schematic representation of the radial segmentation of the cell edge (red, 3.2 µm thickness) and cell body (blue) performed during the time lapse. C) Radial kymograph analysis of cell edge behavior is presented. The upper kymographs represent the integrated intensities of the two proteins (1-3 black arrowheads indicate the specific frames highlighted in the B panel), while the bottom kymographs display the edge speed related to the cell centroid. In D signal intensities are plotted (actin: magenta and βII-spectrin: green) in function of speed (n=9 cells, mean±SEM).

To specifically address the consistence and relevance of our observations during constant cell shape remodelling that occurred during spreading, we developed a software to analyse the protein content at the level of cell edge over the time of the recorded movie, as shown in the schematic representation reported in figure 24 B. We then generated a radial kymograph representing the entire cell circumference of the thickness of 3.2 µm, showing an evident exclusion between the two protein intensities over the entire cell edge and during all the time

of the spreading (Figure 24 C, top). Moreover, by using the same software, we obtained a second kymograph showing the relative speed of the cells at the edge level (Figure 24 C, bottom), and we were able to extrapolate their local speed, as shown in figure 24 D where positive speed correlated with protrusion and negative speed with retractions.

In accordance with the data obtained with fixed samples, actin and spectrin fluorescence intensities displayed opposite trends. Indeed, actin intensity peaked at a speed range consistent with protruding lamellipodia (≈0.08-0.12 μm/sec), decreased slightly at highly positive speeds (>0.15 μm/sec) and dereased more significantly from null to highly negative speeds. These actin dynamics have been previously reported and are consistent with the concept that in fast protruding lamellipodia dilution of the amount of monomeric pool reduces the effective actin tread-milling rate (Mueller et al., 2017; Ryan et al., 2012). Spectrin dynamics, on the other hand, display an opposite behavior suggesting that it might act as a protective meshwork for the PM, alternative to the actin cytoskeleton.

Notably, these opposite and complementary dynamics of the actin and spectrin cytoskeletons were observed in several independent cells (n=9), when cells underwent cycles of protrusions and retractions. For this reason, we wondered if contractility inhibition upon treatment with Blebbistatin, a drug known for its ability to block myosin-II activity, could have effect on actin and spectrin distribution within the cell.

We performed spreading assays, as we did for untreated cells and described above, using live-TIRFM and recorded them.

Interestingly, while during P1 phase cells seemed to spread in a normal way, after the transition (T), they were stuck in P2 and we couldn’t appreciate anymore the presence of lamellipodial protrusions, spectrin-enriched retractions, or the actin stress-fibers formation. Nevertheless, the complementarity between spectrin and actin was still detectable at the cell edge level, as shown in Figure 25 A.

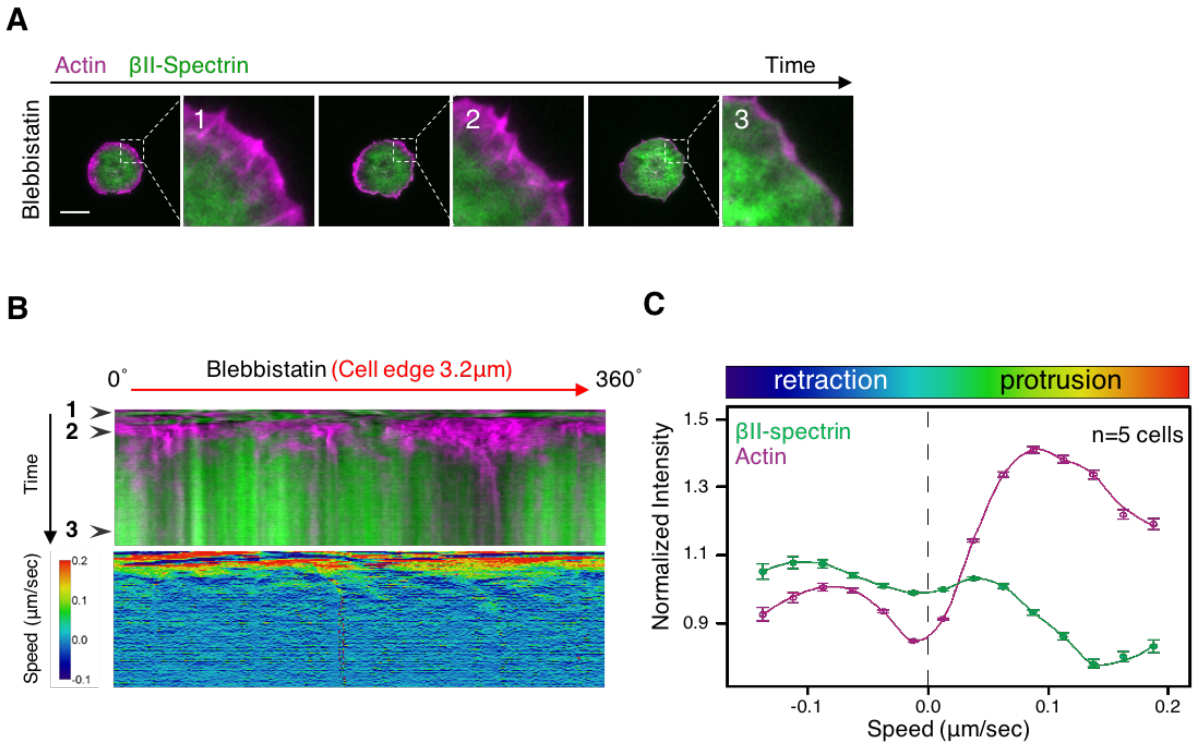


**Figure 25. Myosin inhibition upon blebbistatin treatment impairs cell spreading.**

A) Cells treated with blebbistatin are visualized by live TIRFM and representative images at relevant time points are shown (green: GFP-βII-spectrin, magenta: RFP-actin, scale bar: 20 µm). Peculiar mechanisms are highlighted by white dashed boxes and zoomed in panels 1-3. In 1 is shown a typical non-contractile phase (P1), while the contractile phase (P2) is shown in 2; in absence of myosin II-dependent contractility (blebbistatin) cell spreading is stalled. In 3, blebbistatin treatment impairs these dynamic processes. B) Radial kymograph analysis of cell edge behavior is presented. The upper kymographs represent the integrated intensities of the two proteins (1-3 black arrowheads indicate the specific frames highlighted in the B panel), while the bottom kymographs display the edge speed related to the cell centroid. C) Signal intensities are plotted (actin: magenta and βII-spectrin: green) in function of speed (n=5 cells, mean±SEM).

We then realized a radial kymograph in the same way as described above (Figure 24 B), and obtained the integrated densities related one, showing the inability of the cell to protrude and contract, and the complementarity between actin and spectrin at the level of the cell periphery, (Figure 25 B, top). We also generated the relative speed kymograph (Figure 25 B, bottom), from which we extrapolated the local speed of the cell edge; actin fluorescence intensity peaked,

as expected, at positive speed (≈0.08-0.1 μm/sec) and decreased at higher speed levels (> 0.12 μm/sec), for the same reasons described before, while we couldn't observe any increase in spectrin fluorescence when the speed was negative, confirming that the cell was not undergoing cycles of retraction and protrusion, as consequence of Blebbistatin treatment (figure 25 C).

Altogether these quantitative observations highlight the dynamicity of actin/spectrin complementarity at the cell leading edge during cell shape remodeling events, supporting spectrin role during cellular mechanoadaptation and providing new insight into the counteractivity of the two components.

# 4. Actin nodes as drivers of spectrin organization

Since all the previous observations were performed at the cell edge, we wondered how spectrin and actin were interacting at the cell body level.

By deeply focusing on the previously described spreading assays, we could appreciate a spectrin passive behaviour in following actin-driven cell edge growth during P1. By contrast, during P2, we observed a dramatic remodeling, characterized by cycles of expansion-condensation of the spectrin meshwork localized under the cell body. At the same time, we could also see an increase of actin dynamics, characterized by the formation of actin nodes and their subsequent expansion-contraction, leading to the growth of stress fibers.

By combining actin and spectrin motility by flow analysis, we observed that spectrin, even if never colocalized with actin, moved towards the new synthetized actin nodes, expanding or condensing, depending on their motion, as shown in figure 26 A, B.

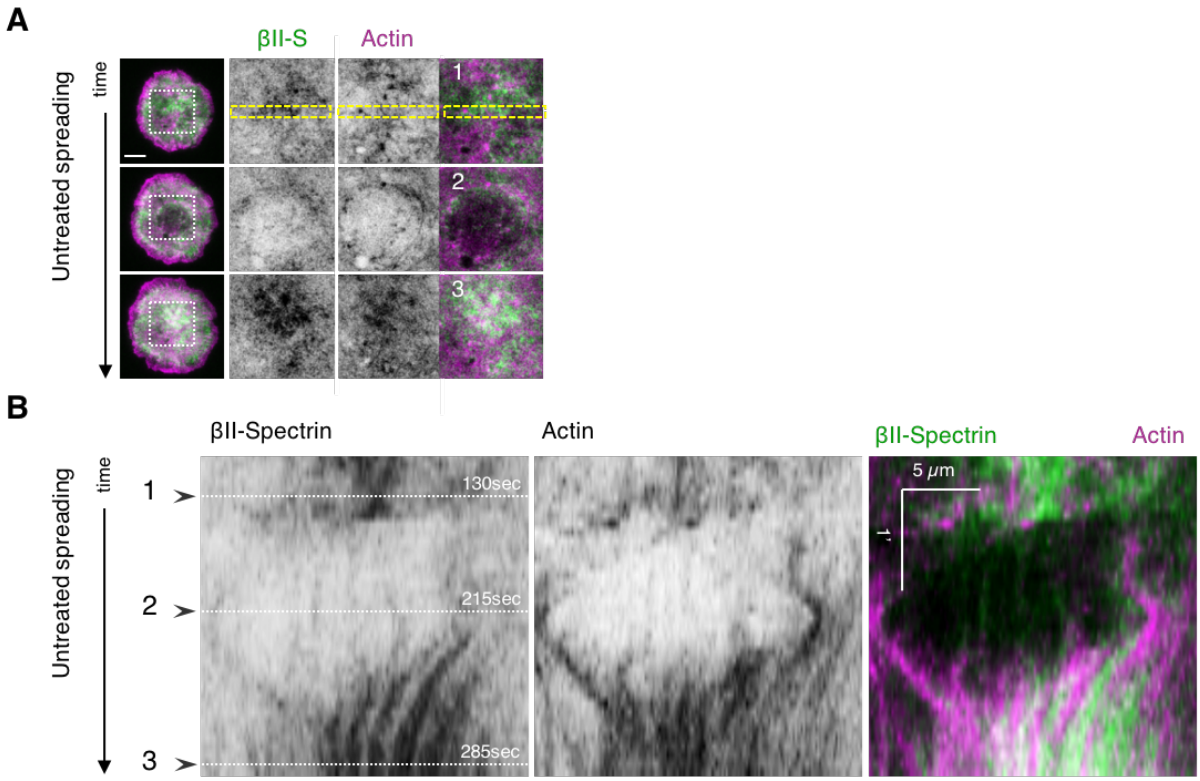


**Figure 26. Spectrin meshwork moves towards new synthetized actin nodes during untreated cell spreading.**

A) Cell spreading analysis at the cell body (zooms corresponding to the dashed white boxes), displayed by live TIRFM images (green: GFP-βII-spectrin, magenta: RFP-actin, Scale bar: 10 μm). Relevant events observed between independent experiments are shown (1-3), displaying endogenous actin nodes formation and correspondent βII-spectrin behavior. B) Kymograph generated in the region highlighted by dashed yellow rectangle. Synchronous condensation and expansion of the two proteins is highlighted by the coordinated side motion in the kymograph, despite the evident absence of colocalization, black arrowheads (1-3) indicate the respective images shown in panel A. Analysis were performed by Marc Antoine Fardin (Institute Jaques Monod, Paris, France).

As already shown, in figure 25, upon myosin-II inhibition after Blebbistatin treatment, such cell body remodeling was completely blocked, whereas actin and spectrin dualism at the cell edge remained unaffected.

To better visualize and quantify these orchestrated motions, we performed correlated particle image velocimetry (PIV) analysis of actin and spectrin flows and extracted integrated cross-correlation values of speed and directionality. The remodeling of the spectrin meshwork organization invariably occurred in correspondence of the formation of mobile actin nodes and resulted in a speed of 22.9±10.4 nm/sec (mean±sem) for spectrin and 33.8±7.8 nm/sec for actin (figure 27 A B).

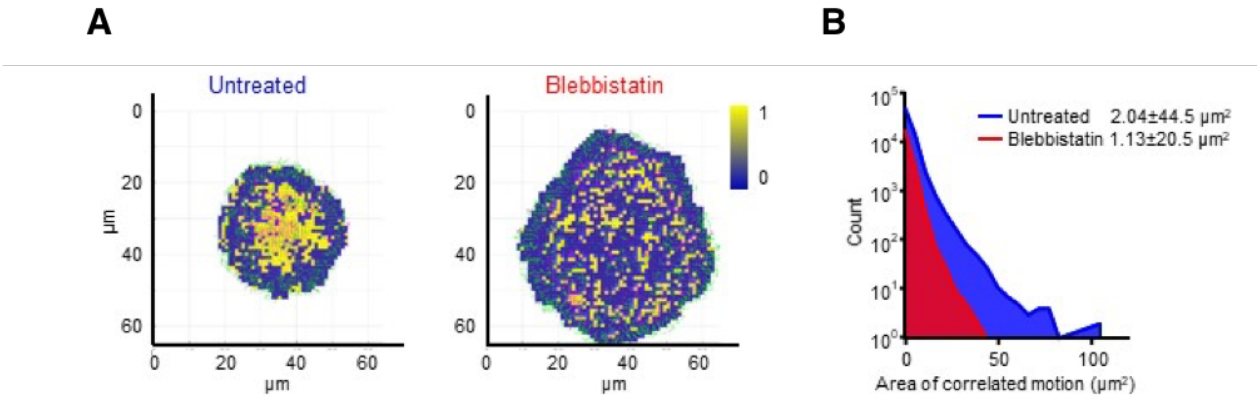


**Figure 27. Spectrin and actin flows cross correlates in terms of speed and directionality.**

A) Two representative images of correlated PIV analyses are shown for the two experimental conditions: cells untreated and treated with 50µM blebbistatin. In yellow are shown areas of high angular and speed correlation between the two proteins, βII-spectrin and actin. Otherwise no correlation is shown in the blue zones (binary LUT). B) Total distribution of "Area of correlated motion" (yellow patches) is shown in the final graph: as predicted untreated cells (blue, n=7 cells) have higher mean area and larger distribution (±SD) compared to blebbistatin-treated cells (red, n=5 cells). Analysis were performed by Marc Antoine Fardin (Institute Jaques Monod, Paris, France).

In order to confirm the role of acto-myosin cytoskeleton in regulating spectrin meshwork organization, we performed drugs-washout experiments during live-TIRFM acquisition.

We treated GFP-βII-spectrin and RFP-actin expressing cells with Latrunculin A and Blebbistatin, drugs that are known for their ability to impair cytoskeleton structure, through actin polymerization and myosin-II activity inhibition respectively, and we monitored actin,

myosin light chain and the relative spectrin dynamics before, during and after drugs administration.

Consistent with our previous observations during cell spreading, we observed an expected spectrin decondensation and redistribution upon acto-myosin stress fibers disruption, as well as a reinforcement at the leading edge level upon cell retraction.

Interestingly, after drugs-washout, cytoskeletal architecture was restored and it was accompained by the formation of new acto-myosin nodes able to drive again spectrin local motion, as reported in figure 28 A-B.

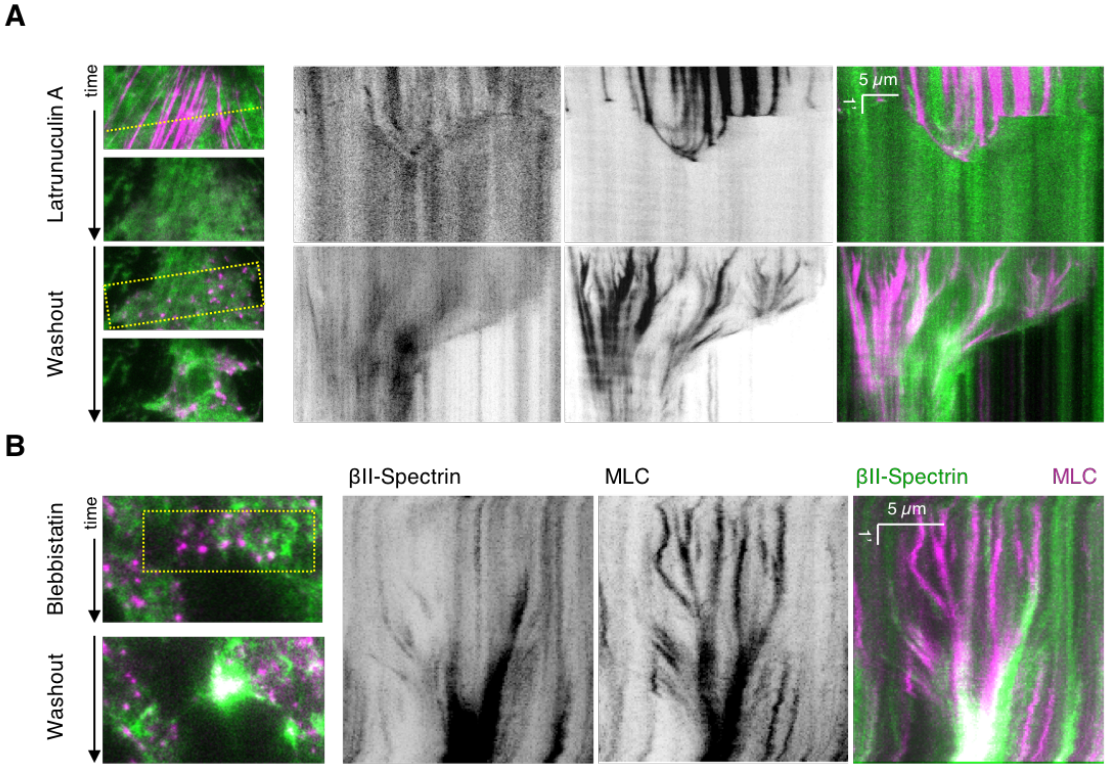


**Figure 28. Spectrin meshwork locally decondenses and redistributes upon acto-myosin fibers disruption.**

A) Representative images during Latrunculin A and subsequent washout experiment visualized by live TIRFM (green: GFP-βII-spectrin, magenta: RFP-actin). Kymographs are generated in correspondence of dashed yellow line and rectangle respectively (scale and time bars are shown). B) The same experimental protocol is repeated with the drug blebbistatin and representative images are shown (green: GFP-βII-spectrin, magenta: RFP-myosin light chain). Kymograph generated in correspondence of dashed yellow box. Similar to endogenous actin nodes formation during spreading, coordinated motion is observed during the drug and washout treatments between the two channels, in absence of colocalization (time scale and scale bar are reported in the kymographs).

Overall, we concluded that the spectrin cytoskeleton is a continuous meshwork tightly associated with the PM, covering it almost entirely. However, its local density under the PM can largely fluctuate upon changes in cell geometry, dynamics and mechanics. Spectrin locally condenses during events characterized by low actin-PM interaction, such as during membrane retraction at cell edges or the remodeling of cortical acto-myosin nodes that leads to the formations of actin fibers, fencing spectrin-rich territories.

# 5. Spectrin molecular turnover depend on contractility

Given our previous observations, we asked if contractility might have been the driver of spectrin dynamics, and we deeply focused on the potential role of the acto-myosin cytoskeleton in the membrane associated spectrin meshwork maturation.

Since spectrin has been shown to build bridges with both actin cytoskeleton and the PM, and to interact with different motors (Holleran et al., 2001; Smith et al., 2018; Takeda et al., 2000), we wondered if its mobility could be dependent on these bonds or, alternatively, on PM-mediated diffusing capabilities through the lipid bilayer.

In order to understand which could be the driving mechanism of spectrin meshwork maturation and dynamics, we started with the investigation of the acto-myosin cytoskeleton, which represented the best candidate for this role.

Cells expressing GFP-βII-spectrin and RFP-actin were treated with actin-impairing drug Latrunculin A and myosin-II inhibitor Blebbistatin, and observed through live-TIRF microscopy. Surprisingly, we couldn't observe any consistent alteration of the meshwork in terms of fluorescence intensity, during the entire experiment (Figure 29 A, B, top).

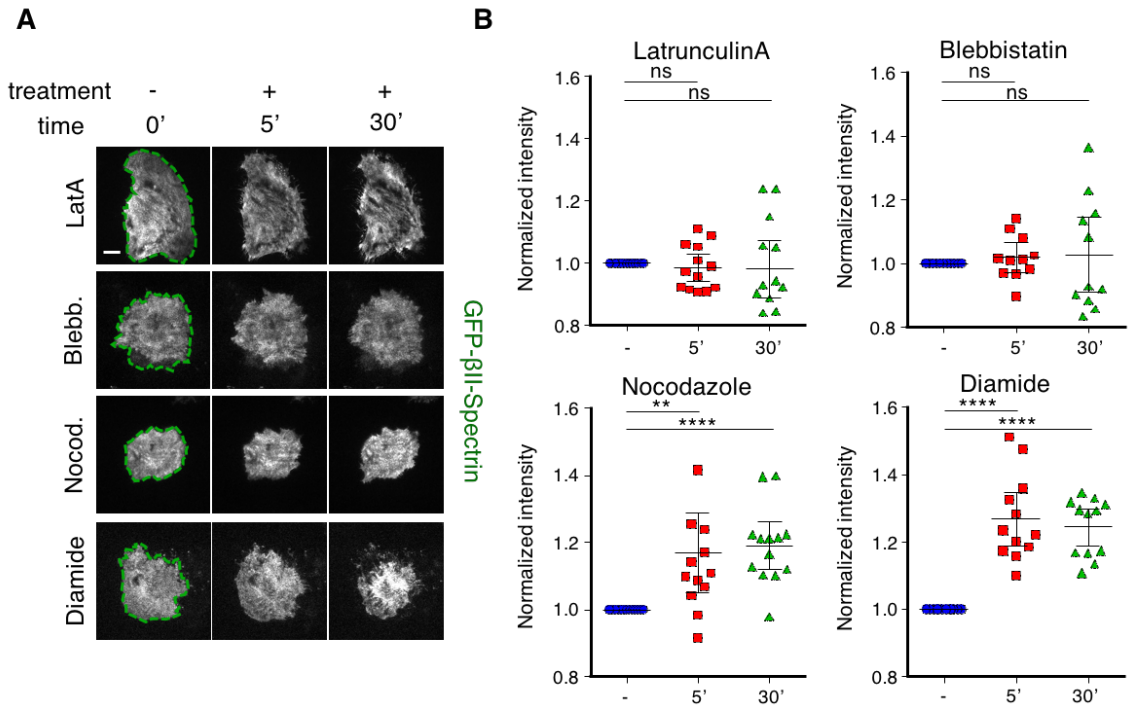


**Figure 29. βII-spectrin reacts differently upon treatments with different drugs.**

A) GFP-βII-spectrin expressing MEFs imaged by live TIRFM during administration of cytoskeletal impairing drugs are shown before (-) and during (+) the treatments (scale bar: 20 μm). Whole-cell mean fluorescence intensities are normalized to the pre-treatment frames (blue circles), and plotted in B at 5 minutes (red square) and 30 minutes (green triangle) of treatment (n=12 cells, mean±SD, paired T-test: ****p<0.0001, **p<0.01).

We indentified two possible explanations: i) the dynamics observed during spreading act locally but fail to organize the meshwork once cell architecture is established, or ii) meshwork dynamics rely on multiple and complex mechanisms that involve also other components like the PM or the microtubule (MT) cytoskeleton.

We performed the same analysis on GFP-βII-spectrin and RFP-actin expressing cells treated with the microtubule impairing drug Nocodazole and the reported spectrin/PM oxidative crosslinker Diamide (Deuticke et al., 1983). Mean fluorescence intensity displayed significant increase already five minutes after those treatments, and this was due to different mechanisms: while the cross-linking compound Diamide strongly affected the cell morphology at the tested concentration, nocodazole-dependent increase in spectrin intensity was not characterized by

cell shape changes, but, actually, by a block of the PM dynamics, as reported in figure 29 A, B (bottom).

In order to quantitatively investigate spectrin meshwork dynamics during the response to the treatments, we performed Fluorescence Recovery After Photobleaching (FRAP) analysis on cells overexpressing GFP-βII-spectrin before and 5 minutes after the drugs injection, as depicted in the schematic representation in figure 30 A, in order to avoid secondary effects due to cytoskeletal perturbations.

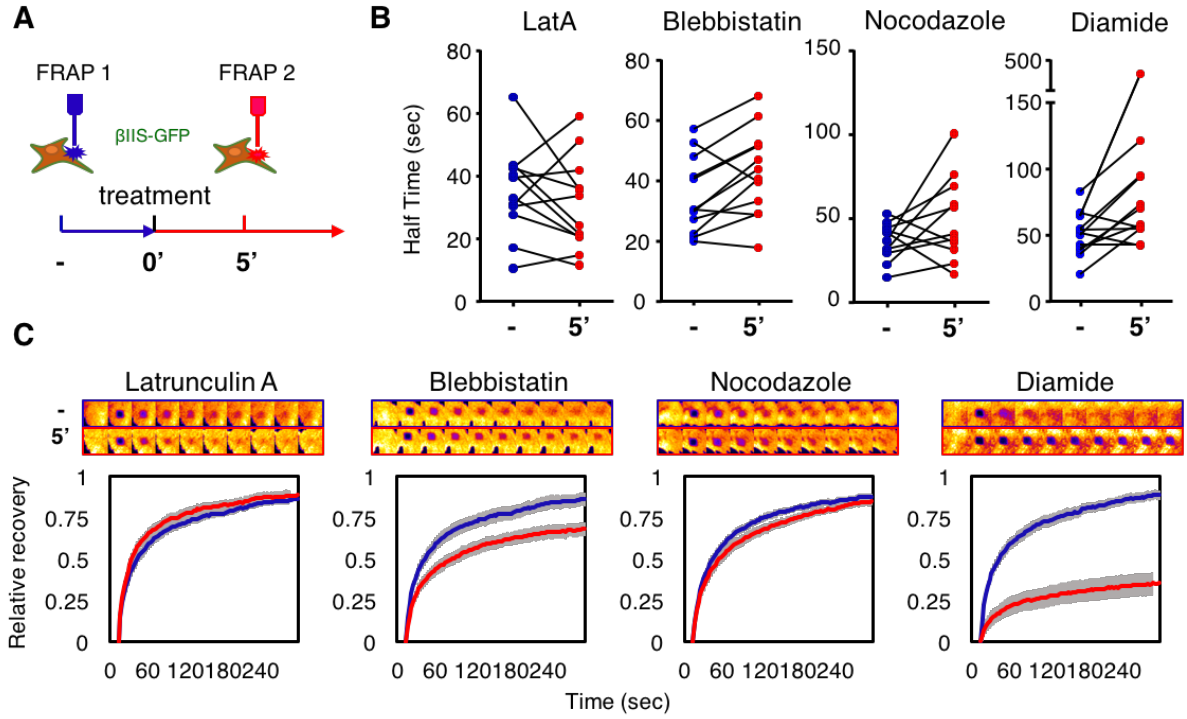


**Figure 30. βII-spectrin turnover relies on myosin-II-dependent contractility.**

A) Schematic representation of the dual-FRAP assay of GFP-βII-spectrin expressing MEFs, performed before (blue) and after 5 minutes treatment (red). The resulting half-time recoveries are presented in B (each individual cell connected by the black lines). Half-time recoveries from the single exponential fitting: latrunculin A treatment from 34.9 (-) to 27.2 (5') seconds, blebbistatin from 34.5 to 40.1 seconds, nocodazole from 35.4 to 46.1 seconds and diamide from 38.4 to 48.2 seconds. C) Recovery curves are plotted (n=12-20 cells, mean ±SEM), while the top inlets show representative ROIs during the recovery phase. Mobile fractions (%) are derived from the curves: during latrunculin A treatment increased from 82.9% to 85.3%, blebbistatin decreased from 83.7% to 66.7%, nocodazole decreased from 85.1% to 82.6% and diamide treatment decreased from 85.6% (-) to 34.5% (mean±SEM are presented in FRAP graphs to visualize the accuracy of the means subjected to the fitting

procedure. See supplemental information for fitting parameters). Experiment and analysis were performed by Andrea Ghisleni (IFOM, Milan).

Although spectrin is able to interact with actin filaments, stress fibers tournover impairment by Latrunculin A treatment, didn't affect its half time recovery ($t_{1/2}$ control= 34.86 sec, $t_{1/2}$ treated= 27.24 sec) within the cell, neither significant variations in the mobile fraction were detected (control=83%, treated= 85%). Taken into account the controversial working mechanism of latrunculin A on small and rigid actin protofilaments (Brieher, 2013), we concluded that, at the molecular level, the spectrin skeleton does not rely on actin fibers turn-over for its physiological dynamics.

Interestingly, myosin-II inhibition through Blebbistatin treatment caused severe reduction in the mobile fraction (82% of control versus 66% of treated cells) and a significant increase in the half-time recovery in 9 cells out of 12 that we tested ($t_{1/2}$ control= 34.51 sec, $t_{1/2}$ treated= 40.83 sec). Together, these results showed us that spectrin requires myosin-II contractility for its dynamic behavior.

During Nocodazole treatment, 8 out of 12 cells displayed slower half-time recovery ($t_{1/2}$ control= 35.36 sec, $t_{1/2}$ treated= 46.08 sec), while the protein mobile fraction was not affected over the time frame of the experiment (85% of control and 83% of treated cells). Indeed, the signal increase observed before might be due to nocodazole secondary effect of increasing contractility (Krendel et al., 1999) in the short term, while the MT-dependent redistribution of spectrin and associated proteins observed in epithelial cells might require long-term adaptation mechanisms (Jenkins et al., 2015). Finally, as expected, diamide-treated cells showed severely reduced spectrin dynamics between the two time points in terms of both mobile fraction, which was highly decreased (85% compared to 34%), and half-time recovery, which was consistently increased ($t_{1/2}$ control= 38.44 sec, $t_{1/2}$ treated= 48.24 sec), in 10 cells out of 12 (Figure 30 B-C).

The dynamic remodeling is therefore essential for an integral spectrin/PM interplay. Overall, we attributed to contractility-dependent activity on highly stable membrane-associated actin protofilaments the main driving force for spectrin dynamics.

# 6. The actin-binding ability of spectrin is needed to coordinate spectrin dynamics with changes in cell mechanics

As already mentioned in the introduction (Chapter 2, paragraph 2.2. Spectrin repeats and other important domains), βII-spectrin posesses various important domains, among which plasma membrane binding domains (PE, PH and PS) and actin binding domain (ABD) were of particular interest four our study.

For this reason, we wondered if actin and these membrane binding domains could somehow contribute to the stability and functionality of the spectrin scaffold.

In order to dissect these mechanisms, we singularly depleted ABD and PE domains from our GFP tagged βII-spectrin construct, as reported in figure 31 A-B, and successfully transfected and overexpressed them in our cells.

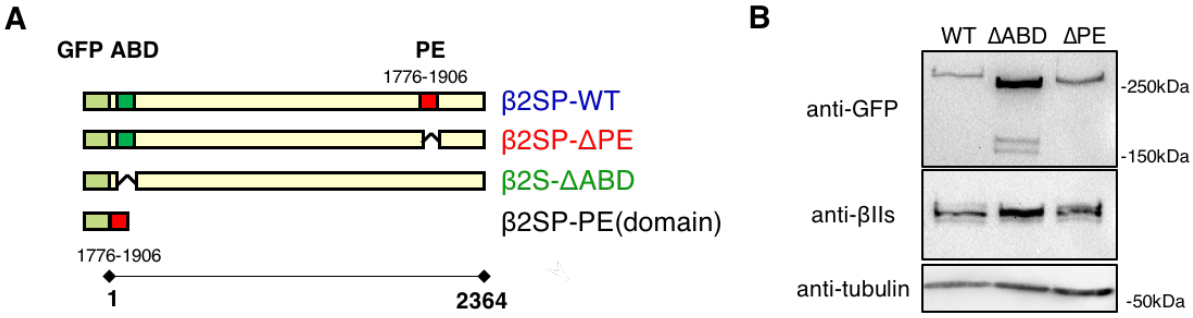


**Figure 31. βII-spectrin mutants representation.**

A) Cartoon representation of the βII-spectrin deletion mutants analyzed in this study. B) Total cell lysates of MEFs expressing exogenous GFP-βII-spectrin variants analyzed by anti-GFP and anti-βII-spectrin antibodies in western blot assay.

We performed FRAP analysis on wild type and mutant cells and compared them in terms of turn over and mobility. Upon the actin binding capability blunt, we observed an increase in the mobile fraction (87.2 %) and a decrease in the half-time recovery ($t_{1/2}$ = 24.56 sec), compared with the wild type in which we obtained a lower level of mobile fraction (74.8 %) and a higher half-time recovery ($t_{1/2}$=41.7 sec). Conversely, ΔPE mutants displayed mildly decreased half-time ($t_{1/2}$=56.8 sec) while the mobile fraction was comparable to the wild type (73.2%) (figure 32 A-C).

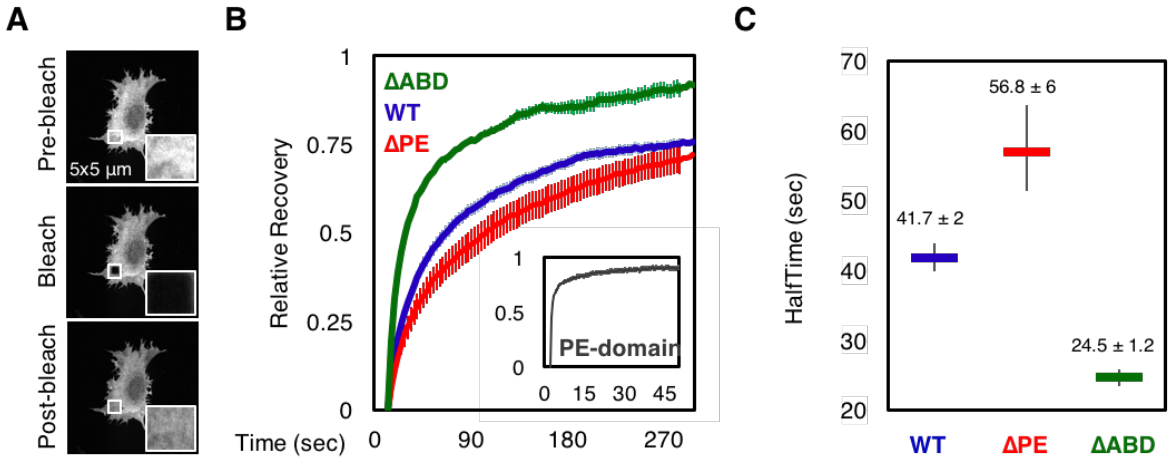


**Figure 32. βII-spectrin mutants display different dynamics.**

A-B) FRAP assay of the βII-spectrin deletion mutants expressed in MEFs. The fit to a single exponential equation is shown (n= 15-20 cells, mean±SEM), and the resulting half time recoveries are plotted in C (mean±95% confidence interval). Wild type protein displays 74.8% of mobile fraction and half-time recovery of 41.7 seconds, ΔABD 87.2% mobility and 24.5 seconds recovery and ΔPE 73.2% and 56.8 seconds. PE-domain only resulted in 87% mobility and 1.45 seconds recovery (inset). Experiment and analysis were performed by Andrea Ghisleni (IFOM, Milan).

We used GFP-tagged PE-only domain construct as control, since it can be used as a marker of membrane free diffusive lipids, and performed the same experiment. As expected, we observed a high mobile fraction (87%) and a very low half-time recovery ($t_{1/2}$= 1.45 sec), as reported in figure 32 B (inset).

Interestingly, individual removal of actin or PM binding domains, failed to affect spectrin localization, as reported in figure 33 C-F.

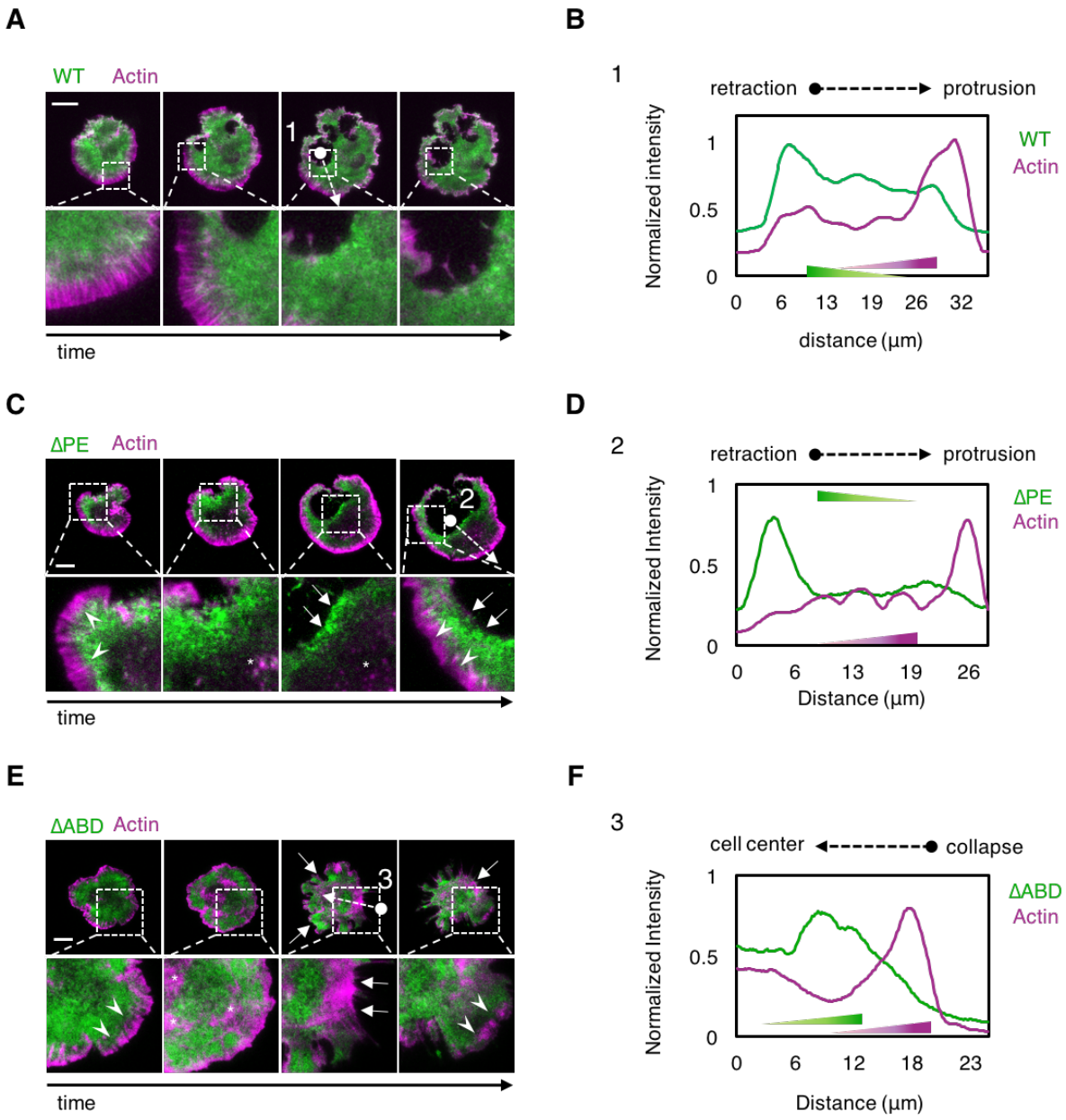


**Figure 33. βII-Spectrin WT, ΔPE and ΔABD show different spreading behaviours but similar accumulation at "cracking" zones formed in a spontaneous way.**

A-C-E) Representative images of spontaneous retractile events observed in MEFs expressing GFP-βII-spectrin variants during cell spreading by live TIRFM (GFP-βII-spectrin variants in green and RFP-Actin in magenta, scale bar: 20 µm). Relevant events are highlighted by the dashed boxes and zoomed in the lower panels: protruding zones are indicated by white arrowheads, retracting zones by white arrows. Line scan analysis of arrows with circular ends (1-2-3) are reported in B-D-F for both proteins, directionality indicated by black arrows.

Indeed, all the mutants were perfectly localized at the plasma membrane level and excluded from stress fibers, behaving as wild type cells.

Overall, these results support the key role of actin binding in spectrin meshwork stabilization but not its localization, while the PM-targeting is ensured by two main reasons. Indeed, both βII-spectrin mutant ability to still dimerize with its counterpart αII-spectrin, and potential cooperative mechanisms between different lipid-binding domains, instead of a single dominant pinning point, ensure the PM-targeting.

We wondered if these differential dynamics might affect cell shape remodeling mechanisms, and we followed cells overexpressing GFP-βII-spectrin mutants during spreading through live-TIRF microscopy. Indeed, ΔABD mutant cells underwent a normal inflationary P1 phase, while, during P2 contractile phase, we observed several collapses of protrusions where the meshwork resilience is instrumental to sustain the PM (Figure 33 E, F). These events were a little bit different from the retractions described earlier where spectrin replaced the actin-based support to the lipid bilayer (Figure 33 A, B); here, simultaneous collapses of actin and spectrin were observed, followed by further attempts of the cell to spread over the substrate. On the contrary, ΔPE cells seemed to spread even faster with a remarkable accumulation of ΔPE-spectrin at the edge of the cell (Figure 33 C, D).

As consequence, a negative Δarea/min increase was recorded in ΔABD cells (10' after transition in P2, n=7 cells), since positive values were offset by negative events. On contrary, wild type cells displayed positive increase in area during P2, while ΔPE cells spread even faster than the wild type and retraction zones highlighted remarkable ΔPE-spectrin accumulation (Figure 34 A, B).

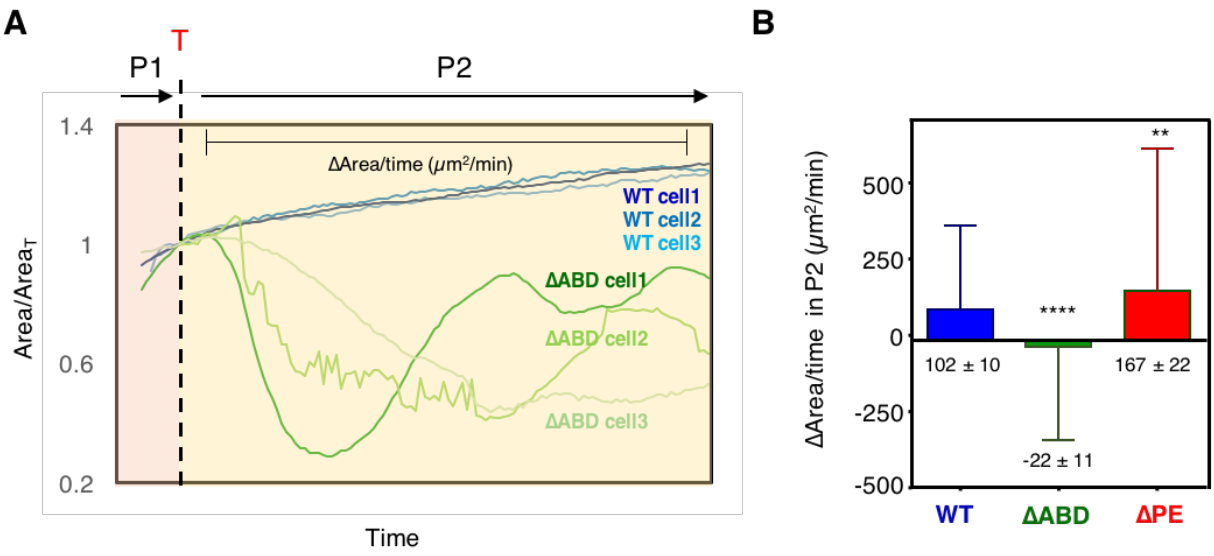


**Figure 34. ΔABD cells display a negative Δarea/min while WT and ΔPE cells have a positive area increase during spreading.**

A) Normalized cell area growth during P2: three stereotypical MEFs transfected with GFP-βII-spectrin WT are plotted in blue, while MEFs expressing ΔABD are shown in green and followed for 10 minutes after transition T by live TIRFM. B) Quantification of ΔArea/time extracted from each frame of time lapses during 10' after transition into P2 (WT n=792 frames, ΔABD n=840 frames, ΔPE n= 502 frames, 7-9 cells. Mean±SD, one-way Anova statistical analysis with multiple comparison, **p<0.008 ****p<0.0001). Analysis were performed by Andrea Ghisleni (IFOM, Milan).

Altogether these results indicate that the binding of βII-spectrin to actin protofilaments rather than PM is a key mechanism for correct meshwork dynamics during myosin II driven contractility. This skeleton confers resilience to the cell, which otherwise would undergo contraction (or retraction) at spectrin-rich PM territories. After establishing the dynamic response of spectrin under cell-driven changes in mechanics, we tested the response of spectrin meshwork to environmentally driven changes in mechanics.

# 7. Spectrin and actin respond differently during extrinsic PM challenges

Since we previously observed an accumulation of spectrin in the retracting zones of the cells during shape remodelling, we hypothesized the existence of a fencing mechanism by spectrin condensation that intervenes to prevent the complete collapse also under extrinsic challenges, like cell stretching. In order to dissect this mechanism, we seeded GFP-βII-spectrin and RFP-actin overexpressing cells on an engineered device, made in IFOM institute (see figure 35 A and chapter 4. Material and methods, paragraph 13 and 19), composed by a silicone membrane, and we selected cells with a characteristic polygonal shape with long arcs between adhesive protrusions.

We then followed those cells during the application of a biaxial stretch until we reached an increase of the area of 30%. Due to the set-up limitations, we were able to use only wide-field illumination imaging method, and for this reason we excluded moderate to high overexpressing cells from the analysis to avoid signal contamination by diffusive cytosolic GFP-βII-spectrin. Under these strong environmental perturbations, GFP-βII-spectrin expressing cells were able to retain the prominent adhesions onto the substrate, while actin treadmilling activity at lamellipodia was blocked by the increased strain (Figure 35 B).

Consistent with previous observations, spectrin signal sharpened in the arc-shaped zones under progressive stretch, creating a frame around the cell that disappeared when the applied stretch was released. Moreover, cell adherence on silicone membrane proved to be challenged and further insights were provided by detachment of weakly anchored protrusions in cells subjected to the gradual stretching protocol (Figure 35 C). Differently from the cell-driven retractions observed during spreading assay, actin and spectrin scaffolds condensed simultaneously in the collapsed protrusions.

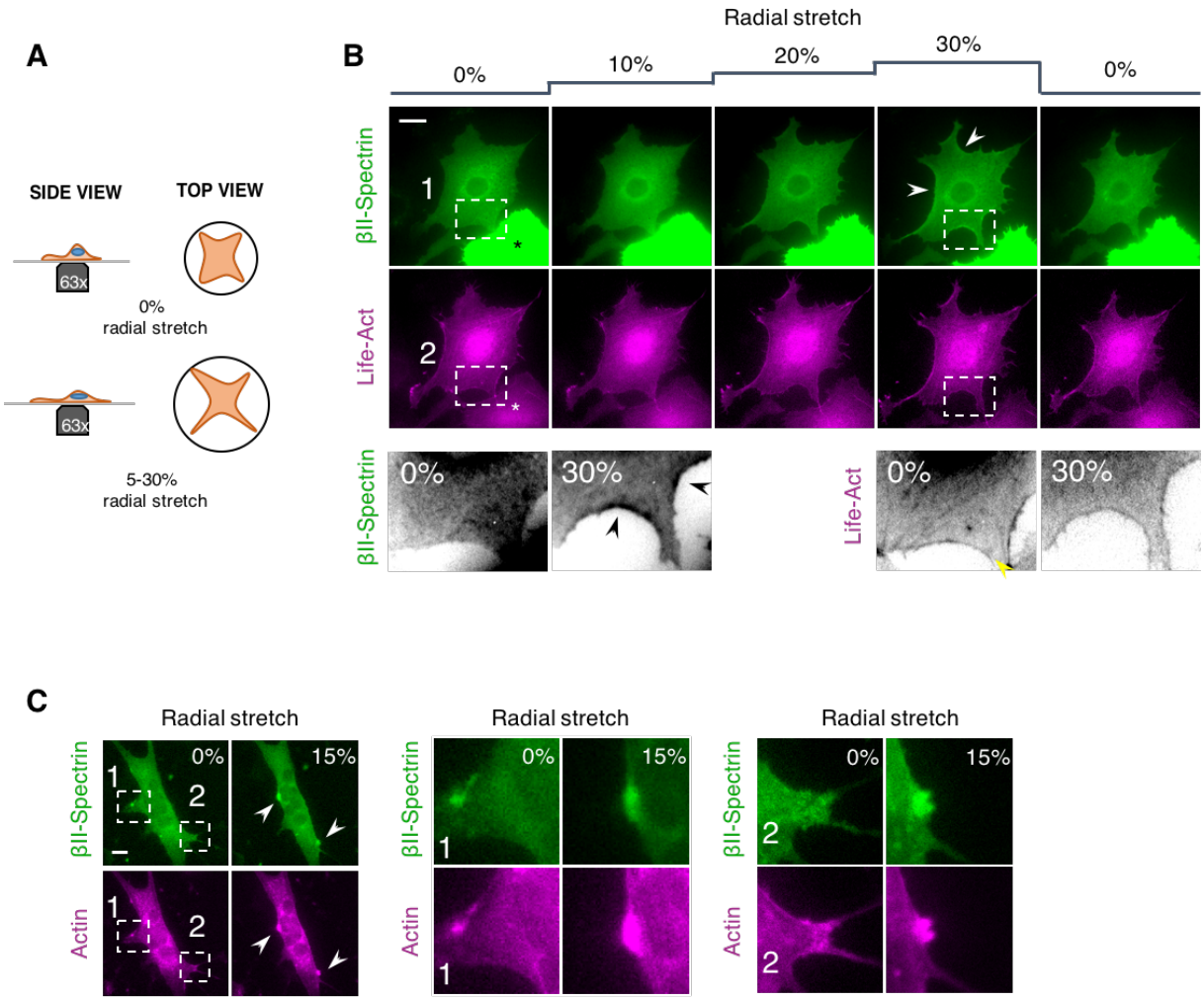


**Figure 35. βII-spectrin reacts with actin during cell stretching.**

A) Cartoon representation of the cell stretching device implemented in this study. B) MEFs transfected with GFP-βII-spectrin (green) and LifeAct-RFP (magenta) seeded on the fibronectin-coated silicone membrane and stretched bi-axially (0-30%) during live EPI fluorescence. In the dashed boxes 1-2, representative cell edge behavior observed among independent experiments, highlighting peculiar condensation of βII-spectrin in curvature zones not enriched by actin (arrowheads) at maximal stretch (30%). C) Bi-axial cell stretching experiment of GFP-**β**II-spectrin (green) and RFP-actin (magenta) expressing MEFs, imaged by live EPI fluorescence microscopy. Dashed boxes 1 and 2 highlights two specific cell protrusions that detached upon 15% stretch. Experiments and analysis were performed by Andrea Ghisleni (IFOM, Milan).

Notably, this was the only mechanical event leading to apparent colocalization between the two cytoskeletons. We interpreted that in those particular fast events, actin and spectrin meshworks react passively as opposed to all the others mechanical perturbations, where the crosstalk

between the two leads to fine-tuned adaptation and reorganization. Spectrin meshwork active condensation in arc-shaped membrane retractions (i.e. spectrin rich membrane curvatures) might be a cell mechanism that operate in the absence of local actin, under extrinsic (stretch) as well as intrinsic (spreading-polarization) mechanical challenges.

# 8. Spectrin concertedly respond with actin during cell compression

Spectrin has been proposed to act as a mechanosensing and mechanoprotector in erythrocytes, neurons and other cell types (Delaunay, 2007; Elgsaeter et al., 1986; Hammarlund et al., 2007; Krieg et al., 2014; Machnicka et al., 2012), but how these functions are exerted and how spectrin meshwork is spatio-temporally organized during these mechanical perturbations are still not clear.

Since under physiological conditions cells can stretch, as we have seen with our stretching device, but also undergo compression (Roca-Cusachs et al., 2017), in order to better understand how spectrin behave upon extrinsic challenges, we performed top-down compression experiments to the cells and followed spectrin and actin reactions through live-TIRF microscopy. We used a custom-developed device (see figure 36 A and Chapter 4. Material and methods, paragraph 14 and 19), composed of a polydimethylsiloxane (PDMS) piston, able to perform cycles of compressions (2 minutes) and relaxations (2 minutes) at increasing strength on our MEFs overexpressing RFP-actin and GFP- βII-spectrin, as reported in the schematic representation of the experimental design in figure 36 B.

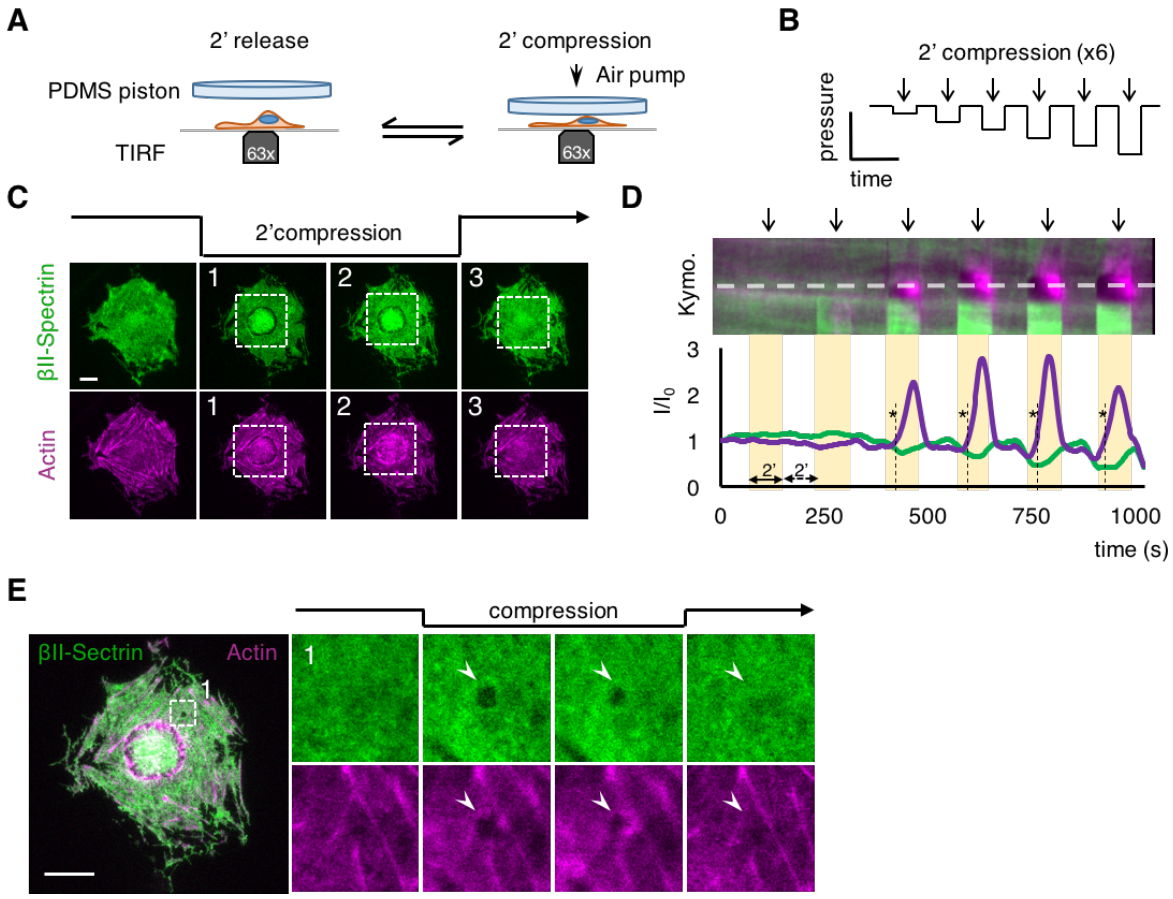


**Figure 36. βII-spectrin and actin show opposite reactions to cell compression.**

A) Cell compression set-up and B) the applied step-increase protocols are schematized. C) GFP-βII-spectrin (green) and RFP-actin (magenta) expressing MEFs are imaged by live TIRFM during the entire compressive protocol. Four relevant time points are shown: pre-compression, early and late compression, and the release phase (scale bar: 10 μm). Key details consistently observed between independent experiments are highlighted by dashed boxes and zoomed in panel 1-2-3. Reaction in correspondence of the nuclear edge, brought into the TIRF plane by the compressive stress (white arrowheads), is quantified by the kymograph analysis (D) over the yellow rectangle. Fluorescence intensities across the dashed line in F are plot in the graph; clearence of βII-spectrin and the delayed actin polimerization is observed (asterisks and dashed lines in the graph). E) Same cell reported in panel C. Zoom 1 highlights the appearance of a vesicular structure (white arrowhead) upon compression, devoid of both βII-spectrin and actin, resembling the clearance effect observed underneath the nucleus (scale bar: 20 μm). Experiment and analysis were performed by Andrea Ghisleni (IFOM, Milan).

Surprisingly, upon cell compression, we observed spectrin and actin reactions under the nucleus, which seemed to work as an additional piston above the cell cortex at the basal level.

Piston contact with the cell roof represented the first compression step and did not affect basal spectrin signal. The pression of the piston was then progressively pushed, and we could observe spectrin fluorescence increase, just right under the nucleus. Simultaneously, an unexpected spectrin- and actin-depleted rim formed in correspondence of the nuclear envelope Remarkably, *de novo* actin-polymerization specifically occurred in this bare PM region within the 2 minutes of compression, and was characterized by concentric inward actin flow. As soon as the piston was released, actin polymerization was blocked and followed by its fast disappereance, whereas spectrin filled again the empty rim (Figure 36 C-D). Occasionally, similar behavior could be observed by compression-relaxation of large cytosolic vesicles (Figure 36 E).

These results represent an exemplar and direct experimental demonstration of our previous observations on the dynamic cooperation between actin and spectrin at the cortex level under mechanical challenges. Moreover, these results pointed out also the role of spectrin/actin cortex meshwork in the protection of the PM. Indeed, by spectrin fluctuations or actin polymerization in order to fill the empty gaps, PM is always under constant support, either mediated by spectrin or actin skeleton.

Interestingly, upon cell compression, we could appreciate the formation of bleb-like structures, caused by the increasing pressure able to affect the cell cortex integrity, as depicted in the scheme in figure 37 B.

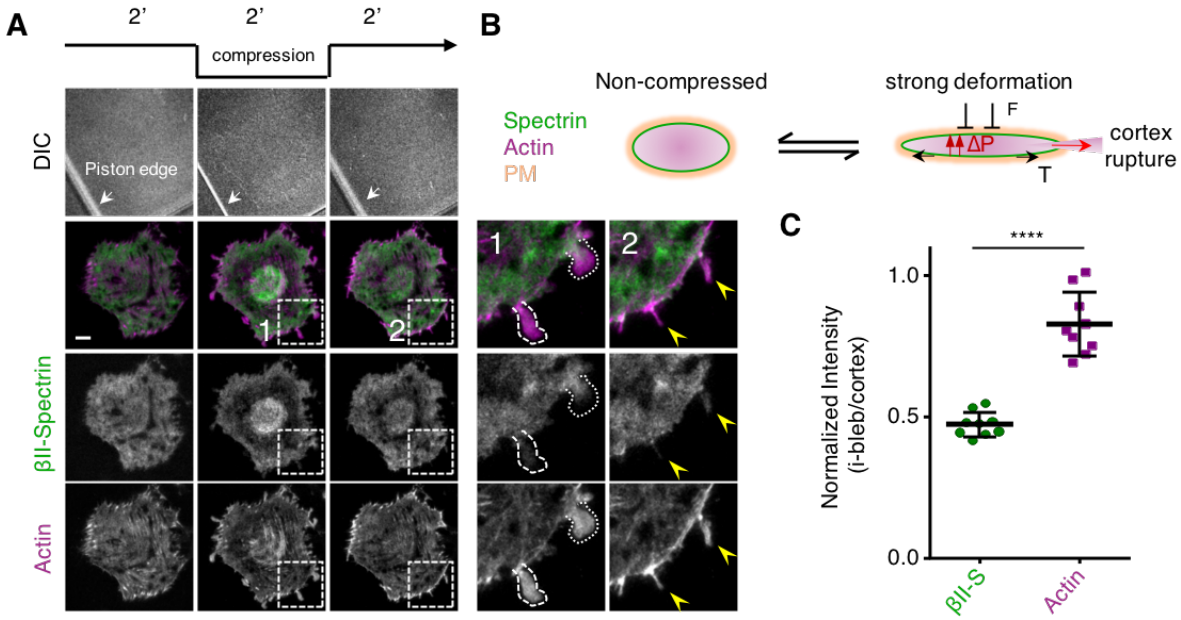


**Figure 37. Compression-induced blebs formation upon cell compression.**

A) Maximal compression experiments of GFP-βII-spectrin (green) and RFP-actin (magenta) expressing MEFs: compression stress is gradually increased until bleb formation is induced. Model of cortex rupture mechanism is schematized in B: key elements are the variation in intracellular pressure (ΔP) and cortex tension (T) during compression. Representative images are shown during (1) and upon release of compression (2), when induced blebs are resorbed into tubular-like actin enriched structures (yellow arrowheads). Actin and βII-spectrin content in the blebs compared to the adjacent cell body are quantified in C (n=9, mean±SD in 3 independent experiments, unpaired T-test: * $p<0.0001$). Experiment and analysis were performed by Andrea Ghisleni (IFOM, Milan).

Surprisingly, these characteristic structures, that we therefore decided to call "compression-induced blebs (i-bleb)", clearly displayed preferential flow of cytosolic actin into the newly formed blebs while the majority of the spectrin signal was retained at the cell body. Furthermore, upon release of the piston, i-blebs were re-absorbed into actin-enriched tubular-like structures devoid of spectrin, as shown in figure 37 A. We then measured the fluorescence intensity of both spectrin and actin in the i-bleb area, thus confirming our previous results, since we obtained a higher actin intensity compared to the spectrin one, as shown in figure 37 C.

These results show that spectrin and actin skeletons, while in cooperation in physiology or during cell-driven mechanoadaptation, display clearly different spatiotemporal dynamics depending on the nature of the mechanical challenge. Indeed, if on one hand, during controlled retraction, spectrin can condense in actin-poor zone and support the plasma membrane, on the other hand, upon fast event like cell detachment (such as after cell stretching), they passively condense together, forming an undistinguishable structure as cell retract. Moreover, in fast protruding zones, which are non-directly driven by the actin cytoskeleton, like in compression-induced blebs, spectrin can be uncoupled from the PM, potentially preserving cytosolic cohesion, while actin flows in the bleb and progressively re-polymerize in defined structures, as already previously observed (Charras et al., 2006).

# 9. Spectrin elastic properties give support to PM during mechanical challenges

In order to better characterize spectrin elastic properties in supporting the PM, we applied cycles of stress and relaxation through osmotic shocks experiments.

Cells transfected with GFP- βII-spectrin and a fluorescent PM marker were left in a 1X-ringer solution and monitored with live-TIRF microscopy. Cycles of hypotonic shocks and isotonic relaxations were performed by changing the medium every 2 minutes during the recording with 0.5X- and 1X-ringer solutions.

Our analyses revealed changes in spectrin fluorescence intensity, which decreased upon hypotonic shocks, whereas increased during isotonic relaxation. Interestingly the ratio between βII-spectrin and PM signal didn't shift significantly from the initial one during several cycles repetition, as reported in figure 38 A-B.

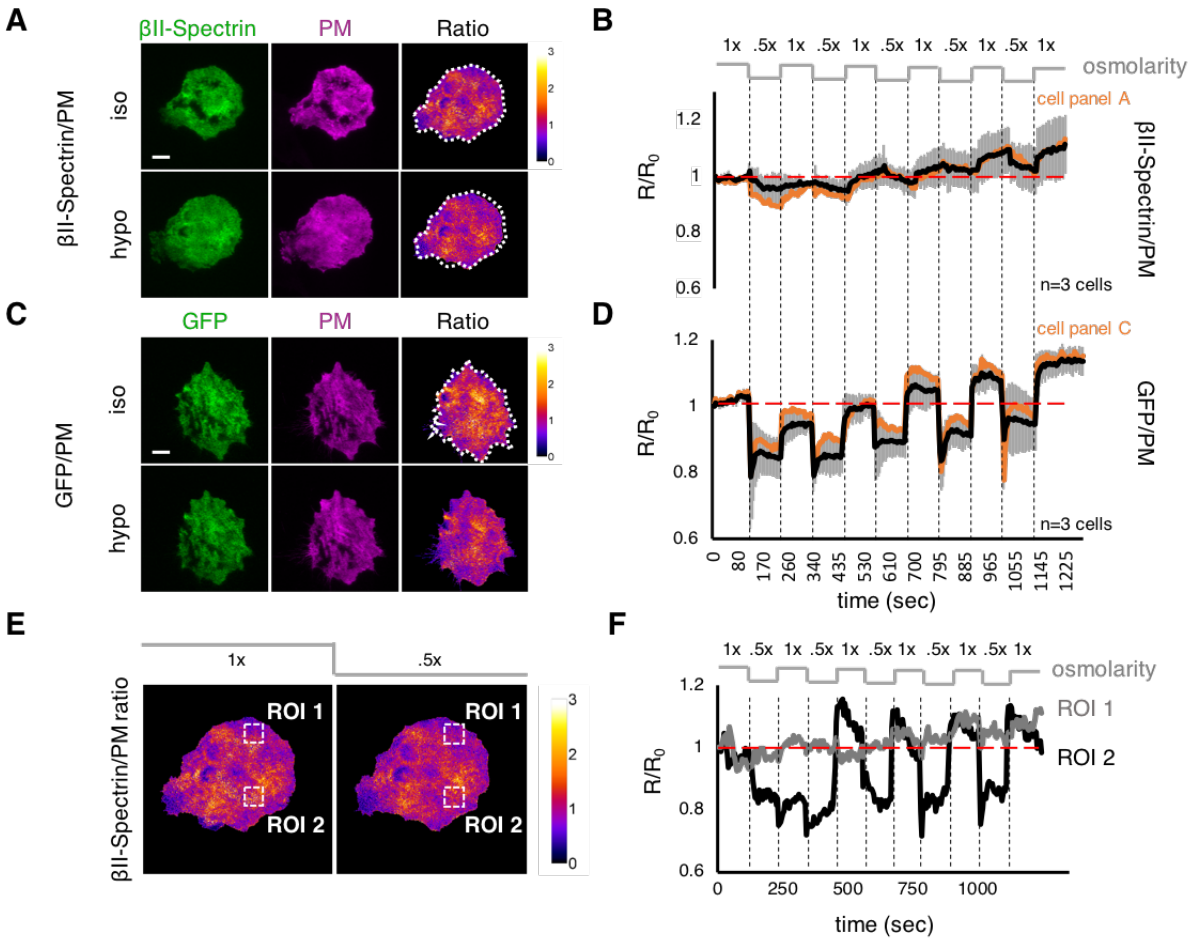


**Figure 38. Global and local βII-spectrin reactions upon cycles of osmotic shocks.**

A) Representative images of GFP-βII-spectrin (green) and PM-marker (magenta) transfected MEFs observed by live TIRFM during osmotic shocks. Five isotonic (1x)-to-hypotonic (0.5x) cycles were applied (B). Initial fluorescent signals are normalized to obtain the non-stoichiometric ratio βII-spectrin/PM (LUT fire, scale bar: 10 μm). Average ratio is plotted in B (black line, n=3 cells, mean±SD), while the ratio of the cell in A is shown by orange line. C-D) As positive control, the same protocol is applied to MEFs transfected with soluble GFP (green) and PM-marker (magenta), while GFP/PM ratio is plotted in D (n=3 cells, mean±SD). Zonal Ratio analysis at two extreme cases is reported in E: ROI1 presents high βII-spectrin/PM ratio, while ROI2 displays lower ratio. As show in the graph (F), the two ROIs behave differently: while ROI1 reacts similarly to the whole-cell analysis graph presented in B, ROI2 shows an initial decrease of the ratio sustained during the first two iso-to-hypotonic cycles, followed by a compensatory effect that restored the initial ratio during the last four cycles.

We used soluble GFP as non-membranous control, and we could observe consistent fluctuations in the βII-spectrin/ PM ratio, as reported in figure 38 C-D.

Interestingly, ratiometric images failed to display homogeneous intensity throughout the entire cell, suggesting enrichment or depletion of one of the two components at specific sites. Local analysis during osmotic shocks displayed initial reduction in the βII-spectrin/PM ratio that was compensated during later shocks, while a second region of the same cell matched the linear ratio shown over the entire cell projected area (Figure 38 E-F).

Altogether, these results support the existence of local redistribution mechanisms at mesoscale level. We concluded that βII-spectrin elastic support of the PM occurs at whole cell level and is maintained by keeping constant the ratio between the two components, while it can locally and transiently drift to allow the occurrence of specific PM-linked events.

# 10. Spectrin meshwork is involved in spatio-temporal regulation of clathrin-mediated endocytosis at PM level

Spectrin dynamics and the complementary interplay with actin pointed out the ability of the two meshworks to create PM microdomains that are consistent with the revised fluid-mosaic model of PM organization (Kusumi et al., 2012).

Since, in epithelial cells, spectrin has been proposed to be confined in microdomains, rather than a uniform structure as the one described in red blood cells or axons, that are able to prevent both clathrin-mediated and bulk endocytosis (Jenkins et al., 2015), we decided to further investigate this mechanism by performing experiment both in fixed and in live specimens.

We immunostained our cells with endogenous clathrin-heavy-chain (CHC), βII-spectrin and actin, and as expected, we found that none of the tree proteins colocalized, as reported in figure 39 A, D.

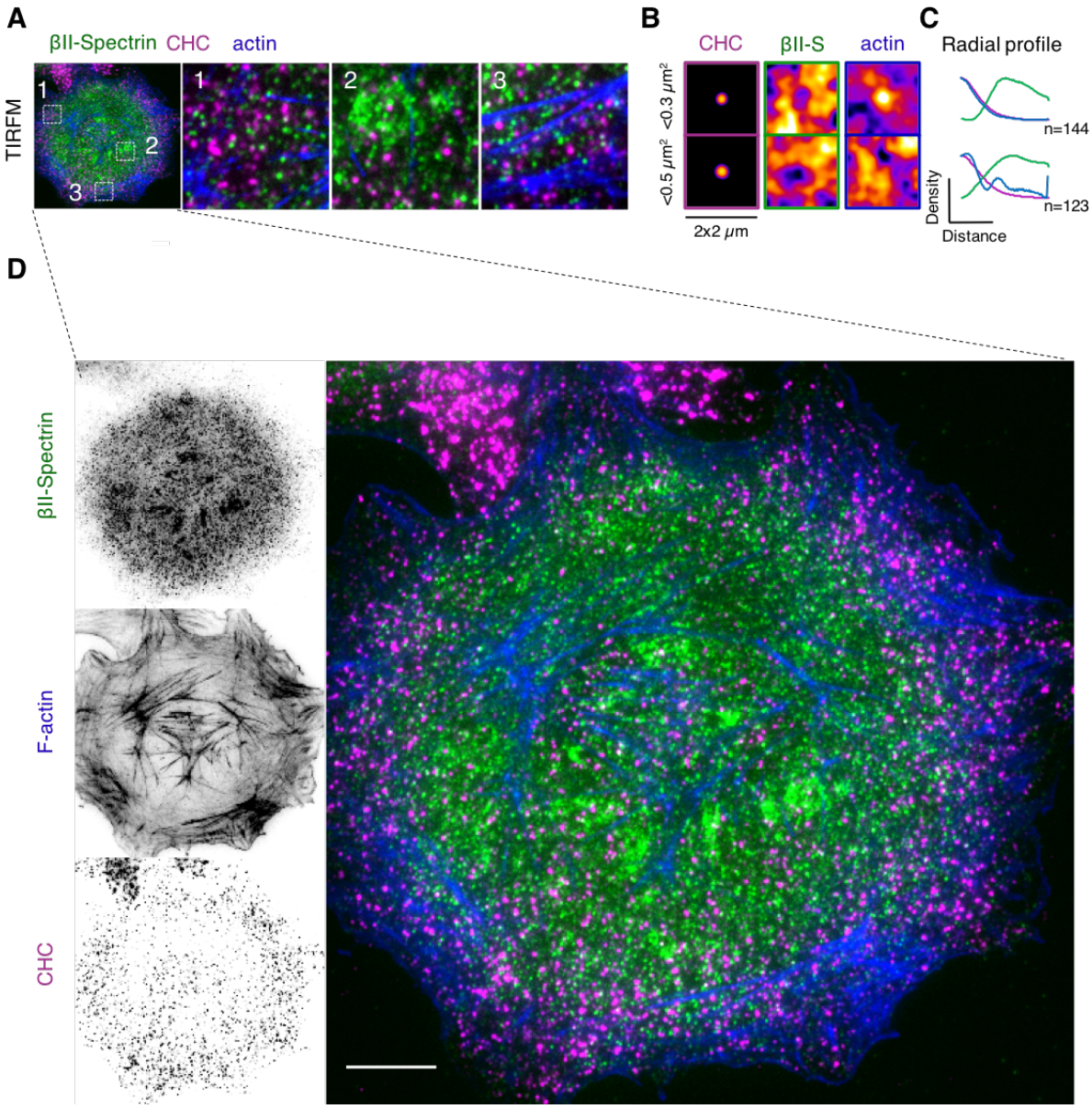


**Figure 39. βII-spectrin, actin and clathrin-heavy-chain never show colocalization.**

A) TIRF microscopy images of MEFs immunostained for endogenous βII-spectrin (green), clathrin heavy chain (CHC, magenta) and F-actin (blue, scale bar: 10 μm). Three different subcellular regions are highlighted (dashed boxes 1-3): high density CHC zone (1), βII-spectrin-rich zone (2) and actin stress fibers (3). B) Density maps generated by aligning discrete clathrin pits of small (<0.3 $\mu m^2$, n=144) and larger size (0.3-0.5 $\mu m^2$, n=123) are shown, while in C correspondent radial intensity profiles for the three channels are presented. D) zoom of the cell presented in panel A (scale bar: 10 μm).

To strengthen this observation multiple discrete clathrin structures were selected, registered in 2x2μm ROIs and clustered into two groups of different size (<300$nm^2$ and 300-500$nm^2$)

following a recently published approach (Mund et al., 2018). The density maps displayed clathrin pits positioned at the center of spectrin-less zones surrounded by spectrin-rich areas. Remarkably, the diameter of the averaged spectrin-less zones almost matched in size the clathrin pits projections (Figure 39 B, C). While most of the actin structures, such as stress fibers, are clearly distinct form the pits, the averaging of >100 pits led to the identification of a discrete actin enrichment in correspondence of the clathrin staining, in particular for smaller group (Figure 39 A-C). These observations fit well with current maturation models of endocytic structures (Kaksonen and Roux, 2018; Kirchhausen, 2009; Scita and Di Fiore, 2010). Our randomized analysis pinpoints to a potential hindrance mechanism through which the spectrin meshwork is able to delimit the zones of the assembly of clathrin pits, in correspondence of loosen spectrin organization.

In order to understand better the dynamics of this mechanism, we performed other analysis in live specimens.

Cells overexpressing GFP- βII-spectrin and mCherry-AP2σ, which is the major chathrin adaptor, were monitored through live-TIRFM, and the exclusion of spectrin from clathrin coated pits was confirmed, since AP2 specifically appeared in the void regions characteristic of the spectrin meshwork (Figure 40 A-C, top).

The same pattern was not displayed when cells were co-transfected with the membrane-binding PE domain only of spectrin, which was used as control for PM staining, and mCherry-Ap2σ, as shown in the bottom part of figure 40 A-C.

CME is a highly dynamic and heterogeneous process with several layers of regulation, including membrane tension modulation by osmolarity (Boulant et al., 2011).

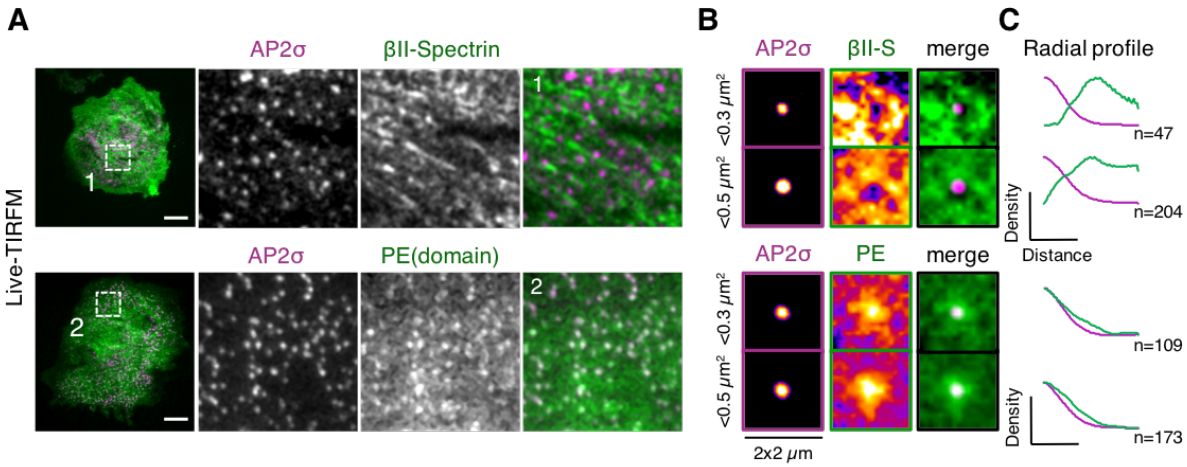


**Figure 40. AP2 specifically localizes in βII-spectrin-voided regions.**

A) Representative live TIRF microscopy images of MEFs transfected with GFP-βII-spectrin (green) and the clathrin adapter AP2σ-mCherry (magenta) (scale bar: 10 μm), Unsharp and Gaussian filters were applied. PE-only domain transfected fibroblasts show homogeneous PM localization and enrichment in correspondence of AP2σ pits, as shown by density maps (B) and radial profile analysis (C) generated as previously described (GFP-βII-spectrin: <0.3 $\mu m^2$, n=47 and 0.3-0.5 $\mu m^2$, n=204; PE-domain: <0.3 $\mu m^2$, n=109 and 0.3-0.5 $\mu m^2$, n=173.

In order to further investigate these processes, which could be potentially linked with spectrin reorganization upon osmolarities changes, we performed osmotic shocks experiments, in the same way as already described in paragraph 9 of this chapter), on cells overexpressing GFP-βII-spectrin and mCherry-AP2σ. As expected, upon hypotonic shock we observed a decrease in spectrin intensity and, concomitantly, an increase in AP2 fluorescence which was soon followed by a strong decrease and then restored upon 1X isotonic relaxation, as shown in figure 41 A, thus suggesting a spectrin regulation of clathrin pits invagination through stretching and relaxation.

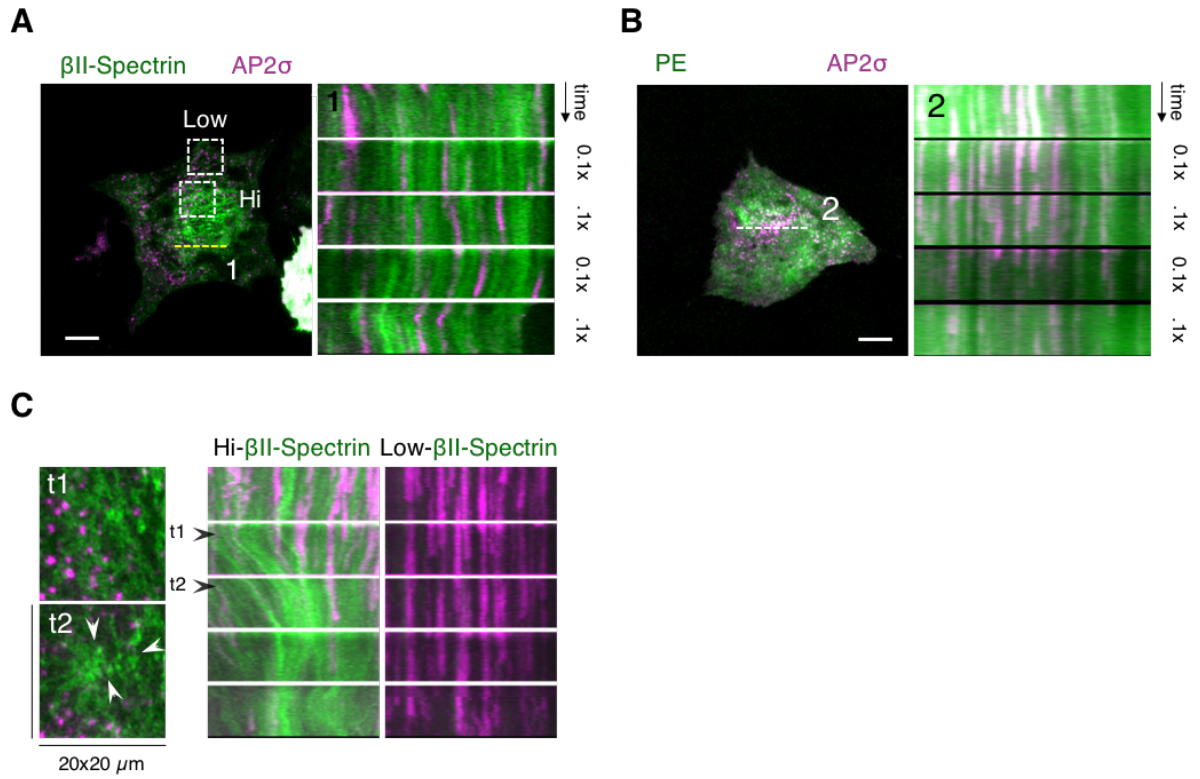


**Figure 41. βII-spectrin act as a fence during clathrin-mediated endocytosis.**

A) Representative time-lapse TIRFM images of cells transfected with - βII-spectrin and mCherry-AP2σ during osmotic shocks: kymograph is generated in correspondence of the dashed yellow line (1), where spectrin mesh and AP2σ pits display coordinated lateral motion in response to osmolarity changes. B) Representative time-lapse TIRFM images of cells transfected with GFP-PE and mCherry-Ap2σ during osmotic shocks: kymograph is generated in correspondence of the dashed yellow line (2) where the same effect was not observed C) 20x20µm ROIs are drawn at low- and high-spectrin density zones around AP2 pits (correspondent to dashed boxes in G, only zooms of Hi-density zone are reported at two different frames). Kymographs display the differential behavior of the pits observed during spectrin remodeling.

We perform the same experiment using our GFP-PE-only membrane binding domain, and we didn't observe the same effect, as represented in figure 41 B.

Further observations of the experiment revealed different behavior in different regions within the same cells; indeed, it was possible to discriminate zones with high GFP-βII-spectrin density, where AP2-pits disappeared from the TIRF plane during the time, and low GFP-βII-spectrin density zones where this event was not happening, as shown in figure 41 C.

These results suggested a fencing capability of spectrin meshwork during clathrin-mediated endocytosis, which was somehow blocked when spectrin concentration was lower.

Overall, these data supported the hypothesis of spectrin involvement in the spatio-temporal reorganization and positioning of endocytic structures.

Of note, several mechanisms have been identified in the regulation of CME, many of them showing discrepancies and controversy with one another (Doherty and McMahon, 2009). Thus far, none of them has clearly taken into consideration the role of the spectrin meshwork and its local re-organization. We propose that the highly dynamic composite nature of the cortex under mechanoresponses is mainly regulated by an orchestrated "*menage a 4*" between PM, spectrin, endocytosis and acto-myosin contraction-polymerization, as proposed in our model reported in figure 45 (see Discussion).

# 11. CRISPR/Cas9 approach for βII-spectrin knock out MEF cell line generation

Given the importance of the effects described upon spectrin depletion (Stankewich et al., 2011) and the interesting results that we obtained and already discussed above, we decided to deeper understand spectrin role in the mesoscale organization of the PM and its possible involvement in the intracellular trafficking, using MEFs completely depleted from βII-spectrin and comparing them with wild type ones.

In order to generate a MEF cell line knock out (KO) for βII-spectrin, we used a CRISPR/Cas9 approach.

RPTP MEFs were transfected with pSpCas9-2A-GFP plasmid and sgRNA designed for *SPTBN1* gene and GFP-positive clones were sorted and expanded.

Knock out efficiency was firstly checked at protein level through western blot analysis on 8 out of the 40 total clones that we obtained, and none of them expressed βII-spectrin protein, as reported in figure 42A.

Moreover, qPCR analysis revealed us a reduction also at mRNA levels, thus confirming βII-spectrin KO cell lines generation success (Figure 42 B).

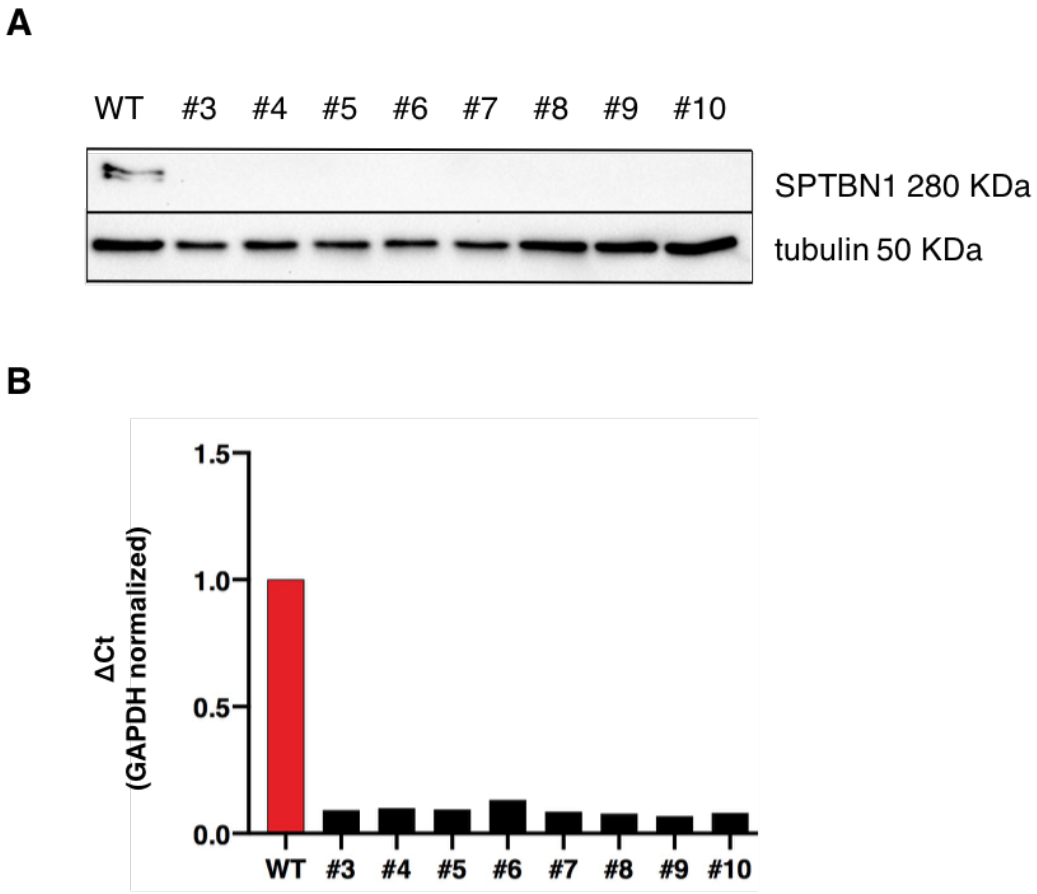


**Figure 42. Generation of RPTP MEF cell lines βII-spectrin knock out.**

A) Total cell lysates of MEFs analyzed by anti-βII-spectrin antibody in western blot assay. B) Gene expression analysis of βII-spectrin in MEFs used for this study, measured by qPCR (n=1).

# 12. βII-spectrin depletion leads to αII-spectrin protein degradation

Since it has been shown that MEFs depleted of αII-spectrin displayed a reduction of 20% also of βII- and βIII- spectrin protein expression levels without any change in their level of mRNA expression (Stankewich et al., 2011), we tested αII-spectrin expression both at protein and mRNA level in #8, #9 and #10 selected βII-spectrin KO clones.

Interestingly, on one hand all the three clones revealed a reduction of αII-spectrin protein expression level in the three clones, while, on the other hand they displayed an almost normal mRNA expression level, as reported in figure 43 A-B.

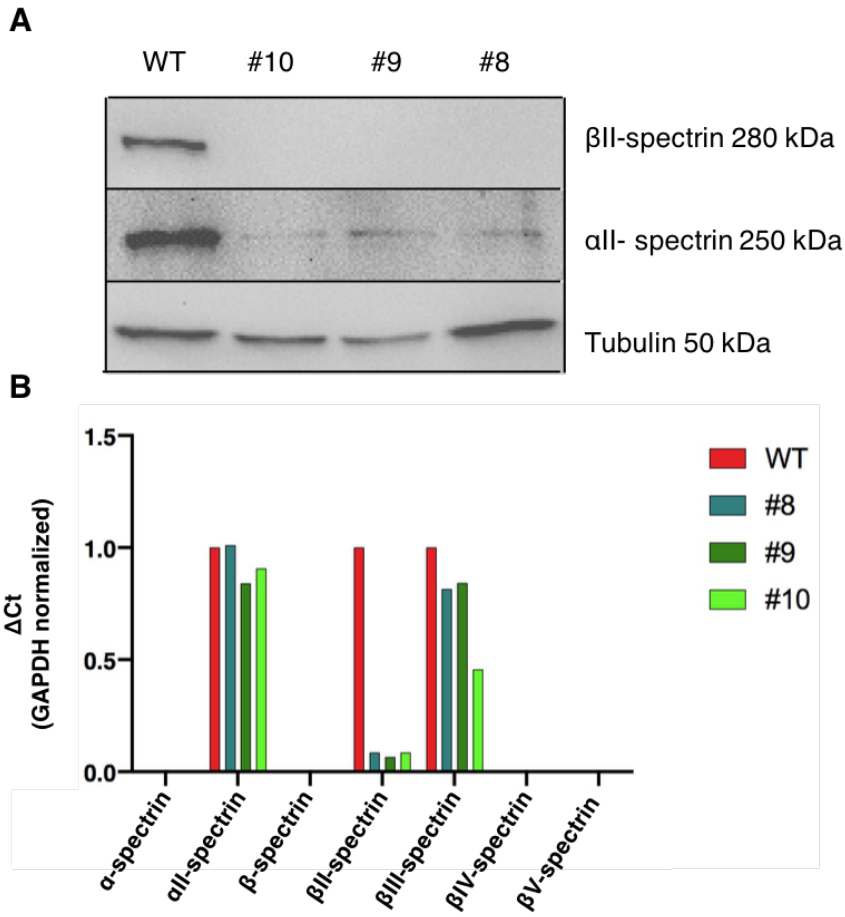


**Figure 43. βII-spectrin KO leads to αII-spectrin protein degradation.**

A) αII- and βII-spectrin protein expression in βII-spectrin KO MEFs analyzed by western blot in total cell lysates. B) Gene expression analysis of different spectrin variants in βII-spectrin KO MEFs used for this study, measured by qPCR (n=1).

We also checked the expression level of the other spectrin isogenes, and, interestingly, the two erythrocytic forms of spectrin (βI and αI) were still undetectable, meaning that their expression was unchanged upon βII-spectrin KO. Moreover, we observed a small decrease in βIII-spectrin expression, while βIV- and V- spectrin expression was too low to be detected by qPCR analysis. Overall, these results support the hypotesis that both βII- and αII-spectrin need to be bound to their respective counterparts in order to perform their proper role in supporting the plasma membrane and to avoid degradation, but further analysis need to be performed to confirm this.

# 13. Spectrin is important for cell shape control in MEF cells

In order to characterize the phenotype of βII-spectrin depleted cells, we performed an over night time lapse on WT, #8, #9 and #10 βII-spectrin KO cells seeded on fibronectin-coated coverslips. Interestingly, βII-spectrin depletion didn't affect cell survival, but KO cells revealed a slower growth and, appeared smaller with a peculiar and elongated shape compared to wild type cells, as shown in the snapshot images extracted from our movies reported in figure 44 A.

In order to better quantify our observations, we transfected MEF RPTP wild type cells with pEGFP empty vector, and clone #8 cells with both pEGFP empty vector and with GFP-βII-spectrin, in order to see if, upon βII-spectrin re-expression, we were able to rescue the WT phenotype. Cells were then fixed with 4% PFA and observed at the microscope.

Indeed, after analysing several cells, we actually observed a reduction in KO cells area, but, βII-spectrin back transfection, wasn't enough to rescue the WT cell dimensions, as shown in the quantification graph reported in figure 44 B.

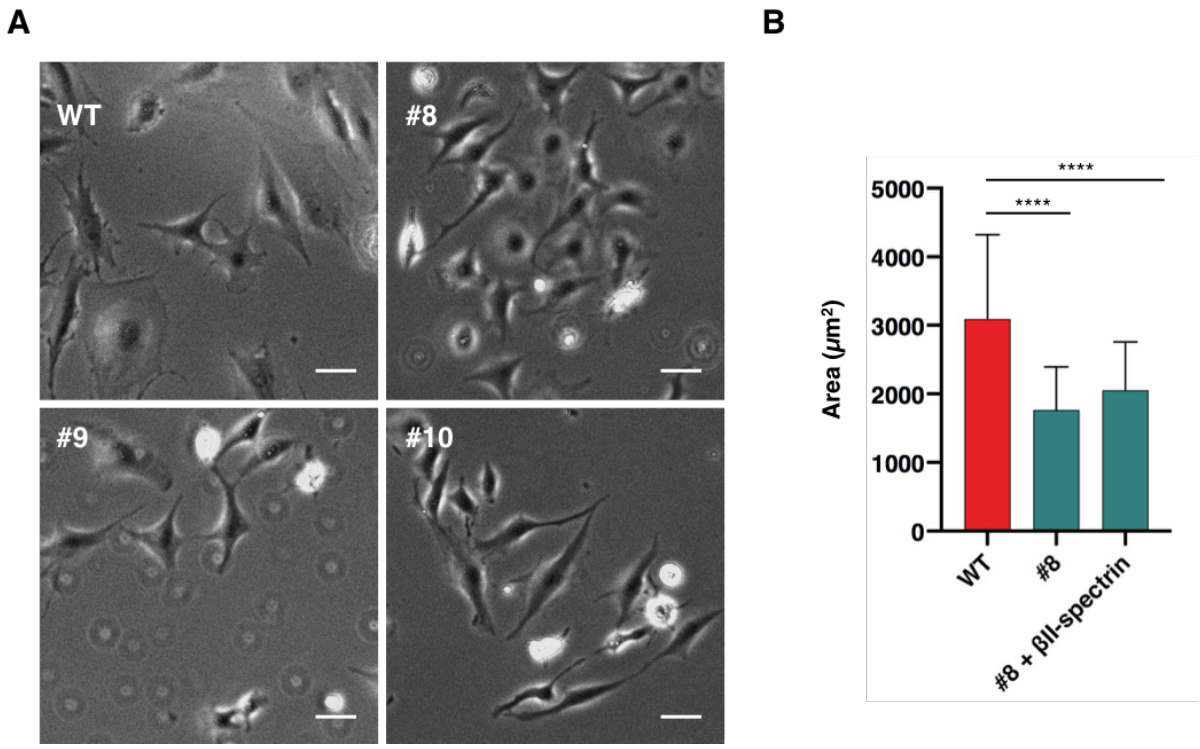


**Figure 44. βII-spectrin KO lead to a cell area decrease.**

A) Snapshot extracted from over night time laps performed on WT cells, #8, #9 and #10 βII-spectrin KO cells. Scale bar: 20 μm. B) Quantification of area of WT, #8 and #8 back-transfected with βII-spectrin (n=42 cells, Statistical analysis: unpaired T-test, $p<0.0001$).

Taken together, these preliminary results, reveal the importance of spectrin in the control of the cell shape in MEFs, accordingly to previous studies performed in erythrocytes.
Further analysis during cell spreading or upon extrinsic mechanical perturbations will be performed in a spectrin-depleted background, in order to assess its role in PM support and cell shape maintenance.

# Materials and Methods

## 1. Cell culture and media

Immortalized mouse embryonic fibroblasts (MEFs) derived from RPTP $\alpha$+/+ murine background (Su et al., 1999) were grown in complete culturing media composed by DMEM (Lonza) supplemented with 10% Fetal Bovine Serum South American (FBS SA, Invitrogen) and 2mM Glutamine at 37°C and 5% $CO_2$. Cells density never exceed 70% confluency to favor single cell analysis instead of tissue-like behaviour. For imaging experiments, MEFs were seeded on glass coverslips of 1½ thickness (Corning) or Nunc Glass Base Dishes (Thermo Scientific) coated with sterile 10µg/ml fibronectin (Sigma-Aldrich). During live imaging experiments, the culturing media was exchanged 30' before experiments in serum-deprived $Ca^{2+}$-buffered RIN GER solution (see supplementary table for buffer composition) to avoid phenol-red background contamination. For experiments with AP2σ construct transient expression, RINGER solution were supplemented with 10% FCS. Other cell lines were obtained from IFOM Cell Bank and cultured as follow: NIH3T3, HS27, RPMI, A-431 were cultured in DMEM (Lonza) supplemented with 10% Fetal Bovine Serum South American (FBS SA, Invitrogen). For MCF-10A DMEM-Ham's F12 was supplemented with 5% Horse Serum, 10ug/ml Insuline, 20ng/ml EGF, 500ng/ml Hydrocortisone, 100ng/ml cholera toxin, 2mM L-Glutamine; MDA-MB 231 were cultured in Leibovitz's L15+ 10% FBS S.A.+ 2mM L-Glutamine; HeLa were cultured in MEM+ 10% FBS S.A.+ 1mM NaPyruvate + 0.1mM NEAA+ 2mM L-Glutamine. HUVEC primary cells were cultured in Endothelial Cell Basal Medium (Sigma-Aldrich)

## 2. Plasmids and transient transfections

All plasmids for mammalian transient expression used in this study are listed in the Resource Table (supplemental information), describing original source and identifier. Specifically, human βII-Spectrin (gene ID: NM_003128) wild type construct was cloned into the pEGFP-C3 backbone (Clonetech) between HindIII and SacII restriction sites, with the fluorescent tag at the N-terminus interspaced by an additional flexible linker composed of 11 residues (KYSDLELKLAA). For the generation of GFP-βII-Spectrin-ΔPE, residues 1776-1907 were deleted from full length βII-Spectrin. The same peptide was cloned in frame with GFP into the pEGFP-N1 backbone to generate GFP-PE domain only. For the generation of GFP-βII-Spectrin-ΔABD, residues 280-2364 were amplified from full length GFP-βII-Spectrin, and cloned into pEGFP-C3 backbone between HindIII and SacII restriction sites. Other plasmids were purchased or obtained from external sources listed in the resource table. Transient expression was obtained by electroporation performed 24h before the experiment using the Neon electroporation system (Thermo Fisher Scientific) as previously described(Pontes et al., 2017b). For each transfection $1x10^6$ cells were trypsinized, washed once with PBS and mixed with 10μg of total DNA in electroporation buffer R (Invitrogen). Cells were singularly electroshocked at 1600mV for 20 ms by placing the electroporation tip into the column filled by E2 buffer (following manufacturer specifications). After the shock, cells were immediately seeded onto tissue-culture grade plastic dishes replenished with complete culturing media.

## 3. CRISPR/Cas9 transfection, plasmid and sgRNA

For transient transfection of MEF cells we used pSpCas9(BB)-2A-GFP (PX458) (Addgene) kindly provided by Giorgio Scita's lab.

sgRNA used (GCCTTACAACTACAACCAAC, Thermo Fisher Scientific) were targeted against: Chr.11: 30197748 - 30197770 on GRCm38.

MEFs cells were transfected with pSpCas9(BB)-2A-GFP (PX458) and, 24 hours later, with sgRNA using the Neon electroporation system (Thermo Fisher Scientific).

For each transfection, $1x10^6$ cells were trypsinized, washed once with PBS and mixed with a total of 10 µg recombinant DNA in electroporation buffer R (Invitrogen), and 7pmol of sgRNA. Cells were singularly electroshocked at 1600mV for 20 msec by placing the electroporation tip into the column filled by E2 buffer (following manufacturer specifications). After the shock, cells were immediately seeded onto tissue-culture grade plastic dishes replenished with complete culturing media and let recover at least 12 hours.

The day after, 74.000 GFP-positive cells were FACS-sorted using Becton Dickinson (BD) FACSAria IIU using a 100 µm nozzle with 20 PSI pressure.

and seeded onto tissue-culture 24 well replenished in complete culturing media.

Clonal selection was performed and 40 βII-spectrin knock out clones were obtained.

# 4. Confocal, TIRF and STED Microscopy

Confocal microscopy was performed on a Leica TCS SP8 laser confocal scanner mounted on a Leica DMi 8 inverted microscope equipped with motorized stage and controlled by the software Leica Application Suite X (LASX) ver. 3.5.2.18963. For the acquisition, we used a HC PL APO CS2 63X/1,40 oil immersion objective. DIC, Epi-Fluorescence and Total Iinternal Reflection Fluorescence (TIRF) microscopy of fixed specimens, live time-lapse of spreading cells, drug treatments, osmotic shocks and cell compression were performed on a Leica AM TIRF MC system. Two different objectives have been used: HCX PL APO 63X/1.47NA oil immersion and HCX PL APO 100X/1.47NA oil immersion. The lasers used for fluorochromes excitation were 488nm, 561nm, 635nm. A specific dichroic and emission filter for each wavelength has

been used. The microscope was controlled by Leica Application Suite AF software (Ver. 2.6.1.7314) and images have been acquired with an Andor iXon DU-8285_VP camera. For live imaging experiments, environmental conditions have been maintained thanks to an Okolab temperature and CO2 control system if needed. STED super resolution microscopy was performed on a Leica TCS SP8 STED 3X system with 3 depletion lasers (592 nm, 660 nm and 775 nm) mounted on a Leica DMi 8 inverted microscope equipped with motorized stage and controlled by the software Leica Application Suite X (LASX) ver. 3.5.2.18963. The objective used for the acquisition was a HC PL APO 100X/1.40 oil immersion.

## 5. Nearest neighbor distribution (nnd) analysis

For nearest neighbor distribution (nnd) analysis we used a Fiji plugin. Gaussian blur filter (2 pixel radius) was applied to the raw image, before using the Find Maxima tool (noise tolerance applied: 10). The image obtained was then converted to a binary format. The centroid of the cell was used as reference to obtain the nearest neighbor distributions within the cell.

All the values were then plotted using Graphpad Prism.

## 6. Micropatterning

Coverslips were washed with 70% Ethanol, airy-dried, activated with plasma cleaner (Harrick Plasma) for few minutes and incubated with 0.1 mg/ml PLL-PEG for 1 hour at room temperature.

A quartz mask (Delta mask B.V.) wash washed with 70% Ethanol and activated under UV light using a UV lamp (UVO Cleaner, Jellght). Pegylated coverslips were put on the desired pattern in the mask, which then was illuminated under UV light. Patterned coverslips were

coated with 5-25 μg/ml fibronectin for 1 hour at room temperature, washed with PBS and ready for the use.

## 7. Stamping

Coverslips were washed with 70% Ethanol, airy-dried, activated with plasma cleaner (Harrick Plasma) for 3-5 minutes. Polydimethylsiloxane (Sylgard 184 silicone elastomere kit, Dow Corning) was prepared by mixing its two reagents in a ratio of 1:10 and degassed. It was then poured on the mold, degassed again and cured over night at 65°C. PDMS was peeled of the molds and plasma cleaned to make the surface hydrophilic. The stamps were then coated with 10-30 μg/ml fibronectin for 30 minutes at room temperature. Excess of fibronectin was airy-dried and the stamps were gently pressed onto the glass bottom dish for 1 minute and then carefully removed. To passivate the surface of the non-fibronectin coated glass, the surface was treated with a solution of 0.5% PEG-PLL (Ruixibio) for 1 hour in order to avoid cell attachment on the unstamped area. After the incubation, the dishes were rinsed several times with PBS and 1-5x$10^4$ RPTP cells were seeded and cultured at 37 °C in the same media described before.

## 8. Immunofluorescences

The antibody used in this study were the following: mouse anti-βII-spectrin dilution 1:200 (BD-bioscience), rabbit anti-βII-spectrin dilution 1:200 (Abcam), mouse anti-αII-spectrin dilution 1:200 (Invitrogen), rabbit anti β-actin dilution 1:200 (Cell Signaling) and mouse anti-Clathrin Heavy Chain dilution 1:500 (Thermo Fisher, clone X22). Before fixation, cells were seeded on 10 μg/ml fibronectin coated coverslips/glass bottom dishes. Cells of different lines were fixed in 4% paraformaldehyde in PBS for 10 minutes and then neutralized using 10 mM $NH_4Cl$ in PBS for 10 min. Alternatively, fixation was performed in ice-cold methanol for 2’ at -20°C

when cells were immunostained by anti β-actin antibody. Cells were subsequently washed three times with PBS (5' each), permeabilized using PBS containing 0.1% Triton X-100 and blocked with 3-5% BSA for 10 minutes at room temperature. Then, cells were incubated with primary antibody for 1h at room temperature or over-night at 4°C. After 3 washing steps in PBS, cells were incubated with Alexa 488/647-conjugated goat anti-mouse or anti-rabbit dilution 1:400 and Alexa 488/647-conjugated phalloidin dilution 1:400 for 1h at room temperature. For STED microscopy ATTO 594-conjugated goat anti-mouse or anti-rabbit dilution 1:400, ATTO 647N-conjugated goat anti-mouse or anti-rabbit dilution 1:400 and CHROMEO 488-conjugated goat anti-muse or anti-rabbit dilution 1:400 were used. After three washes in PBS of 5' each, cells were mounted with glycerol (for confocal microscopy) or in PBS (for TIRF microscopy) and stored at 4°C. All primary antibodies and fluorophore-conjugated secondary antibodies are listed in supplemental information.

# 9. Spreading assay

The spreading assay was performed on custom-designed 2-way aluminum slides, sealed on the two planar faces by 22x22 mm glass coverslips welded with high vacuum grease (Sigma-Aldrich). Coverslips were previously acid-washed with a 20% $HNO_3$ solution for 2 h at room temperature, followed by a wash in pure acetone before being dried and coated with 10 µg/ml fibronectin for 1 h at 37°C. The chamber was rinsed with 1x RINGER solution and incubated on stage at 37˚, the dual glass surfaces allow simultaneous fluorescence and DIC illumination during media addition/exchange. MEFs were transfected 24h before imaging with the opportune plasmid combinations. Before the experiment, cells were trypsinized, centrifuged 5' at 1200 rpm, washed once with PBS and serum-starved in suspension for 30' at 37˚ in $CO_2$-independent 1X RINGER solution. Suspended cells were thereafter kept at room temperature up to 3 h. For each time lapse, 1-5x$10^4$ cells were fluxed into the imaging chamber to optimally

observe single-cell spreading; for this reason, cell aggregates or debris were carefully avoided during imaging. The time lapse started after a positively double-transfected cell engaged with the fibronectin-coated substrate; this cell was then followed for 15-20' at time rates of 2-5 seconds/frame. For experiments in presence of myosinII-inhibitor blebbistatin (Sigma-Aldrich), cells were suspended in 1x RINGER solution supplemented with blebbistatin at 50μM final concentration; imaging chambers were filled with the same 1x RINGER solution supplemented with blebbistatin to avoid rebound effects. The correct cell behaviour was monitored by DIC acquisition in terms of cell integrity, isotropic spreading, lamellipodia formation and buckling, while the fluorescent channels were analysed as described in the next sections.

# 10. Spectrin and actin intensities at the cell edge

For cell edge analysis a custom macro for Fiji was written. Signal background was subtracted, while edge-preserving filters were applied to the actin fluorescence signal to generate a binary mask of the growing cell area over time. The centroid of the cell was used as reference point to identify each angle between $0^0$ and $359^0$ on the cell outer circumference. From the edge, the signal was eroded by 25 pixel (≈3.2μm at resolution of ≈130nm/pixel) and mean intensity of the fluorescent signals were computed into the final kymographs composed of 360 pixel on the x axis, one for each angle, while the y axis represents the total number of frames. Speed of the cell edge was extrapolated from the variation in pixel from the centroid at known pixel size and time frame. Values were considered positive when the edge moved away from the centroid and negative when it moved closer. For comparisons between independent cells, actin and spectrin intensity measurements were normalized to 1 at null speed. Results were analyzed and plotted with R and the ggplot2 R package.

## 11. Correlated Spectrin and actin flow velocity analysis (PIV)

Correlation between speed and directionality of the two fluorescent channels have been performed on the same live TIRFM datasets during the spreading analyzed for cell edge dynamics. Signal background was subtracted. Particle Image Velocimetry (PIV) was performed independently on single fluorescent channels by a custom macro in Fiji, excluding the portion of the cell close to the edge (50 pixel) and the frames corresponding to the initial spreading phase P1 from the analysis (50 frames). The resulting vector fields of the two channels (i.e. RFP-actin and GFP-βII-spectrin) mapped both the speed magnitude and directionality (angle) of the channels independently. To identify synchronous angular and speed correlations between the two channels, their correlation was binarized by giving a value of 1 to areas where the speeds of the two channels were within +/-50% of each other, and where the directions shared the same quadrant (i.e. when the difference of angle was less than $\pi/2$). Areas that did not meet these criteria were assigned a value of 0. The fraction of correlated flow velocities was then given as the ratio between the area covered by correlated velocities and the area of the cell after excluding the edge portion.

## 12. Cytoskeletal Drug Perturbation and osmotic shocks

MEFs were transfected 24h before imaging with opportune pair of constructs as previously described. Before imaging, cells were trypsinized and seeded on glass coverslip coated with 10µg/ml fibronectin ($1x10^3$). Cells were seed and let attach to the substrate for 1 h; the media was replaced with $CO_2$-independent 1x RINGER solution and mounted on a 2-way imaging chamber that allow on-stage media exchange as previously described for the spreading assay. Time lapse consisted of an initial phase of 5’ where sufficient frames were acquired at steady-

state (internal control), the media was then replaced by 1x RINGER solution supplemented with the opportune cytoskeletal impairing drugs exceeding the volume of the imaging chamber to avoid dilution of final drug concentrations. Specifically, 1μM Latrunculin A, 10μM Blebbistatin, 5 μM Nocodazole and 5mM Diamide were singularly used (Sigma-Aldrich). Perturbed cells were then imaged for 30' at 1-5 minute/frame. Intensity calculations were carried out in Fiji by subtracting the background and creating a dynamic binary mask of the GFP-βII-Spectrin signal; the built-in "analyze particle" tool was applied to obtain mean fluorescence intensity values at different time points. Only untreated, 5' and 30' after treatment time points were plotted using the software Graphpad Prism.

For experiments that required osmotic shocks, MEFs cells were treated following the same procedure described earlier for cytoskeletal perturbations. Time lapse was obtained at higher temporal resolution (2-5 second/frame). At given time points (every 3' or 5' depending on the experiment), the media was replaced with hypotonic 0.5x or 0.1x RINGER solution, exceeding the volume of the imaging chamber to avoid incomplete media exchange. Mean intensity calculation was done in Fiji by subtracting the background and creating a dynamic binary mask to derive fluorescence intensity parameters over the time frame. In case of ratio measurements between the two fluorescent channels, mean intensities of the first two frames of the two channels were averaged and arithmetically matched to obtain the initial ratio value of 1. Indeed, the purpose of these experiments was to calculate the fluctuation in content more than a stoichiometric measurement between the two fluorescent proteins. Intensity data were then averaged, analyzed and plotted using the software Graphpad Prism.

# 13. Cell stretching

Cell stretching experiments were performed using an automated cell stretching dish (International patent: WO 2018/149795 A1). The components of the cell stretching dish were

designed using SolidWorks software and 3D printed using a stereolithography-based 3D printer (Formlabs) coupled with an autoclavable and biocompatible dental resin (Dental SG resin, Formlabs). The printed parts were rinsed in isopropyl alcohol for 5 minutes to remove any uncured resin from their surface, and then in a UV box to finalize the polymerization process and stabilize mechanical properties. The printed parts were then polished and assembled to create the lower (cell chamber) and the upper portion (aperture driver) characterizing the stretching dish. Prior to the experiments, the components of the lower portion were autoclaved to be sterilized and assembled to clamp a deformable silicone membrane (thickness 0.005″, SMI), thus creating a cell culture chamber. The dish was coated with fibronectin (10 µg/ml) and incubated at 37 °C for 1 hour. A total of $10^5$ cells were seeded in the cell chamber and let spread for 1-2 hours at 37 °C. Before starting the imaging, the whole cell stretching dish was assembled by connecting the upper portion, consisting in the driving unit, to the cell culture chamber. Biaxial stretching was applied to all the samples under investigation. The EPI-fluorescence mode of the Leica AM TIRF MC system was used. Due to technical limitations such as re-focusing and re-centering of the cell under investigation, after each 5% step increase in the biaxial stretch obtained by the software-controlled motorized device, a single frame in the two fluorescent channels was recorded.

# 14. Cell compression

Cell compression experiments were performed using a cell compression device (International patent: WO 2019/086702 A1, see picture below) capable of applying dynamic compression stress to single cells. The main components of the compression device were designed using SolidWorks software and 3D printed using a stereolithography-based 3D printer (Form 2, Formlabs), following the same procedure described in for the cell stretching device. The cell compression device consists of an air chamber connected to an air pressure regulator. Prior to

the experiments, a Polydimethylsiloxane (PDMS, Sylgard 184) piston was microfabricated to have circular pillars (200 μm in diameter) on its surface, and attached to a deformable silicone membrane (thickness 0.005″, SMI) through plasma bonding. The membrane with the piston was then clamped to the air chamber. The assembled cell compression device was connected to the air pressure regulator and then locked to cell culture dish (seeded with cells) through mechanical ribs. In particular, a total of $10^5$ cells were seeded on 27mm Ø Nunc Glass Base Dishes (Thermo Scientific), exchanged to 1x RINGER solution 30 minutes before imaging and the original Petri lid replaced by the compression device. A dynamic compressive load was applied to cells by increasing the air pressure inside the compression device through the pressure regulator, thus controlling the movement of the membrane and the piston to compress the cells underneath. DIC and TIRF illumination was used to monitor cell reaction at 5 seconds/frame rate. ROIs to measure fluorescence intensity fluctuation were drawn in Fiji, while the DIC was used to monitor the engagement of the piston with the cell roof. As the compression strain increased, the cell became flatter and DIC imaging decreased its contrast in physiologically flat fibroblasts. Due to cell height variation, the device does not allow precise absolute read-out of the pressure applied to cells, being cell deformation a non-controllable variable. For this reason, two different approaches were applied. The first one was intended to cause maximal cell response: compression pressure was slowly increased until bleb formation was observed. For i-bleb/cortex ratio, mean fluorescence intensities in the two channels were obtained in the projected bleb area, and divide by the mean fluorescence intensities in the adjacent cortical region of similar area. The second approach was designed to better control the applied strain: the initial compression was thus set at the first value required to engage the piston with the top of the cell as monitored by DIC. This first step hardly caused a reaction monitorable by TIRF at basal cell level but allowed consistency between independent experiments, for this reason six different cycles of compression (2 minutes) and relaxation (2 minutes) were performed at increasing pressure, as schematized in

D; the 2 minutes compression step duration was chosen to allow adaptive mechanisms to occur and avoid long-term detrimental effects on cell integrity. Intensity calculations were carried out in Fiji by subtracting the background and drawing ROIs across the perinuclear rim formed during compression. Pre-stretch mean intensity for each single compressive event was divided by maximal mean intensity registered during the subsequent 2 minutes compressive step. Data were plotted using the software Graphpad Prism.

## 15. Frap experiments

MEFs cells expressing GFP-βII-spectrin constructs were imaged 24 hours after transfection with a Confocal Spinning disk microscope (Olympus) equipped with a iXon 897 Ultra camera (ANDOR) and a FRAP module furnished with a 405nm laser. The environmental control was maintained with an OKOlab incubator. Images are acquired using a 100x/1.35Sil silicone oil immersion objective. MEFs were trypsinized and seeded on glass-bottom dishes (Matek, Sigma-Aldrich) coated with 10 µg/ml fibronectin. Before imaging, $CO_2$-independent media without phenol-red was exchanged. Squared Regions Of Interest of 5x5µm length were photo-bleached with the 405 nm laser at 50% intensity and post-bleach images were followed with 15 to 20% laser intensity for 100 frames (1 frame every 5 seconds for full length and truncated GFP-βII-spectrin constructs and 0.5 seconds for PE-only). FRAP data were analyzed and curves fitted to the one-exponential recovery equations (one-phase association) by the software Graphpad Prism:

$$I= I_0+Imax*[1-e^{-(k)*(t)}]$$

Where I is the relative intensity compared to the pre-bleach value, k represents the association rate, and t is the half time recovery expressed in seconds.

For the dual FRAP assay, cells were seeded on fibronectin-coated glass coverslip and mounted on the 2-way imaging chamber that allow on-stage media exchange as previously described for spreading assay and osmotic shocks. The first FRAP measurements was conducted in serum-free 1x Ringer solution; at completion, the media was exchanged and independently supplemented with the cytoskeletal drugs at the concentration used before. Specifically, 1 μM Latrunculin A, 10 μM Blebbistatin, 5 μM Nocodazole and 5 mM Diamide (Sigma-Aldrich). Cells were allowed to equilibrate with the new media for 5 minutes; afterward, a second FRAP analysis was started on the same cell previously analyzed.

# 16. Clathrin pits density maps

TIRF images were acquired as previously described. For analysis of fixed specimens, 2x2μm ROIs were selected by segmenting discrete pits of random sizes, not overlapping with neighbouring structures. All images were stacked in FIJI for pit size calculation. CHC/AP2 Images were scaled by a factor of 10, Yen auto-threshold applied to create a binary mask and particle size calculated by the "Analyse particle" tool in FIJI. ROIs were divided at this point according to size that considered the diffraction limitation of TIRF microscopy (<300nm$^2$ and 300-500nm$^2$); particle bigger that 500nm$^2$ were not considered informative. Raw images of the two cluster were then independently stacked and z-projected for median intensity values. Gaussian blur filter (1pixel radius) and a scale factor of 10 were applied to the projected images to homogenize the signals. Scaled-projected images of the two particle-size groups were then matched for signal intensities between corresponding channels. Normalized radial plots were generated by the Radial Profile plugin (FIJI) on the final 2x2μm projected images.

For live imaging datasets, Unsharp Mask (1pixel radius, 0.6 weight) and Gaussian blur filter (1pixel radius) were applied to the raw images before ROIs selection. No additional filters were applied to the final projected images.

## 17. Statistical analysis

All the graphs and plots are presented as mean ± SD, with the exception of the FRAP recovery curves that are presented as mean ± SEM. These experiments were further analysed by fitting to an exponential equation, therefore the authors considered trivial to show the accuracy of the mean (better described by definition by SEM) instead of the intrinsic variability between independent experiments. Statistical analysis by unpaired T-test was performed when comparison between two experimental groups was required (i.e. normalized i-bleb/cortex ratio). One-way Anova analysis was performed when multiple experimental groups were present, multiple comparison between two groups were also performed in parallel, as shown for the quantification of maximal intensity at the cell body during the sequential compression protocol. All the experiments were performed in triplicate or more, as specifically indicated in the figure legends.

## 18. RNA extraction and qPCR analysis

Cells were lysed and RNA was extracted with the RNAeasy Mini Kit (Qiagen).

1 µg of RNA was retrotranscribed using "qScript cDNA Synthesis kit" (Quantabio).

For gene expression analysis, 5ng of cDNA was amplified (in triplicate) in a reaction volume of 10 uL containing the following reagents: 5ul of "TaqMan® Fast Advanced Master Mix, Thermofisher", 0.5 ul of "TaqMan Gene expression assay 20x, Thermofisher" (Mm01315345_m1, Mm01180701_m1, Mm01326617_m1, Mm00661691_m1, Mm01284057_m1, Mm01239117_m1); SPTBN5 primers were custom designed (Fw: GGACGCCAGTGTTCACCAA Rev: GCCCCCTTGTAGCAGCTT). Real-time PCR was carried out on the 7500 Real-Time PCR System (Thermofisher), using a pre-PCR step of 20s at 95°C, followed by 40 cycles of 1s at 95°C and 20s at 60°C. Samples were amplified with primers and probes for each target and for all the targets one NTC sample was run.

Raw data (Ct) were analyzed with “Biogazelle qbase plus” software and the fold change was expressed as CNRQ (Calibrated Normalized Relative Quantity) with Standard Error (SE). Gapdh was used as reference to normalize the data.

The entire process (retrotranscription, gene expression and data analysis) was performed by the qPCR-Service at Cogentech-Milano.

# 19. Resource Tables and Schemes

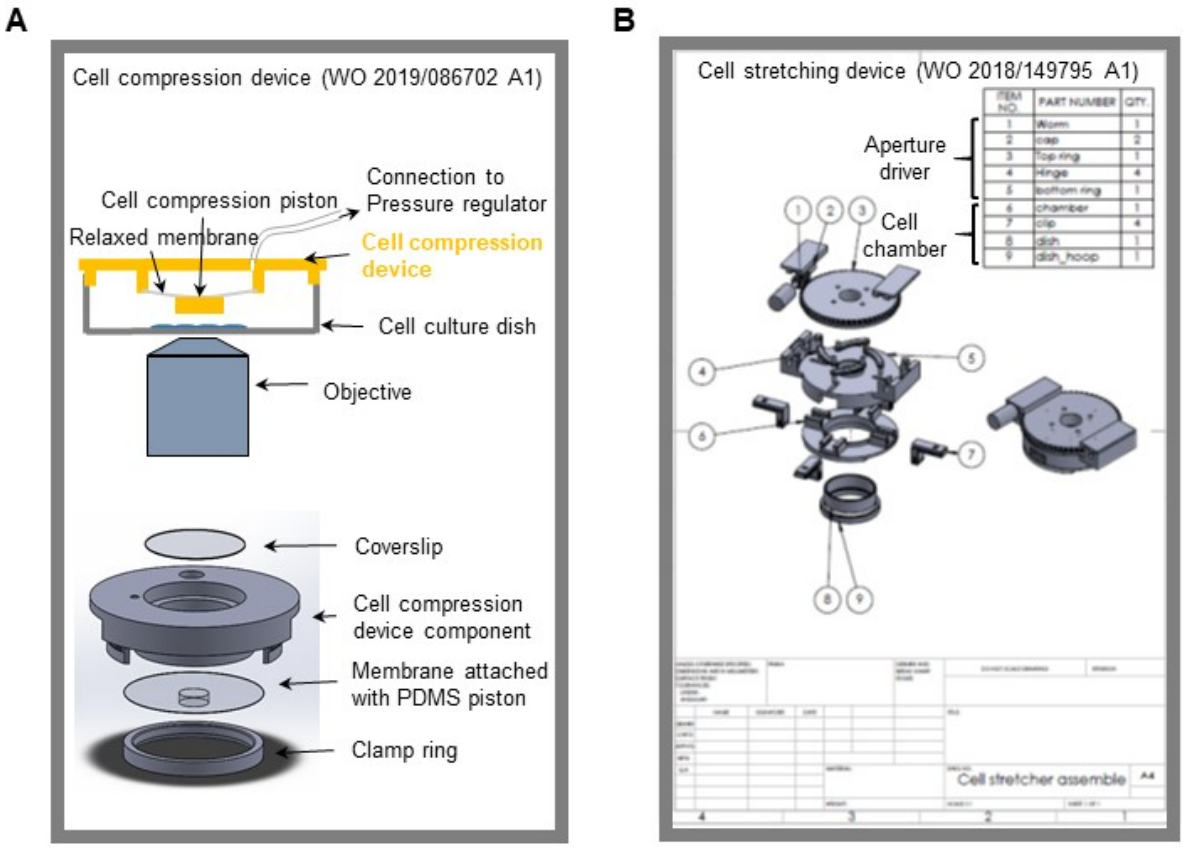


# 20. Schematical representation of the devices used for cell compression/stretching experiments

| List of Antibodies | Source | Identifier |
|---|---|---|
| Mouse anti-SPTBN1 | BD Bioscience | BD-612563 |
| Rabbit anti-SPTBN1 | Abcam | AB-72239 |
| Rabbit anti-SPATN1 | Invitrogen | PA5-35383 |
| Rabbit-anti β-Actin | Cell Sign | D6A8 |
| Mouse-anti Tubulin | Sigma | T9026 |
| Mouse Clathrin-heavy chain | Thermo Fisher | clone X22 |
| Phalloidin AlexaFluor488 | Invitrogen | A12379 |
| Phalloidin AlexaFluor568 | Invitrogen | A12380 |
| Rabbit-anti mouse HRP | BioRad | 1706516 |
| Mouse-anti rabbit HRP | BioRad | 1706515 |
| Donkey anti-mouse AlexaFluor488 | Thermo Fisher | A21202 |
| Donkey anti-rabbit AlexaFluor488 | Thermo Fisher | A21206 |
| Donkey anti-mouse AlexaFluor647 | Thermo Fisher | A31571 |
| Donkey anti-rabbit AlexaFluor647 | Thermo Fisher | A31573 |
| Donkey anti-mouse Cy3 | Jackson Imm Res | 715-165-150 |
| Donkey anti-rabbit Cy3 | Jackson Imm Res | 711-165-152 |
| Goat anti-rabbit ATTO 594 | Sigma Aldrich | 77671 |
| Goat anti-mouse ATTO 594 | Sigma Aldrich | 76085 |
| Goat anti-rabbit ATTO 647N | Sigma Aldrich | 40839 |
| Goat anti-mouse ATTO 647N | Sigma Aldrich | 50185 |
| HRP Goat-anti rabbit CHROMEO 488 | Active Motif | 15014 |
| HRP Goat-anti mouse CHROMEO 488 | Active motif | 15014 |

| Ringer buffer for Live Microscopy | Composition |
|---|---|
| 1x | 150 mM NaCl, 1mM $MgCl_2$, 1mM $CaCl_2$, 20 mM Hepes (pH 7.4), 5 mM KCl and 2g/l glucose |
| 0.5x | 75 mM NaCl, 1mM $MgCl_2$, 1mM $CaCl_2$, 10 mM Hepes (pH 7.4), 2.5 mM KCl and 1g/l glucose |
| 0.1x | 15 mM NaCl, 1mM $MgCl_2$, 1mM $CaCl_2$, 2 mM Hepes (pH 7.4), 0.5 mM KCl and 0.2g/l glucose |
| 1.5x | 225 mM NaCl, 1mM $MgCl_2$, 1mM $CaCl_2$, 30 mM Hepes (pH 7.4), 7.5 mM KCl and 3g/l glucose |

| *List of Plasmids* | *Source* | *Identifier* |
|---|---|---|
| GFP-SPTBN1 | This manuscript | |
| GFP-Actin | MBI | |
| RFP-Actin | MBI | |
| mCherry-SPTBN1 | This manuscript | |
| GFP-SPTBN1-mCherry | This manuscript | |
| GFP-PM (Lyn) | Addgene | 21213 |
| Scarlet-PM (Lck) | Addgene | 98821 |
| GFP-SPTBN1 ΔPE | This manuscript | |
| GFP-SPTBN1 ΔPS | This manuscript | |
| GFP-SPTBN1 ΔABD | This manuscript | |
| GFP-SPTBN1 PE only | This manuscript | |
| mCherry-AP2σ | DiFiore' Lab | |
| LifeAct-Ruby | MBI | |
| RFP-Myosin Light Chain | MBI | |
| pSpCas9(BB)-2A-GFP | Scita's Lab | |

| *List of cell lines* | *Source* |
|---|---|
| Immortalized MEF (RPTP $\alpha$ +/+ background) | Sheetz' Lab |
| NIH-3T3 | IFOM cell bank |
| HS27 | IFOM cell bank |
| RPMI | IFOM cell bank |
| A431 | IFOM cell bank |
| MCF-10A | IFOM cell bank |
| MDA-MB231 | IFOM cell bank |
| Hela | IFOM cell bank |
| HUVEC | IFOM cell bank |

| *List of Reagents* | *Source* | *Identifier* |
|---|---|---|
| Nitric acid | Sigma | 438073 |
| Latrunculin A | Sigma | L5163 |
| Blebbistatin | Sigma | B0560 |
| Nocodazole | Sigma | M1404 |
| Diamide | Sigma | D3648 |
| Hexamethyldisilazane | Sigma | 440191 |
| Sylgard 184 silicone elastomere kit | Dow Corning | 1064291 |
| PEG-PLL | Ruixibio | R-PL1226 |
| Silicone membrane | SMI | |
| Dow Corning® high-vacuum silicone grease | Sigma | Z273554-1EA |
| FM4-64 FX | Thermo Scientific | F34653 |

| *List of cell culture reagents* | *Source* | *Identifier* |
|---|---|---|
| DMEM High Glucose | Lonza | BE12-614F |
| HAM'S F12 | Biowest (VWR) | L0136-500 |
| Leibovitz L15 | Biowest (VWR) | L0300-500 |
| Endothelial Cell Growth Medium | Cell Applications, inc | 211-500 |
| Fetal Bovine Serum | Euroclone | ECS0182L |
| Horse Serum | Life Technologies | 16050-122 |
| Cholera Toxin | Sigma-Aldrich | C8052-2MG |
| Holo Transferrin | Sigma-Aldrich | T0665-100MG |
| Hydrocortisone | Sigma-Aldrich | H0888-1G |
| Insulin (Bovine pancreas) | Sigma-Aldrich | I0516-5ML |
| L-Glutamine | Euroclone | LOBE17605F |
| Sodium Pyruvate | Microtech | L0642 |
| Trypsin-EDTA | Euroclone | ECB3052D-20 |
| Penicillin Streptomycin | Euroclone | ECB3001L |
| Puromycin | Vinci-Adipogen | AG-CN2-0078-M100 |
| Fibronectin | Roche | 11080938001 |

| ***Microscopes*** | ***Brand*** |
|---|---|
| TIRF | Leica |
| SP5 laser scanning confocal | Leica |
| SP8 laser scanning confocal | Leica |
| Spinning Disk Confocal Unit | Olympus |

| ***Devices*** | ***Source*** | ***Patent number*** |
|---|---|---|
| Cell compression | IFOM | WO 2019/086702 A1 |
| Cell stretcher | IFOM | WO 2018/149795 A1 |
| Aluminum coverslip holder | Nils Gauthier | |
| Micropatterning wafer | MBI/IFOM | |

| ***Softwares*** | ***Brand*** |
|---|---|
| LAS X | Leica |
| CellSense | Olympus |
| Prism | Graphpad |
| Image Lab (5.0) | Biorad |
| Fiji | NIH |
| R studio | |
| Illustrator | Adobe |

## STED analysis, one phase decay

| One phase decay | |
|---|---|
| **Best-fit values** | |
| Y0 | 132.6 |
| Plateau | -14.52 |
| K | 2.878 |
| Half Life | 0.2409 |
| Tau | 0.3475 |
| Span | 147.2 |
| **95% CI (profile likelihood)** | |
| Y0 | 115.1 to 154.9 |
| Plateau | -43.44 to 5.899 |
| K | 1.820 to 4.173 |
| Half Life | 0.1661 to 0.3810 |
| Tau | 0.2397 to 0.5496 |
| **Goodness of Fit** | |
| Degrees of Freedom | 193 |
| R squared | 0.4657 |
| Sum of Squares | 52971 |
| Sy.x | 16.57 |
| **Constraints** | |
| K | K > 0 |
| | |
| **Number of points** | |
| # of X values | 196 |
| # Y values analyzed | 196 |

**Spreading area/specrin and area/actin linear regression analysis**

| | ***Actin Integrated Density*** | ***Spectrin Integrated Density*** |
|---|---|---|
| Pearson correlation coefficient Linear regression | 0.5386254 | 0.7296664 |
| **Best-fit values** | | |
| B0 | 4.758e+02 | 4.708e+02 |
| B1 | 4.459e-05 | 4.405e-05 |
| **Std. Error** | | |
| B0 | 4.260e+01 | 2.821e+01 |
| B1 | 3.962e-06 | 2.345e-06 |
| **T value** | | |
| B0 | 11.17 | 16.69 |
| B1 | 11.26 | 18.79 |
| **Goodness of Fit** | | |
| Degrees of Freedom | 371 | 301 |
| Multiple R-squared | 0.2901 | 0.5324 |
| Adjusted R-squared | 0.2878 | 0.5309 |
| p-value | 2.2e-16 | 2.2e-16 |
| Beta estimate | 4.45906e-05 | 4.40486e-05 |
| Standard error | 3.96159e-06 | 2.344543-06 |
| T value | 11.25574 | 18.78771 |
| P value | 7.35929e-25 | 4.67908e-53 |
| F statistic | 7.16465e-25 | 7.16465e-25 |
| F | 4.45906e-05 | 4.40486e-05 |
| Model p | 3.96159e-06 | 2.34454e-06 |
| Outliers | 12 | 12 |

## Dual FRAP Analysis

| Diamide | | | Nocodazole | | Latrunculin A | | Blebbistatin | |
|---|---|---|---|---|---|---|---|---|
| Control | | Treated (5') | Control | Treated (5') | Control | Treated (5') | Control | Treated (5') |
| **One-phase association Best-fit values** | | | | | | | | |
| Y0 | 0.009453 | 0.01164 | -0.05037 | 0.02238 | -0.01107 | -0.08307 | -0.004542 | -0.002546 |
| Plateau | 0.8569 | 0.3446 | 0.8513 | 0.8262 | 0.8294 | 0.8526 | 0.8371 | 0.6676 |
| K | 0.01803 | 0.01437 | 0.0196 | 0.01504 | 0.01989 | 0.02544 | 0.02008 | 0.01698 |
| Tau | 55.45 | 69.59 | 51.01 | 66.48 | 50.29 | 39.3 | 49.79 | 58.91 |
| Half-time (sec) | 38.44 | 48.24 | 35.36 | 46.08 | 34.86 | 27.24 | 34.51 | 40.83 |
| Span | 0.8474 | 0.3329 | 0.9017 | 0.8038 | 0.8405 | 0.9357 | 0.8417 | 0.6701 |
| Std. Error | | | | | | | | |
| Y0 | 0.02527 | 0.03849 | 0.01835 | 0.02037 | 0.02294 | 0.03224 | 0.02625 | 0.02802 |
| Plateau | 0.006448 | 0.01448 | 0.004094 | 0.007067 | 0.005005 | 0.004843 | 0.00564 | 0.007901 |
| K | 0.000843 | 0.003078 | 0.0005928 | 0.0006812 | 0.0007993 | 0.001125 | 0.0009171 | 0.00116 |
| Span | 0.02315 | 0.0336 | 0.01704 | 0.01798 | 0.02135 | 0.03085 | 0.02447 | 0.02539 |
| **95% Confidential Interval** | | | | | | | | |
| Y0 | -0.04013 to 0.05903 | -0.06389 to 0.08716 | -0.08638 to -0.01436 | -0.01760 to 0.06236 | -0.05608 to 0.03393 | -0.1463 to -0.01982 | -0.05606 to 0.04698 | -0.05753 to 0.05244 |
| Plateau | 0.8442 to 0.8695 | 0.3161 to 0.3730 | 0.8433 to 0.8594 | 0.8123 to 0.8401 | 0.8196 to 0.8392 | 0.8431 to 0.8621 | 0.8260 to 0.8482 | 0.6521 to 0.6831 |
| K | 0.01638 to 0.01969 | 0.008330 to 0.02041 | 0.01844 to 0.02077 | 0.01371 to 0.01638 | 0.01832 to 0.02145 | 0.02324 to 0.02765 | 0.01828 to 0.02188 | 0.01470 to 0.01925 |
| Tau | 50.80 to 61.05 | 49.00 to 120.0 | 48.15 to 54.22 | 61.05 to 72.96 | 46.61 to 54.59 | 36.17 to 43.04 | 45.70 to 54.69 | 51.95 to 68.03 |
| Half-time | 35.21 to 42.32 | 33.96 to 83.21 | 33.38 to 37.59 | 42.32 to 50.57 | 32.31 to 37.84 | 25.07 to 29.83 | 31.67 to 37.91 | 36.01 to 47.15 |
| Span | 0.8020 to 0.8928 | 0.2670 to 0.3988 | 0.8683 to 0.9351 | 0.7685 to 0.8391 | 0.7986 to 0.8824 | 0.8751 to 0.9962 | 0.7936 to 0.8897 | 0.6203 to 0.7199 |
| **Goodness of Fit** | | | | | | | | |
| Degrees of Freedom | 1149 | 1149 | 1053 | 1053 | 1149 | 1149 | 957 | 1149 |
| R square | 0.6867 | 0.1122 | 0.8441 | 0.7471 | 0.7357 | 0.6725 | 0.7202 | 0.5177 |
| Absolute Sum of Squares | 15.39 | 47.97 | 6.027 | 10.69 | 10.97 | 14.27 | 9.822 | 20.59 |
| Sy.x | 0.1157 | 0.2043 | 0.07566 | 0.1007 | 0.09771 | 0.1114 | 0.1013 | 0.1339 |

**FRAP analysis deletion mutants**

| | WT | ΔPE | ΔABD | PE-only |
|---|---|---|---|---|
| **One-phase association Best-fit values** | | | | |
| Y0 | -0.05615 | -0.01408 | -0.1411 | -2.811 |
| Plateau | 0.7485 | 0.7320 | 0.8718 | 0.8699 |
| K | 0.01662 | 0.01220 | 0.02823 | 0.0004781 |
| Tau | 60.18 | 81.94 | 35.43 | 2091 |
| Half-time (seconds) | 41.71 | 56.80 | 24.56 | 1450(msec) |
| Span | 0.8046 | 0.7461 | 1.013 | 3.681 |
| Std. Error | | | | |
| Y0 | 0.01209 | 0.01963 | 0.02240 | 0.3488 |
| Plateau | 0.003295 | 0.009428 | 0.002599 | 0.002656 |
| K | 0.0003987 | 0.0006632 | 0.0007211 | 2.293e-005 |
| Span | 0.01091 | 0.01635 | 0.02164 | 0.3483 |
| **95% Confidence Intervals** | | | | |
| Y0 | -0.07986 to -0.03244 | -0.05258 to 0.02442 | -0.1850 to -0.09716 | -3.495 to -2.126 |
| Plateau | 0.7420 to 0.7549 | 0.7135 to 0.7505 | 0.8667 to 0.8769 | 0.8647 to 0.8751 |
| K | 0.01584 to 0.01740 | 0.01090 to 0.01350 | 0.02681 to 0.02964 | 0.0004332 to 0.0005231 |
| Tau | 57.48 to 63.15 | 74.05 to 91.72 | 33.74 to 37.30 | 1912 to 2309 |
| Half-time | 39.84 to 43.77 | 51.33 to 63.57 | 23.38 to 25.85 | 1325 to 1600(msec) |
| Span | 0.7832 to 0.8260 | 0.7140 to 0.7781 | 0.9704 to 1.055 | 2.997 to 4.364 |
| **Goodness of Fit** | | | | |
| Degrees of Freedom | 2205 | 1437 | 1341 | 1533 |
| R square | 0.8218 | 0.6519 | 0.8362 | 0.5420 |
| Absolute Sum of Squares | 12.62 | 20.83 | 6.211 | 14.52 |
| Sy.x | 0.07565 | 0.1204 | 0.06806 | 0.09732 |

# Discussion

Here, we provide a comprehensive understanding of how the ubiquitous and highly conserved protein spectrin dynamically interacts with the acto-myosin cortex, PM and the endocytic machinery in order to sustain the cell during both intrinsic and extrinsic mechanoadaptive events, as represented in the cartoon in figure 43.

## 1. Spectrin and actin define a universal and 21. complementary pattern, suggesting an interchangeable role in PM sustainment

Our analysis on different cell types, grown under different constrains, revealed the presence of different PM territories either supported by actin or spectrin cytoskeletons. Particularly, we identified four different subcellular regions where this mutual exclusion was more evident, thus suggesting their complementary distributions and roles (Figure 45; zones I, IV, VII and stress fibers at cortex cycle 3).

Spreading assays on living cells well described spectrin and actin dynamic distribution and organization during early phases of cell interaction and adhesion with the substrate, giving more details about their interplay. By deeply focusing on spreading movies, it was possible to discriminate between two different behaviours; indeed, at the cell edge, actin-enriched protrusions and spectrin-enriched retractions suggested cooperative but opposite roles in supporting the plasma membrane during intrinsic mechanoadaptive processes (Figure 45; zones I and VII). On the contrary, at the cell body level, actin and spectrin seemed to move in a more coordinated and homogeneous way, even if never colocalized. Particularly, we observed the formation of peculiar actin nodes, which were passively followed by spectrin mesh, even after

treatments with cytoskeleton impairing drugs. These results highlighted, for the first time, a possible involvement of spectrin in the cell sustainment whenever actin is not present, like in cell retractions or upon acto-myosin cortex remodelling; working as an additional scaffold for the PM which can mutate its density depending on changes in cell shape, dynamics or mechanics (Figure 45; cell cortex cycles 1 to 3).

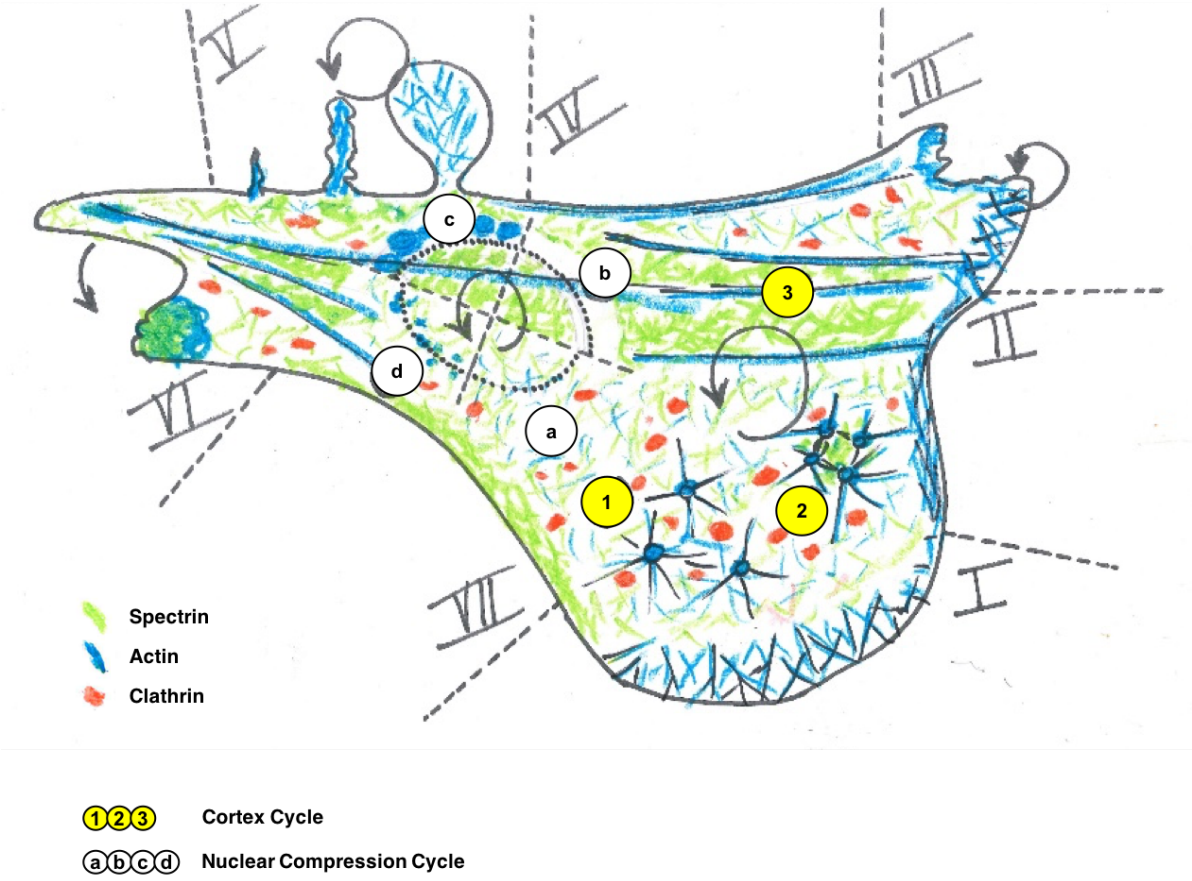


**Figure 45. Model of the mesoscale organization and dynamics of spectrin-actin-plasma membrane territories.**

(I) to (VII) highlight the cell edge behavior. (I) Upon protrusion actin polymerization dominates. (II) During contraction actin is condensed and forms transverse arcs. In I and II spectrin is secluded and "passively" follow acto-myosin lead. (III) Deletion of the Actin binding domain of spectrin induce edge instability upon contraction activation. (IV) Mature actin bundles sustain the PM, spectrin is not recruited to those actin curvatures. (V) Upon cell compression blebs enriched with actin but devoid of spectrin are formed. While actin polymerize and condense in the bleb, spectrin localizes and marks the former position of the cell edge before compression. (VI) Abrupt cell detachment induces a "plug-like" formation in which actin and spectrin seem to colocalize. (VII) In actin depleted

but spectrin-rich edge curvature, spectrin condenses as the edge move inward, potentially holding the PM and responding to the increased membrane load. (a) to (d) highlight the cell cortex behavior under nuclear compressive stress. (a) to (b) The native acto-spectrin cortex get cleared under the edges of the nuclear envelope upon compression. (c) During compression, in this gap of cleared membrane, actin polymerization occurs and fills up progressively the bare bilayer. (d) Upon relaxation, spectrin meshwork elastically recoils, entangling the polymerizing actin and restoring the original cortex organization. Stress fibers under the nucleus are not affected by the compression. (1) to (3) highlight the cell cortex behavior. (1) In spectrin-less zones, actin nodes can form. (2) These aster-like structures move and coalesce upon myosin II mediated contractility. This mechanism modifies spectrin meshwork local density synchronously, with expansion and condensation between coalescing nodes. Further acto-myosin condensation lead to bundles formation interleaved by spectrin-rich territories. (3) These high-density zones impede clathrin-mediated endocytosis (red dots), which otherwise occurs between spectrin fences. Those steps occur cyclically upon cell control or drugs/mechanical stimuli.

## 2. Myosin contractility and actin protofilaments are both necessary for spectrin ability in the PM stabilization

Interestingly, when we performed Blebbistatin treatment during spreading, cells were not able to undergo cycles of contraction and protrusions, and we couldn't appreciate the presence of actin-rich protrusions or spectrin-rich retractions anymore. This, suggested a possible involvement of the acto-myosin contractile machinery in the regulation of spectrin meshwork dynamics.

Indeed, FRAP experiments confirmed our hypothesis, showing how spectrin turnover is mainly regulated by myosin contractility. Interestingly, despite the presence of an actin binding domain, which is well conserved among all the proteins belonging to the "spectrin

superfamily", Latrunculin A treatment didn't have any significant effect on spectrin molecular turnover, whereas contributed to spectrin remodelling at a mesoscale level, in correspondence of the new formed actin nodes. This could be due to the fact that spectrin binding capability is restricted only to actin protofilaments, composed by 13-15 G-actin monomers (Bañuelos et al., 1998; Picart and Discher, 1999), that are too short and rigid to generate contractility and, probably, since they are protected by other capping proteins, to be affected by that specific drug treatment (Koenderink and Paluch, 2018). Moreover, this peculiar actin binding ability, could also explain the characteristic exclusion of spectrin from actin stress fibers and protrusive structures such as lamellipodia or filopodia.

Given the acto-myosin cortex ability to regulate the meshwork dynamics, it is not really clear how this mechanism could generate a homogenous movement within the cell (Koenderink and Paluch, 2018). The presence of small actin protofilaments, holding together spectrin heterotetramers, could explain this paradox. Indeed, ABD removal from βII-Spectrin, impaired the protein dynamics and cell spreading capacity, thus leading to cell edge instability, characterized by synchronous spectrin/actin retractions (Figure 45, zone III). Taken together all these observations, we speculated that spectrin meshwork can act as a "veil-like" structure, underneath the PM, able to transmit the force by creating a continuum between the edge of the cell and the contractile machinery. However, also long-term perturbations of others cytoskeleton structures, such as Nocodazole mediated microtubule disruption, affected spectrin meshwork organization, probably through depalmitoylation or dephosphorilation of residues important for its association with the PM, thus impairing membrane trafficking regulation (Jenkins et al., 2015), but further investigations regarding the time scale and the mechanisms in our cellular system are still required.

# 3. Spectrin is an elastic and continuous meshwork

Spectrin has been described in literature as an elastic meshwork, which can be stretched or relaxed, with a variable length between 50 and 200 nm, depending on the cell type and on the sample processing protocol used (Pan et al., 2018). Here, we found a distribution in which spectrin intramolecular distance peaked at 150 nm, and the 95% of the values ranged from 70 nm to 220 nm. These results suggested a spectrin elastic characteristic, which length was able to fluctuate among different regions of the same cell. A recent work performed on erythrocytes, has proposed that the presence of spectrin-void regions at the PM level did not affect membrane integrity; indeed, these cytoskeleton-empty zones can work as weak regions that help red blood cells in changing their shape during circulation (Pan et al., 2018).

Given these observations, we speculated that spectrin in fibroblasts exists as a dynamic and continuous meshwork, which appear to be less uniform, compared to the polymeric structure described both in erythrocytes and axons. Indeed, from our results, spectrin meshwork seems to be similar to the model proposed by Jenkins et al., 2015 for lateral membranes of epithelial cells, where spectrin is proposed to be confined into microdomains at plasma membrane level, in a dynamic equilibrium with the endocytic machinery. Non-homogeneous spectrin distributions within the cell hinted at its protective role, thus suggesting spectrin ability to act as a fence at the plasma membrane level, helping the cell to resist both extrinsic and cell-driven mechanical perturbations.

# 4. Spectrin fencing mechanism depends on cycles of condensation/decondensation upon different mechanical stimuli

Further confirmations to our hypothesis came from stretching, compression and osmotic shocks experiments; indeed, spectrin meshwork reacted differently depending on the nature of the applied mechanical cues. Upon cell detachment from the substrate, due to mechanical stretch for example, spectrin and actin displayed a "plug-like" behavior, and collapsed together in the region where the stress was applied, probably because the event was too fast to allow the proteins to organize and adapt to the perturbation (Figure 45; zone VI). On the contrary, during induced mechanical cell compression, spectrin clearance triggered actin polymerization as a protective mechanism in response to its displacement, both at new-formed blebs level (Figure 45, zone V) and under the nucleus, which was completely reverted once the piston was released (Figure 43, compression cycles a-d). Together with spectrin exclusion from protrusive lamellipodia, these results suggest the existence of a previously neglected hindrance mechanism that prevents potential Arp2/3-driven actin polymerization in presence of a spectrin-enriched cortex.

Moreover, upon cycles of stretching and relaxation through osmotic shocks, we observed that globally spectrin was kept at a constant ratio with all the plasma membrane area, whereas in restricted regions, we could observe different reactions characterized by local meshwork condensation as a cell-protective mechanism.

These results support a spectrin fencing role through a local condensation mechanism upon different mechanical stimuli, which has been firstly proposed in neuronal axons of *C. Elegans* under constant compressive or bending forces (Krieg et al., 2014; Krieg et al., 2017). Moreover, a recent work performed in *D. Melanogaster* highlighted a spectrin mechanoprotective role, by

a transient and stable binding with the shear-deformed actin network at cell fusion level, thanks to its extensibility and flexibility properties (Duan et al., 2018). Here, we propose a spectrin protective role upon mechanical cues through an accumulation mechanism rather than a meshwork *de-novo* recruitment or stretching/relaxation model, as it has been proposed and based on the intramolecular distances measured in previous studies in erythrocytes and neurons.

## 5. Spectrin skeleton dynamics is a crucial element for the control of the cell shape and various PM-linked processes

Finally, it has been shown that spectrin can act as a patrol which can control lateral membrane organization in epithelial cells by blocking receptors internalization (Jenkins et al., 2015), further supporting our theory of a spectrin protective role at the PM level.

Our observations of the spectrin and actin reactions upon different environmental perturbations strongly support the existence of a non-Brownian diffusion mode through the PM. Indeed, it has been shown that diffusion barriers across the membrane, which regulate its dynamic and topological microdomain organization, depend on the so called “fencing and picket” mechanism due to the actin cytoskeleton and transmembrane proteins interaction (Kusumi and Suzuki, 2005).

Given its ability in defining PM microdomains which constantly remodel over time in response to both intrinsic and extrinsic cues, spectrin meshwork can well integrate in the mesoscale dynamic organization of the PM (Kusumi et al., 2012; Nicolson, 2014)

In this scenario, and given the above-mentioned model of a spectrin-mediated regulation of cargoes internalization in epithelial cells (Jenkins et al., 2015), we observed that endocytic events, such as CME, take place at the level of PM microdomains, which are delimited by

spectrin skeleton. In addition, we observed that clathrin-coated pits (CCPs) maturation, which is sustained by actin polymerization, occurred at restricted regions within spectrin fenestrations (Figure 45, cell cortex cycles 1 to 3).

It is still not clear if this mechanism could be exclusive for CME or if spectrin meshwork can spatio-temporally regulate other surface trafficking events like non-clathrin endocytosis (NCE) or membrane trafficking pathways with opposite directionality such as exocytosis. Indeed, spectrin has been identified at the level of many intracellular membranes, such as Golgi, synaptic vesicles, the endoplasmic reticulum (ER), the nuclear membrane, thus supporting a growing body of evidence that many other compartments of the endo/lysosomal pathway can be associated to spectrin. A major issue will be to understand which is the role of spectrin given its association with different intracellular compartments (De Matteis and Morrow, 2000), and further analysis still need to be performed in order to address all these open questions.

Such role in organizing PM trafficking events is consistent with a recent report proposing spectrin as a general ruler for cell-cell adhesion molecules organization in neurons (Hauser et al., 2018).

All these widely utilized mechanisms may unveil why spectrin is a highly evolutionary conserved protein, which is ubiquitously expressed in all eukaryotic cells together with its membrane anchor partner ankyrin (Bennett and Lorenzo, 2013).

More generally, these results indicate that the spectrin skeleton dynamics is a crucial element critical to shape and coordinate many PM-linked cellular processes in physiology and pathology.

# 6. α/β-spectrin heterotetramer stability is necessary for its correct functioning and for cell shape maintentenance

We successfully generated βII-spectrin KO cell lines taking advantage of the CRISPR/Cas9 system and selected 3 clones among the ones that we obtained, for deeper investigations.

The reduction of αII-spectrin expression at protein but not at the mRNA level, upon βII-spectrin depletion, suggested that the protein is correctly synthesized, but it undergoes protein degradation probably because of the lack of its binding with βII-spectrin.

These findings are consistent with early studies in vertebrates showing that βII-spectrin is degraded when it is not assembled with the α counterpart (Woods and Lazarides, 1985).

Overall, these results reveal the need of the presence of a whole and stable α/β-spectrin heterotetramer, otherwise the two proteins will not be able to accomplish their role and will undergo protein degradation.

Moreover, after checking the mRNA expression level of all the other spectrin genes, we didn't observe any protein compensation from the two erythrocytic versions, which, despite their structural and functional similarities are confirmed to be exclusively expressed in red blood cells.

Interestingly, we observed a little reduction of the *SPTBN2* gene, which encodes for βIII-spectrin. One possible explanation to this result could be that αII-spectrin, in non-erythroid cells, not only binds βII-spectrin, but also all the other spectrin variants. Indeed, the αII-spectrin degradation, consequently to βII-spectrin KO, could probably affect also the stability of the other β-spectrins. Unfortunately, βIV- and βV- espression levels were too low to be detected, so the impact of βII-spectrin depletion on their fate couldn't be evaluated, and further analysis need to be performed in order to better understand this possible process.

Finally, we here provide preliminary results supporting the role of spectrin in the control and maintenance of the cell shape.

Indeed, we investigated the effect of spectrin removal on the cell morphology by performing time lapse analysis, which revealed us a peculiar and elongated shape in cells βII-spectrin KO, compared to the WT ones, thus suggesting the importance of spectrin is sustaining plasma membrane and avoiding its collapse.

Furthermore, after measuring the area of both WT and βII-spectrin KO cells, we observed a consistent reduction of cell area upon βII-spectrin depletion, compared with control cells. Interestingly, GFP-βII-spectrin re-expression in KO cells wasn't enough to completely rescue the wild type phenotype, even if we observed a slight increase in their area. This could probably due to the altered αII-spectrin expression, which normal level was probably not restored after βII-spectrin back-transfection.

These results are in line with what have been shown in MEFs depleted of αII-spectrin, which appeared spikier and displayed an impaired growth and spreading (Stankewich et al., 2011).

In general, these preliminary results reveal the importance of the α/β-heterotetramer as a PM scaffold able to sustain and regulate the shape of the cell; future analysis on cell spreading or during extrinsic mechanical challenges will be performed in a βII-spectrin KO background for a deeper understanting.

Moreover, given our previous results suggesting a spectrin meshwork role in the regulation of PM-linked processes, it would be of great interest to follow clathrin-mediated endocytosis and measure the internalization rate upon spectrin KO, in order to further support our hypothesis.

# 7. Author contributions

I contributed to the following publication:

**A RAB35-p85/PI3K axis controls oscillatory apical protrusions required for efficient chemotactic migration (Corallino et al., 2018)**

with the execution and analysis of cell migration on suspended fibronectin coated nanofibers experiments.

# 8.

# References


1. An, X., Guo, X., Zhang, X., Baines, A.J., Debnath, G., Moyo, D., Salomao, M., Bhasin, N., Johnson, C., Discher, D.*, et al.* (2006). Conformational stabilities of the structural repeats of erythroid spectrin and their functional implications. J Biol Chem *281*, 10527-10532.
2. Andrade, D.M., Clausen, M.P., Keller, J., Mueller, V., Wu, C., Bear, J.E., Hell, S.W., Lagerholm, B.C., and Eggeling, C. (2015). Cortical actin networks induce spatio-temporal confinement of phospholipids in the plasma membrane--a minimally invasive investigation by STED-FCS. Sci Rep *5*, 11454.
3. Autore, F., Pfuhl, M., Quan, X., Williams, A., Roberts, R.G., Shanahan, C.M., and Fraternali, F. (2013). Large-scale modelling of the divergent spectrin repeats in nesprins: giant modular proteins. PLoS One *8*, e63633.
4. Baines, A.J. (2009). Evolution of spectrin function in cytoskeletal and membrane networks. Biochemical Society transactions *37*, 796-803.
5. Bañuelos, S., Saraste, M., and Carugo, K.D. (1998). Structural comparisons of calponin homology domains: implications for actin binding. Structure *6*, 1419-1431.
6. Bennett, V., and Baines, A.J. (2001). Spectrin and Ankyrin-Based Pathways: Metazoan Inventions for Integrating Cells Into Tissues. Physiol Rev *81*, 1353-1392.
7. Bennett, V., and Lorenzo, D.N. (2013). Spectrin- and ankyrin-based membrane domains and the evolution of vertebrates. Curr Top Membr *72*, 1-37.
8. Berghs, S., Aggujaro, D., Dirkx, R., Maksimova, E., Stabach, P., Hermel, J.M., Zhang, J.P., Philbrick, W., Slepnev, V., Ort, T.*, et al.* (2000). BetaIV spectrin, a

new spectrin localized at axon initial segments and nodes of ranvier in the central and peripheral nervous system. Journal of Cell Biology *151*, 985-1001.

9. Bershadsky, A., Chausovsky, A., Becker, E., Lyubimova, A., and Geiger, B. (1996). Involvement of microtubules in the control of adhesion-dependent signal transduction. Curr Biol *6*, 1279-1289.
10. Bialkowska, K., Saido, T.C., and Fox, J.E. (2005). SH3 domain of spectrin participates in the activation of Rac in specialized calpain-induced integrin signaling complexes. J Cell Sci *118*, 381-395.
11. Boulant, S., Kural, C., Zeeh, J.C., Ubelmann, F., and Kirchhausen, T. (2011). Actin dynamics counteract membrane tension during clathrin-mediated endocytosis. Nat Cell Biol *13*, 1124-1131.
12. Bovellan, M., Romeo, Y., Biro, M., Boden, A., Chugh, P., Yonis, A., Vaghela, M., Fritzsche, M., Moulding, D., Thorogate, R.*, et al.* (2014). Cellular control of cortical actin nucleation. Curr Biol *24*, 1628-1635.
13. Brieher, W. (2013). Mechanisms of actin disassembly, Vol 24.
14. Broderick, M.J., and Winder, S.J. (2005). Spectrin, alpha-actinin, and dystrophin. Adv Protein Chem *70*, 203-246.
15. Burlacu, S., Janmey, P.A., and Borejdo, J. (1992). Distribution of actin filament lengths measured by fluorescence microscopy. Am J Physiol *262*, C569-577.
16. Byers, T.J., and Branton, D. (1985). Visualization of the protein associations in the erythrocyte membrane skeleton. Proc Natl Acad Sci U S A *82*, 6153-6157.
17. Castello, M., Tortarolo, G., Hernandez, I.C., Bianchini, P., Buttafava, M., Boso, G., Tosi, A., Diaspro, A., and Vicidomini, G. (2016). Gated-sted microscopy with

subnanosecond pulsed fiber laser for reducing photobleaching. Microsc Res Tech *79*, 785-791.

18. Chalut, K.J., and Paluch, E.K. (2016). The Actin Cortex: A Bridge between Cell Shape and Function. Dev Cell *38*, 571-573.
19. Charras, G.T., Hu, C.K., Coughlin, M., and Mitchison, T.J. (2006). Reassembly of contractile actin cortex in cell blebs. J Cell Biol *175*, 477-490.
20. Chesarone, M.A., and Goode, B.L. (2009). Actin nucleation and elongation factors: mechanisms and interplay. Curr Opin Cell Biol *21*, 28-37.
21. Chugh, P., and Paluch, E.K. (2018). The actin cortex at a glance. J Cell Sci *131*.
22. Cianci, C.D., Zhang, Z., Pradhan, D., and Morrow, J.S. (1999a). Brain and muscle express a unique alternative transcript of ??II spectrin. Biochemistry *38*, 15721-15730.
23. Cianci, C.D., Zhang, Z., Pradhan, D., and Morrow, J.S. (1999b). Brain and muscle express a unique alternative transcript of alphaII spectrin. Biochemistry *38*, 15721-15730.
24. De Matteis, M.A., and Morrow, J.S. (2000). Spectrin tethers and mesh in the biosynthetic pathway. Journal of cell science *113*, 2331-2343.
25. Delalande, O., Czogalla, A., Hubert, J.F., Sikorski, A., and Le Rumeur, E. (2017). Dystrophin and Spectrin, Two Highly Dissimilar Sisters of the Same Family. Subcell Biochem *82*, 373-403.
26. Delaunay, J. (2007). The molecular basis of hereditary red cell membrane disorders. Blood Rev *21*, 1-20.
27. Derbala, M.H., Guo, A.S., Mohler, P.J., and Smith, S.A. (2018). The role of betaII spectrin in cardiac health and disease. Life Sci *192*, 278-285.

28. Deuticke, B., Poser, B., Lutkemeier, P., and Haest, C.W. (1983). Formation of aqueous pores in the human erythrocyte membrane after oxidative cross-linking of spectrin by diamide. Biochim Biophys Acta *731*, 196-210.

29. Devarajan, P., Stabach, P.R., De Matteis, M.A., and Morrow, J.S. (1997). Na,K-ATPase transport from endoplasmic reticulum to Golgi requires the Golgi spectrin-ankyrin G119 skeleton in Madin Darby canine kidney cells. Proc Natl Acad Sci U S A *94*, 10711-10716.

30. Discher, D.E., and Carl, P. (2001). New insights into red cell network structure, elasticity, and spectrin unfolding--a current review. Cell Mol Biol Lett *6*, 593-606.

31. Djinovic-Carugo, K., Gautel, M., Ylanne, J., and Young, P. (2002). The spectrin repeat: a structural platform for cytoskeletal protein assemblies. FEBS Lett *513*, 119-123.

32. Doherty, G.J., and McMahon, H.T. (2009). Mechanisms of endocytosis. Annu Rev Biochem *78*, 857-902.

33. Duan, R., Kim, J.H., Shilagardi, K., Schiffhauer, E.S., Lee, D.M., Son, S., Li, S., Thomas, C., Luo, T., Fletcher, D.A.*, et al.* (2018). Spectrin is a mechanoresponsive protein shaping fusogenic synapse architecture during myoblast fusion. Nat Cell Biol *20*, 688-698.

34. Dubreuil, R.R. (2006). Functional links between membrane transport and the spectrin cytoskeleton. J Membr Biol *211*, 151-161.

35. Dubreuil, R.R., Byers, T.J., Sillman, A.L., Bar-Zvi, D., Goldstein, L.S., and Branton, D. (1989). The complete sequence of Drosophila alpha-spectrin: conservation of structural domains between alpha-spectrins and alpha-actinin. J Cell Biol *109*, 2197-2205.

36. Dubreuil, R.R., and Grushko, T. (1998). Genetic studies of spectrin: new life for a ghost protein. Bioessays *20*, 875-878.

37. DuFort, C.C., Paszek, M.J., and Weaver, V.M. (2011). Balancing forces: architectural control of mechanotransduction. Nat Rev Mol Cell Biol *12*, 308-319.

38. Elgsaeter, A., Stokke, B.T., Mikkelsen, A., and Branton, D. (1986). The molecular basis of erythrocyte shape. Science *234*, 1217-1223.

39. Emoto, K., Kobayashi, T., Yamaji, A., Aizawa, H., Yahara, I., Inoue, K., and Umeda, M. (1996). Redistribution of phosphatidylethanolamine at the cleavage furrow of dividing cells during cytokinesis. Proc Natl Acad Sci U S A *93*, 12867-12872.

40. Engelhardt, H., and Sackmann, E. (1988). On the measurement of shear elastic moduli and viscosities of erythrocyte plasma membranes by transient deformation in high frequency electric fields. Biophys J *54*, 495-508.

41. Evans, E.A. (1973). New membrane concept applied to the analysis of fluid shear- and micropipette-deformed red blood cells. Biophys J *13*, 941-954.

42. Falkenburger, B.H., Jensen, J.B., Dickson, E.J., Suh, B.C., and Hille, B. (2010). Phosphoinositides: lipid regulators of membrane proteins. J Physiol *588*, 3179-3185.

43. Fung, Y.C., and Tong, P. (1968). Theory of the sphering of red blood cells. Biophys J *8*, 175-198.

44. Galiano, M.R., Jha, S., Ho, T.S., Zhang, C., Ogawa, Y., Chang, K.J., Stankewich, M.C., Mohler, P.J., and Rasband, M.N. (2012). A distal axonal

cytoskeleton forms an intra-axonal boundary that controls axon initial segment assembly. Cell *149*, 1125-1139.

45. Gauthier, N.C., Masters, T.A., and Sheetz, M.P. (2012). Mechanical feedback between membrane tension and dynamics. Trends in Cell Biology *22*, 527-535.
46. Gauthier, N.C., Rossier, O.M., Mathur, A., Hone, J.C., and Sheetz, M.P. (2009). Plasma Membrane Area Increases with Spread Area by Exocytosis of a GPI-anchored Protein Compartment. Molecular biology of the cell *20*, 3261-3272.
47. Giannone, G., Dubin-Thaler, B.J., Dobereiner, H.G., Kieffer, N., Bresnick, A.R., and Sheetz, M.P. (2004). Periodic lamellipodial contractions correlate with rearward actin waves. Cell *116*, 431-443.
48. Goldman, R.D., Cleland, M.M., Murthy, S.N., Mahammad, S., and Kuczmarski, E.R. (2012). Inroads into the structure and function of intermediate filament networks. J Struct Biol *177*, 14-23.
49. Gowrishankar, K., Ghosh, S., Saha, S., C, R., Mayor, S., and Rao, M. (2012). Active remodeling of cortical actin regulates spatiotemporal organization of cell surface molecules. Cell *149*, 1353-1367.
50. Grum, V.L., Li, D., MacDonald, R.I., and Mondragon, A. (1999). Structures of two repeats of spectrin suggest models of flexibility. Cell *98*, 523-535.
51. Hammarlund, M., Jorgensen, E.M., and Bastiani, M.J. (2007). Axons break in animals lacking beta-spectrin. J Cell Biol *176*, 269-275.
52. Han, B., Zhou, R., Xia, C., and Zhuang, X. (2017). Structural organization of the actin-spectrin-based membrane skeleton in dendrites and soma of neurons. Proc Natl Acad Sci U S A *114*, E6678-e6685.

53. Hauser, M., Yan, R., Li, W., Repina, N.A., Schaffer, D.V., and Xu, K. (2018). The Spectrin-Actin-Based Periodic Cytoskeleton as a Conserved Nanoscale Scaffold and Ruler of the Neural Stem Cell Lineage. Cell Reports *24*, 1512-1522.

54. He, J., Zhou, R., Wu, Z., Carrasco, M.A., Kurshan, P.T., Farley, J.E., Simon, D.J., Wang, G., Han, B., Hao, J.*, et al.* (2016). Prevalent presence of periodic actin-spectrin-based membrane skeleton in a broad range of neuronal cell types and animal species. Proceedings of the National Academy of Sciences of the United States of America, 1605707113-.

55. Helfer, E., Panine, P., Carlier, M.F., and Davidson, P. (2005). The interplay between viscoelastic and thermodynamic properties determines the birefringence of F-actin gels. Biophys J *89*, 543-553.

56. Hell, S.W., and Wichmann, J. (1994). Breaking the diffraction resolution limit by stimulated emission: stimulated-emission-depletion fluorescence microscopy. Opt Lett *19*, 780-782.

57. Henon, S., Lenormand, G., Richert, A., and Gallet, F. (1999). A new determination of the shear modulus of the human erythrocyte membrane using optical tweezers. Biophys J *76*, 1145-1151.

58. Hochmuth, R.M., and Mohandas, N. (1972). Uniaxial loading of the red-cell membrane. J Biomech *5*, 501-509.

59. Hochmuth, R.M., and Waugh, R.E. (1987). Erythrocyte membrane elasticity and viscosity. Annu Rev Physiol *49*, 209-219.

60. Holleran, E.A., Ligon, L.A., Tokito, M., Stankewich, M.C., Morrow, J.S., and Holzbaur, E.L. (2001). beta III spectrin binds to the Arp1 subunit of dynactin. J Biol Chem *276*, 36598-36605.

61. Holmes, K.C., Popp, D., Gebhard, W., and Kabsch, W. (1990). Atomic model of the actin filament. Nature *347*, 44-49.

62. Horikoshi, N., Pandita, R.K., Mujoo, K., Hambarde, S., Sharma, D., Mattoo, A.R., and Chakraborty, S. (2016). β2-spectrin depletion impairs DNA damage repair. *7*.

63. Howes, M.T., Mayor, S., and Parton, R.G. (2010). Molecules, mechanisms, and cellular roles of clathrin-independent endocytosis. Curr Opin Cell Biol *22*, 519-527.

64. Huang, B., Babcock, H., and Zhuang, X. (2010). Breaking the diffraction barrier: super-resolution imaging of cells. Cell *143*, 1047-1058.

65. Hulsmeier, J., Pielage, J., Rickert, C., Technau, G.M., Klambt, C., and Stork, T. (2007). Distinct functions of alpha-Spectrin and beta-Spectrin during axonal pathfinding. Development *134*, 713-722.

66. Iida, N., Lokeshwar, V.B., and Bourguignon, L.Y. (1994). Mapping the fodrin binding domain in CD45, a leukocyte membrane-associated tyrosine phosphatase. J Biol Chem *269*, 28576-28583.

67. Ikeda, Y., Dick, K.A., Weatherspoon, M.R., Gincel, D., Armbrust, K.R., Dalton, J.C., Stevanin, G., Durr, A., Zuhlke, C., Burk, K.*, et al.* (2006). Spectrin mutations cause spinocerebellar ataxia type 5. Nat Genet *38*, 184-190.

68. Iskratsch, T., Wolfenson, H., and Sheetz, M.P. (2014). Appreciating force and shape [mdash] the rise of mechanotransduction in cell biology. Nature Reviews Molecular Cell Biology *15*, 825-833.

69. Jacobson, K., Sheets, E.D., and Simson, R. (1995). Revisiting the fluid mosaic model of membranes. Science *268*, 1441-1442.

70. Jenkins, P.M., He, M., and Bennett, V. (2015). Dynamic spectrin/ankyrin-G microdomains promote lateral membrane assembly by opposing endocytosis.

71. Kaksonen, M., and Roux, A. (2018). Mechanisms of clathrin-mediated endocytosis. Nat Rev Mol Cell Biol *19*, 313-326.

72. Kaksonen, M., Toret, C.P., and Drubin, D.G. (2006). Harnessing actin dynamics for clathrin-mediated endocytosis. Nat Rev Mol Cell Biol *7*, 404-414.

73. Kalappurakkal, J.M., Anilkumar, A.A., Patra, C., van Zanten, T.S., Sheetz, M.P., and Mayor, S. (2019). Integrin Mechano-chemical Signaling Generates Plasma Membrane Nanodomains that Promote Cell Spreading. Cell *177*, 1738-1756.e1723.

74. Kirchhausen, T. (2009). Imaging endocytic clathrin structures in living cells. Trends Cell Biol *19*, 596-605.

75. Kitisin, K., Ganesan, N., Tang, Y., Jogunoori, W., Volpe, E.A., Kim, S.S., Katuri, V., Kallakury, B., Pishvaian, M., Albanese, C.*, et al.* (2007). Disruption of transforming growth factor-beta signaling through beta-spectrin ELF leads to hepatocellular cancer through cyclin D1 activation. Oncogene *26*, 7103-7110.

76. Kizhatil, K., Davis, J.Q., Davis, L., Hoffman, J., Hogan, B.L., and Bennett, V. (2007a). Ankyrin-G is a molecular partner of E-cadherin in epithelial cells and early embryos. J Biol Chem *282*, 26552-26561.

77. Kizhatil, K., Yoon, W., Mohler, P.J., Davis, L.H., Hoffman, J.A., and Bennett, V. (2007b). Ankyrin-G and beta2-spectrin collaborate in biogenesis of lateral membrane of human bronchial epithelial cells. J Biol Chem *282*, 2029-2037.

78. Koenderink, G.H., and Paluch, E.K. (2018). Architecture shapes contractility in actomyosin networks. Curr Opin Cell Biol *50*, 79-85.

79. Komada, M., and Soriano, P. (2002). [Beta]IV-spectrin regulates sodium channel clustering through ankyrin-G at axon initial segments and nodes of Ranvier. J Cell Biol *156*, 337-348.

80. Korobova, F., and Svitkina, T. (2008). Arp2/3 complex is important for filopodia formation, growth cone motility, and neuritogenesis in neuronal cells. Mol Biol Cell *19*, 1561-1574.

81. Korsgren, C., and Lux, S.E. (2010). The carboxyterminal EF domain of erythroid alpha-spectrin is necessary for optimal spectrin-actin binding. Blood *116*, 2600-2607.

82. Kottke, M.D., Delva, E., and Kowalczyk, A.P. (2006). The desmosome: cell science lessons from human diseases. J Cell Sci *119*, 797-806.

83. Krendel, M., Gloushankova, N.A., Bonder, E.M., Feder, H.H., Vasiliev, J.M., and Gelfand, I.M. (1999). Myosin-dependent contractile activity of the actin cytoskeleton modulates the spatial organization of cell–cell contacts in cultured epitheliocytes. In Proc Natl Acad Sci U S A, pp. 9666-9670.

84. Krieg, M., Dunn, A.R., and Goodman, M.B. (2014). Mechanical Control of the Sense of Touch by β Spectrin. *16*, 224-233.

85. Krieg, M., Stuhmer, J., Cueva, J.G., Fetter, R., Spilker, K., Cremers, D., Shen, K., Dunn, A.R., and Goodman, M.B. (2017). Genetic defects in beta-spectrin

and tau sensitize C. elegans axons to movement-induced damage via torque-tension coupling. Elife *6*.

86. Kusumi, A., Fujiwara, T.K., Chadda, R., Xie, M., Tsunoyama, T.A., Kalay, Z., Kasai, R.S., and Suzuki, K.G. (2012). Dynamic organizing principles of the plasma membrane that regulate signal transduction: commemorating the fortieth anniversary of Singer and Nicolson's fluid-mosaic model. Annu Rev Cell Dev Biol *28*, 215-250.

87. Kusumi, A., and Suzuki, K. (2005). Toward understanding the dynamics of membrane-raft-based molecular interactions. Biochim Biophys Acta *1746*, 234-251.

88. Kusunoki, H., MacDonald, R.I., and Mondragon, A. (2004). Structural insights into the stability and flexibility of unusual erythroid spectrin repeats. Structure *12*, 645-656.

89. Law, R., Carl, P., Harper, S., Dalhaimer, P., Speicher, D.W., and Discher, D.E. (2003a). Cooperativity in forced unfolding of tandem spectrin repeats. Biophys J *84*, 533-544.

90. Law, R., Liao, G., Harper, S., Yang, G., Speicher, D.W., and Discher, D.E. (2003b). Pathway shifts and thermal softening in temperature-coupled forced unfolding of spectrin domains. Biophys J *85*, 3286-3293.

91. Legendre, K., Safieddine, S., Kussel-Andermann, P., Petit, C., and El-Amraoui, A. (2008). alphaII-betaV spectrin bridges the plasma membrane and cortical lattice in the lateral wall of the auditory outer hair cells. J Cell Sci *121*, 3347-3356.

92. Leluk, J., Hanus-Lorenz, B., and Sikorski, A.F. (2001). Application of genetic semihomology algorithm to theoretical studies on various protein families. Acta Biochim Pol *48*, 21-33.

93. Lemmon, M.A. (2007). Pleckstrin homology (PH) domains and phosphoinositides. Biochem Soc Symp, 81-93.

94. Leshchyns'ka, I., Sytnyk, V., Morrow, J.S., and Schachner, M. (2003). Neural cell adhesion molecule (NCAM) association with PKCbeta2 via betaI spectrin is implicated in NCAM-mediated neurite outgrowth. J Cell Biol *161*, 625-639.

95. Liem, R.K. (2016). Cytoskeletal Integrators: The Spectrin Superfamily. Cold Spring Harb Perspect Biol *8*.

96. Liu, S.C., Derick, L.H., and Palek, J. (1987). Visualization of the hexagonal lattice in the erythrocyte membrane skeleton. J Cell Biol *104*, 527-536.

97. Machnicka, B., Czogalla, A., Hryniewicz-Jankowska, A., Boguslawska, D.M., Grochowalska, R., Heger, E., and Sikorski, A.F. (2014). Spectrins: a structural platform for stabilization and activation of membrane channels, receptors and transporters. Biochim Biophys Acta *1838*, 620-634.

98. Machnicka, B., Grochowalska, R., Boguslawska, D.M., Sikorski, A.F., and Lecomte, M.C. (2012). Spectrin-based skeleton as an actor in cell signaling. Cell Mol Life Sci *69*, 191-201.

99. Marchesi, V.T., and Steers, E., Jr. (1968). Selective solubilization of a protein component of the red cell membrane. Science *159*, 203-204.

100. Mayor, S., and Pagano, R.E. (2007). Pathways of clathrin-independent endocytosis. Nat Rev Mol Cell Biol *8*, 603-612.

101. McMahon, H.T., and Boucrot, E. (2011). Molecular mechanism and physiological functions of clathrin-mediated endocytosis. Nat Rev Mol Cell Biol *12*, 517-533.

102. McMahon, L.W., Zhang, P., Sridharan, D.M., Lefferts, J.A., and Lambert, M.W. (2009). Knockdown of alphaII spectrin in normal human cells by siRNA leads to chromosomal instability and decreased DNA interstrand cross-link repair. Biochem Biophys Res Commun *381*, 288-293.

103. Metral, S., Machnicka, B., Bigot, S., Colin, Y., Dhermy, D., and Lecomte, M.C. (2009). AlphaII-spectrin is critical for cell adhesion and cell cycle. J Biol Chem *284*, 2409-2418.

104. Moorthy, S., Chen, L., and Bennett, V. (2000). Caenorhabditis elegans beta-G spectrin is dispensable for establishment of epithelial polarity, but essential for muscular and neuronal function. J Cell Biol *149*, 915-930.

105. Morris, C.E., and Homann, U. (2001). Cell surface area regulation and membrane tension. J Membr Biol *179*, 79-102.

106. Mozzi, R., Buratta, S., and Goracci, G. (2003). Metabolism and functions of phosphatidylserine in mammalian brain. Neurochem Res *28*, 195-214.

107. Mueller, J., Szep, G., Nemethova, M., de Vries, I., Lieber, A.D., Winkler, C., Kruse, K., Small, J.V., Schmeiser, C., Keren, K.*, et al.* (2017). Load Adaptation of Lamellipodial Actin Networks. Cell *171*, 188-200 e116.

108. Mund, M., van der Beek, J.A., Deschamps, J., Dmitrieff, S., Hoess, P., Monster, J.L., Picco, A., Nedelec, F., Kaksonen, M., and Ries, J. (2018). Systematic Nanoscale Analysis of Endocytosis Links Efficient Vesicle Formation to Patterned Actin Nucleation. Cell *174*, 884-896.e817.

109. Munro, S. (2003). Lipid rafts: elusive or illusive? Cell *115*, 377-388.

110. Nans, A., Mohandas, N., and Stokes, D.L. (2011). Native ultrastructure of the red cell cytoskeleton by cryo-electron tomography. Biophys J *101*, 2341-2350.

111. Nicolson, G.L. (2014). The Fluid-Mosaic Model of Membrane Structure: still relevant to understanding the structure, function and dynamics of biological membranes after more than 40 years. Biochim Biophys Acta *1838*, 1451-1466.

112. Odde, D.J., Ma, L., Briggs, A.H., DeMarco, A., and Kirschner, M.W. (1999). Microtubule bending and breaking in living fibroblast cells. J Cell Sci *112 ( Pt 19)*, 3283-3288.

113. Ono, S. (2007). Mechanism of depolymerization and severing of actin filaments and its significance in cytoskeletal dynamics. Int Rev Cytol *258*, 1-82.

114. Pampaloni, F., and Florin, E.L. (2008). Microtubule architecture: inspiration for novel carbon nanotube-based biomimetic materials. Trends Biotechnol *26*, 302-310.

115. Pan, L., Yan, R., Li, W., and Xu, K. (2018). Super-Resolution Microscopy Reveals the Native Ultrastructure of the Erythrocyte Cytoskeleton. Cell Rep *22*, 1151-1158.

116. Pecheur, E.I., Martin, I., Maier, O., Bakowsky, U., Ruysschaert, J.M., and Hoekstra, D. (2002). Phospholipid species act as modulators in p97/p47-mediated fusion of Golgi membranes. Biochemistry *41*, 9813-9823.

117. Picart, C., and Discher, D.E. (1999). Actin Protofilament Orientation at the Erythrocyte Membrane. Biophysical Journal *77*, 865-878.

118. Pielage, J., Fetter, R.D., and Davis, G.W. (2005). Presynaptic spectrin is essential for synapse stabilization. Curr Biol *15*, 918-928.

119. Pielage, J., Fetter, R.D., and Davis, G.W. (2006). A postsynaptic spectrin scaffold defines active zone size, spacing, and efficacy at the Drosophila neuromuscular junction. J Cell Biol *175*, 491-503.

120. Pontes, B., Monzo, P., and Gauthier, N.C. (2017a). Membrane tension: A challenging but universal physical parameter in cell biology. Semin Cell Dev Biol *71*, 30-41.

121. Pontes, B., Monzo, P., Gole, L., Le Roux, A.L., Kosmalska, A.J., Tam, Z.Y., Luo, W., Kan, S., Viasnoff, V., Roca-Cusachs, P.*, et al.* (2017b). Membrane tension controls adhesion positioning at the leading edge of cells. J Cell Biol.

122. Pontes, B., Monzo, P., Gole, L., Le Roux, A.L., Kosmalska, A.J., Tam, Z.Y., Luo, W., Kan, S., Viasnoff, V., Roca-Cusachs, P.*, et al.* (2017c). Membrane tension controls adhesion positioning at the leading edge of cells. J Cell Biol *216*, 2959-2977.

123. Ponti, A., Machacek, M., Gupton, S.L., Waterman-Storer, C.M., and Danuser, G. (2004). Two distinct actin networks drive the protrusion of migrating cells. Science *305*, 1782-1786.

124. Raghupathy, R., Anilkumar, A.A., Polley, A., Singh, P.P., Yadav, M., Johnson, C., Suryawanshi, S., Saikam, V., Sawant, S.D., Panda, A.*, et al.* (2015). Transbilayer lipid interactions mediate nanoclustering of lipid-anchored proteins. Cell *161*, 581-594.

125. Rand, R.P., and Burton, A.C. (1964). MECHANICAL PROPERTIES OF THE RED CELL MEMBRANE. I. MEMBRANE STIFFNESS AND INTRACELLULAR PRESSURE. Biophys J *4*, 115-135.

126. Robertsson, J., Petzold, K., Lofvenberg, L., and Backman, L. (2005). Folding of spectrin's SH3 domain in the presence of spectrin repeats. Cell Mol Biol Lett *10*, 595-612.

127. Roca-Cusachs, P., Conte, V., and Trepat, X. (2017). Quantifying forces in cell biology. Nat Cell Biol *19*, 742-751.

128. Ryan, G.L., Petroccia, H.M., Watanabe, N., and Vavylonis, D. (2012). Excitable actin dynamics in lamellipodial protrusion and retraction. Biophys J *102*, 1493-1502.

129. Salbreux, G., Charras, G., and Paluch, E. (2012). Actin cortex mechanics and cellular morphogenesis. Trends Cell Biol *22*, 536-545.

130. Salomao, M., An, X., Guo, X., Gratzer, W.B., Mohandas, N., and Baines, A.J. (2006). Mammalian alpha I-spectrin is a neofunctionalized polypeptide adapted to small highly deformable erythrocytes. Proc Natl Acad Sci U S A *103*, 643-648.

131. Sato, M., Schwartz, W.H., Selden, S.C., and Pollard, T.D. (1988). Mechanical properties of brain tubulin and microtubules. J Cell Biol *106*, 1205-1211.

132. Scita, G., and Di Fiore, P.P. (2010). The endocytic matrix. Nature *463*, 464-473.

133. Sezgin, E., Levental, I., Mayor, S., and Eggeling, C. (2017). The mystery of membrane organization: composition, regulation and roles of lipid rafts. Nat Rev Mol Cell Biol *18*, 361-374.

134. Shen, B.W., Josephs, R., and Steck, T.L. (1986). Ultrastructure of the intact skeleton of the human erythrocyte membrane. J Cell Biol *102*, 997-1006.

135. Shewan, A., Eastburn, D.J., and Mostov, K. (2011). Phosphoinositides in cell architecture. Cold Spring Harb Perspect Biol *3*, a004796.

136. Shotton, D.M., Burke, B.E., and Branton, D. (1979). The molecular structure of human erythrocyte spectrin. Biophysical and electron microscopic studies. J Mol Biol *131*, 303-329.

137. Singer, S.J., and Nicolson, G.L. (1972). The fluid mosaic model of the structure of cell membranes. Science *175*, 720-731.

138. Smith, A.S., Nowak, R.B., Zhou, S., Giannetto, M., Gokhin, D.S., Papoin, J., Ghiran, I.C., Blanc, L., Wan, J., and Fowler, V.M. (2018). Myosin IIA interacts with the spectrin-actin membrane skeleton to control red blood cell membrane curvature and deformability. Proc Natl Acad Sci U S A *115*, E4377-e4385.

139. Sridharan, D., Brown, M., Lambert, W.C., McMahon, L.W., and Lambert, M.W. (2003). Nonerythroid alphaII spectrin is required for recruitment of FANCA and XPF to nuclear foci induced by DNA interstrand cross-links. J Cell Sci *116*, 823-835.

140. Sridharan, D.M., McMahon, L.W., and Lambert, M.W. (2006). alphaII-Spectrin interacts with five groups of functionally important proteins in the nucleus. Cell Biol Int *30*, 866-878.

141. Stabach, P.R., and Morrow, J.S. (2000). Identification and characterization of beta V spectrin, a mammalian ortholog of Drosophila beta H spectrin. J Biol Chem *275*, 21385-21395.

142. Stankewich, M.C., Cianci, C.D., Stabach, P.R., Ji, L., Nath, A., and Morrow, J.S. (2011). Cell organization, growth, and neural and cardiac development require alphaII-spectrin. J Cell Sci *124*, 3956-3966.

143. Stankewich, M.C., Tse, W.T., Peters, L.L., Ch'ng, Y., John, K.M., Stabach, P.R., Devarajan, P., Morrow, J.S., and Lux, S.E. (1998). A widely expressed betaIII

spectrin associated with Golgi and cytoplasmic vesicles. Proceedings of the National Academy of Sciences of the United States of America *95*, 14158-14163.

144. Su, J., Muranjan, M., and Sap, J. (1999). Receptor protein tyrosine phosphatase alpha activates Src-family kinases and controls integrin-mediated responses in fibroblasts. Curr Biol *9*, 505-511.

145. Sun, R., Meng, X., Wang, W., Liu, B., Lv, X., Yuan, J., Zeng, L., Chen, Y., Yuan, B., and Yang, S. (2019). Five genes may predict metastasis in non-small cell lung cancer using bioinformatics analysis. Oncol Lett *18*, 1723-1732.

146. Swihart, A.H., Mikrut, J.M., Ketterson, J.B., and Macdonald, R.C. (2001). Atomic force microscopy of the erythrocyte membrane skeleton. J Microsc *204*, 212-225.

147. Takeda, S., Yamazaki, H., Seog, D.H., Kanai, Y., Terada, S., and Hirokawa, N. (2000). Kinesin superfamily protein 3 (KIF3) motor transports fodrin-associating vesicles important for neurite building. J Cell Biol *148*, 1255-1265.

148. Tang, Y., Katuri, V., Dillner, A., Mishra, B., Deng, C.X., and Mishra, L. (2003). Disruption of transforming growth factor-beta signaling in ELF beta-spectrin-deficient mice. Science *299*, 574-577.

149. Thompson, J.M., Ellis, R.E., Green, E.M., Winlove, C.P., and Petrov, P.G. (2008). Spectrin maintains the lateral order in phosphatidylserine monolayers. Chem Phys Lipids *151*, 66-68.

150. Tojkander, S., Gateva, G., and Lappalainen, P. (2012). Actin stress fibers--assembly, dynamics and biological roles. J Cell Sci *125*, 1855-1864.

151. Ursitti, J.A., Pumplin, D.W., Wade, J.B., and Bloch, R.J. (1991). Ultrastructure of the human erythrocyte cytoskeleton and its attachment to the membrane. Cell Motil Cytoskeleton *19*, 227-243.

152. Ursitti, J.A., and Wade, J.B. (1993). Ultrastructure and immunocytochemistry of the isolated human erythrocyte membrane skeleton. Cell Motil Cytoskeleton *25*, 30-42.

153. Vance, J.E., and Steenbergen, R. (2005). Metabolism and functions of phosphatidylserine. Prog Lipid Res *44*, 207-234.

154. Vance, J.E., and Tasseva, G. (2013). Formation and function of phosphatidylserine and phosphatidylethanolamine in mammalian cells. Biochim Biophys Acta *1831*, 543-554.

155. Vogel, V., and Sheetz, M. (2006). Local force and geometry sensing regulate cell functions. Nat Rev Mol Cell Biol *7*, 265-275.

156. Wang, G., Simon, D.J., Wu, Z., Belsky, D.M., Heller, E., O'Rourke, M.K., Hertz, N.T., Molina, H., Zhong, G., Tessier-Lavigne, M.*, et al.* (2019). Structural plasticity of actin-spectrin membrane skeleton and functional role of actin and spectrin in axon degeneration. Elife *8*.

157. Winkelmann, J.C., Chang, J.-G., Tsef, W.T., Scarpa, A.L., Marchesi, V.T., and Forget, B.G. (1990). Full-lenght sequence of the cDNA for human erythroid beta-spectrin. The Journal of Biological Chemistry *265*, 11827-11832.

158. Winkelmann, J.C., and Forget, B.G. (1993). Erythroid and nonerythroid spectrins. Blood *81*, 3173-3185.

159. Wolny, M., Grzybek, M., Bok, E., Chorzalska, A., Lenoir, M., Czogalla, A., Adamczyk, K., Kolondra, A., Diakowski, W., Overduin, M.*, et al.* (2011). Key

amino acid residues of ankyrin-sensitive phosphatidylethanolamine/phosphatidylcholine-lipid binding site of betaI-spectrin. PLoS One *6*, e21538.

160. Woods, C.M., and Lazarides, E. (1985). Degradation of unassembled alpha- and beta-spectrin by distinct intracellular pathways: regulation of spectrin topogenesis by beta-spectrin degradation. Cell *40*, 959-969.
161. Writzl, K., Primec, Z.R., Strazisar, B.G., Osredkar, D., Pecaric-Meglic, N., Kranjc, B.S., Nishiyama, K., Matsumoto, N., and Saitsu, H. (2012). Early onset West syndrome with severe hypomyelination and coloboma-like optic discs in a girl with SPTAN1 mutation. Epilepsia *53*, e106-110.
162. Xu, K., Zhong, G., and Xiaowei, Z. (2013). Actin, spectrin and associated proteins form a periodic cytoskeletal structure in axons. Science *339*.
163. Yeung, T., Gilbert, G.E., Shi, J., Silvius, J., Kapus, A., and Grinstein, S. (2008). Membrane phosphatidylserine regulates surface charge and protein localization. Science *319*, 210-213.
164. Zhang, R., Zhang, C., Zhao, Q., and Li, D. (2013). Spectrin: Structure, function and disease. Science China Life Sciences *56*, 1076-1085.
165. Zhang, Y., Abiraman, K., Li, H., Pierce, D.M., Tzingounis, A.V., and Lykotrafitis, G. (2017). Modeling of the axon membrane skeleton structure and implications for its mechanical properties. PLoS Comput Biol *13*, e1005407.
166. Zhong, G., He, J., Zhou, R., Lorenzo, D., Babcock, H.P., Bennett, V., and Zhuang, X. (2014). Developmental mechanism of the periodic membrane skeleton in axons. Elife *3*.

167. Zhou, R., Han, B., Xia, C., and Zhuang, X. (2019). Membrane-associated periodic skeleton is a signaling platform for RTK transactivation in neurons. Science *365*, 929-934.

# Acknowledgments

*My first acknowledgment goes to my boss Nils for giving me the opportunity to work at this challenging project and for all the long meetings we had, discussing about science and more, thanks to him I learned that in the scientific world, but also in the everyday life, we should always think a bit out of the box,*

*Then, I would like to thank all the members of my group, for supporting me, for helping me everytime I was in need and for all the precious suggestions they gave me during all these years, helping me to grow personally and as a scientist,*

*Thanks to Pascale, for helping me in the everyday practical life in the lab,*

*Thanks to Andrea, or AG, for sharing with me all the great adventures in the spectrin world, helping and supporting me patiently every day, encouraging me always with a smile,*

*Thanks to Michele, also known as Corbetta, for giving me "the best year of my PhD since he arrived in the lab" as he always reminds me,*

*To both of them, thanks for all the nice moments inside and outside the lab, for all the coffee they offered me and for being not only simple collegues, but also good friends,*
*I would also like to thank Paolo, for all the help with data analysis that contributed to the evolution of the spectrin story,*

*Thanks to Paulina, for all the times she comforted me, when I was almost crying after lab meetings,*

*Thanks to Ale and Fabri, for all the laughs we had together during these months, helping me a lot during my thesis writing, it's a pity we didn't meet before,*

*To all NG-PM group…thanks for all the interesting, crazy and never-ending discussions we had during our "paper of the week" sessions.*

*I would like to thank all the people from lab B, for helping me everytime I was in need and because of the nice atmosphere that made me feel like at home during these years.*

*Thanks to Chiara Bruckmann, my favourite professional, who, from the first day, adopted me, helped me and supported me, becoming more than a simple colleague.*

*Thanks to Roberta, Nikos and Irene for being amazing friends during all the PhD, and for all the moments we shared together, from the hardest to the funniest… they made my PhD life softer,*

*Thanks to Ceci and Seba, for sharing with me the amazing ENABLE adventure, for all the never-ending skype calls and all the laughs we had in our "amazing" room in Copenaghen. I have heard that friends are the family that you choose, and I think that with all of them I have made one of my best choice ever!*

*I would like to thank my "disagiate", Chiara, Buts, Nena, Pelle, Bobo, Chicca and Frengo, because, as one of my favourite songs says: "I get by, with a little help from my friends", and they are the best I could have ever asked for,*

*Thanks to Maddi and Gio, my crazy friends, for all the evenings together having "just few beers", and for all the mornings that "I will never drink a beer anymore", but also for being always present both in the happiest and in the most difficult moments,*

*Thanks to all my friends from Ostello Bello, for being like a second family since more than 4 years,*

*Thanks to Eugenia, for all our evenings started with a simple beer, and ended with never-ending discussions about nothing and everything; and also for being always in the first line when I was in need, knowing always the right things to say to me,*

*Thanks to Alice, for being always present, despite the thousand miles that separate us,*

*Thanks to Pucci, for our special friendship and for being my certainty all the time, since more than 20 years.*

*Thanks to Simone, for teaching me how to climb a rock wall, even if I still don't know how to make a longe! But also thanks for being so patient with me, not only on the rocks, but also in the daily life.*
*And last but not least,*

*A special thanks to the Family,*
*For making me become the person I am,*
*For helping me every time I was in need,*
*For supporting me in every decision I made and giving me the strength to reach this important step,*

*And of course, for all the times we met in front of a good drink accompanied with great laughs, enjoying the moments together and celebrating life,*
*years are passing by...but we are still the most amazing family all over the world!*

*Thanks to my mum, for the energy and love she puts in every single thing she does, always with a smile, helping me in facing my day with optimism and serenity Thanks for being so genuine, teaching me that in life, the best things are the simplest ones,*

*Thanks to my dad, for transmitting me passion and curiosity and for teaching me that, we can fall many times in life, but the secret is to be stronger enough to wake up again and keep going on…Pol is waiting for us!*

*Thanks to my brother Jack, for being an important model for me, because of his determination in life, which is always accompanied by a good amount of sense of humour! Thanks for all the good advices and for being always present despite we do not see each other so often!*

*Thanks to Giò, for being my super sister, for her strength and energy and for being always a source of inspiration for me. For all the times we were screaming together during concerts and all the special moments we had together. For all the time we had fights when we used to share the same apartment, but then we solved the problems just with a simple smile. Thanks for being present in the most important moments, from the best to the worst!*

*Thanks to Mati, Cocò and Greg, for all the cheerfulness and joy they bring with always them,*

*Thanks to my aunt Giuly, for being always present and for all her beautiful words that she is used to tell me.*

*The last four years have been absolutely the most challenging, but also the most important of my life, they made me grow a lot, shaped myself, and made me become the person I am, full of passions, energy, love and amazing people around me…and if I think about my future, I am not really sure about where I will be, but I certainly know that all these persons I love, will always come with me!*